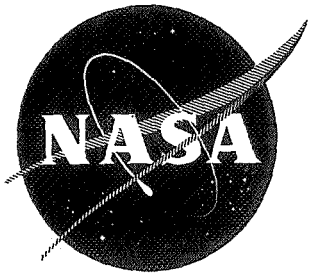

NASA CR-72796
ALRC-2100-5

FINAL REPORT

DESIGN AND EXPERIMENTAL EVALUATION OF A TURBOPUMP LIFT-OFF SEAL

by

J. A. RITTER

AEROJET LIQUID ROCKET COMPANY
SACRAMENTO, CALIFORNIA 95813

Prepared for

NATIONAL AERONAUTICS AND SPACE ADMINISTRATION

NASA Lewis Research Center
Contract NAS 3-11202
D. D. Scheer, Project Manager

NOTICE

This report was prepared as an account of Government sponsored work. Neither the United States, nor the National Aeronautics and Space Administration (NASA), nor any person acting on behalf of NASA:

A.) Makes any warranty or representation, expressed or implied, with respect to the accuracy, completeness, or usefulness of the information contained in this report, or that the use of any information, apparatus, method or process disclosed in this report may not infringe privately owned rights, or

B.) Assumes any liabilities with respect to the use of, or for damages resulting from the use of any information, apparatus, method or process disclosed in this report.

As used above, "person acting on behalf of NASA" includes any employee or contractor of NASA, or employee of such contractor, to the extent that such employee or contractor of NASA, or employee of such contractor prepares, disseminates, or provides access to, any information pursuant to his employment or contract with NASA, or his employment with such contractor.

Requests for copies of this report should be referred to:

National Aeronautics and Space Administration
Scientific and Technical Information Facility
~~P.O. Box 33~~
~~College Park, Md. 20740~~

NASA CR-72796
ALRC-2100-5

FINAL REPORT

DESIGN AND EXPERIMENTAL EVALUATION OF A TURBOPUMP LIFT-OFF SEAL

Prepared For

NATIONAL AERONAUTICS AND SPACE ADMINISTRATION

12 May 1971

CONTRACT NAS 3-11202

Prepared by:

AEROJET LIQUID ROCKET COMPANY
P. O. Box 13222
Sacramento, California 95813

AUTHOR: J. A. Ritter
Project Engineer

APPROVED: W. W. Heath
Project Manager

Technical Management:

NASA LEWIS RESEARCH CENTER
21000 Brookpark Road
Cleveland, Ohio 44135

APPROVED: D. D. Scheer
Project Manager
Chemical Rocket
Division

FOREWORD

This final report is a summary of the work conducted by the Aerojet Liquid Rocket Company, Sacramento, California, under Contract NAS 3-11202. The contract was sponsored by the Lewis Research Center of the National Aeronautics and Space Administration and was administered under the technical direction of the Chemical Rocket Division with Mr. D. D. Scheer as Project Manager.

ABSTRACT

Hydrogen static "zero leakage" rates and "zero wear" rubbing life predictions were developed for various seal interface geometries and material combinations. A hydrostatic lift-off seal and a related tester unit for use with liquid hydrogen were designed and fabricated. The seal was designed for "zero leakage" of hydrogen after operation which simulated 300 liquid hydrogen turbopump duty cycles. For the seal size studied in this program, "zero leakage" was defined as one standard cc/sec at a differential pressure of 85 psi. A hardware discrepancy precluded operation of the seal at design conditions. However, static sealing and rubbing tests in liquid hydrogen were accomplished. The seal functioned effectively as a static seal through a known life of 176 rubbing cycles with leakage below 1 std cc/sec at differential pressures to 45 psi.

TABLE OF CONTENTS

TABLE OF CONTENTS (cont.)

LIST OF TABLES

LIST OF TABLES (cont.)

LIST OF FIGURES

LIST OF FIGURES (cont.)

LIST OF FIGURES (cont.)

I. SUMMARY

The objective of the four-task Effective Lift-Off Seal Program was to design and develop a lift-off seal for liquid hydrogen service which would function as a "zero leakage" static seal with pressurized liquid hydrogen in the seal cavity as well as function as a dynamic seal during simulated turbopump transient and steady-state operation.

A. TASK I - CONCEPTUAL DESIGN

A design study was performed wherein a number of lift-off seal design concepts were formulated. These included designs where seal lift-off occurs as a function of sealed cavity pressure and/or shaft rotation (self-actuating) as well as designs requiring an external or auxiliary system for disengaging the sealing elements (externally-actuated). In addition, a "zero leakage" definition was conceived which relates the maximum permissible flow of hydrogen with the physical size of the turbomachinery and engine for which the seal is intended.

Concurrent with the conceptual design of the seals, a theoretical relationship was established between sealing loads, "zero wear" rubbing life, and "zero leakage" hydrogen flow for various seal interface geometries and material combinations. This relationship was developed by combining common elements derived from a review of results of extensive leakage and wear experiments.

B. TASK II - DETAIL DESIGN AND ANALYSIS

At the completion of the Task I effort, two of the design concepts were selected for further design and analysis. Both of these concepts were hydrostatic face-type bellows seals. The basic difference between these two concepts was that one design relied upon the bellows spring force, fluid pressure, and the hydrostatic forces to achieve the program objectives while the alternative design included an externally-pressurized bellows chamber to provide positive control of the sealing loads.

Mechanical design, structural and hydraulic analyses, and detail manufacturing drawings were completed during Task II for both of the seal concepts. In addition, an existing turbine-driven seal test unit design was modified to provide for installation of either of the lift-off seals and for liquid hydrogen evaluation in accordance with program requirements.

At the conclusion of Task II, the externally-pressurized seal design was designated as the most logical selection for fabrication and subsequent experimental evaluation. The control of seal loading made possible by this design offered the means to more fully explore the load-leakage-life relationship and provided a more adequate foundation for future seal design work.

C. TASK III - FABRICATION

The mechanical design approach taken during the Task II effort was based upon the use of fabrication and assembly techniques that had been demonstrated in previous designs. Significant effort was expended, but the completed seal did not meet all of the drawing design requirements because of bellows fabrication problems. However, a subsequent review of the design indicated that a meaningful test program could be conducted for evaluating the basic features of the design without expending the additional funds required for repair of the discrepancies.

D. TASK IV - TESTING AND DEVELOPMENT

A program was established for liquid hydrogen evaluation of the lift-off seal for comparison with predicted performance. Tests were conducted to determine the static "zero leakage" flow across the seal interfaces at several pressure gradients. Additional tests were conducted to evaluate the transient wear characteristics of the sealing surfaces in a liquid hydrogen environment.

E. PROGRAM RESULTS

Good correlation was obtained between actual and predicted static leakage flow rates and the achievement of the "zero leakage" program goal. Wear life of the interface materials was not as predicted, but was reasonably good considering the severity of the test conditions.

II. INTRODUCTION

Contractual effort for the effective Lift-Off Seal Program was initiated during July 1967 and the technical portion was completed during June 1970. The following contractual tasks were accomplished.

Task I - Conceptual Design

Task II - Detail Design and Analysis

Task III - Fabrication

Task IV - Testing and Development

The detailed accomplishments in each task are provided in the ensuing sections of this report.

The seal development efforts in several NASA Programs (i.e., M-1, J-2, and SNAP 8) have established that there are significant potential benefits to be derived from the use of lift-off seals which would prevent propellant leakage during static or non-rotating conditions and control leakage under dynamic operation. Experience has shown that although reasonably accurate predictions can be made for seal dynamic leakage rates, both static leakage and the duration capability of the sealing elements had to be determined experimentally for each design under consideration.

Both a static "zero leakage" limit and a duration capability were expressed as program goals; therefore, it was considered appropriate to develop an analytical approach toward the prediction of the sealing loads required to achieve this leakage limit as well as the rubbing life of the sealing elements. The load-leakage-life relationship established during this program constituted a significant portion of the design effort involved in the creation of the required lift-off seal manufacturing drawings.

III. BASIC DESIGN CONSIDERATIONS

A. SEAL SPECIFICATIONS

The lift-off seal concepts considered for this program were designed to meet the following contractual requirements.

1. Fluid to be sealed: Liquid Hydrogen

2. Design Parameters:

Condition	Sealed Fluid Cavity Pressure	Leakage Cavity Pressure	Allowable Leakage
(a)	100 ± 10 psia	0 psig	"zero leakage" as defined during Task I
(b)	500 ± 10 psia	0 psig	To be established during Task I

Condition (a) - Seal faces in contact at zero rpm.

Condition (b) - Seal faces separated, shaft at design rpm.

3. Seal face surface speed at design condition (b) shall be in the range of 500 ft/sec to 700 ft/sec.

4. Life: Goal - 10 hours which shall include 300 duty cycles.

5. Separation of the sealing surfaces shall be accomplished during shaft acceleration from zero rpm to design rpm. Acceleration to design rpm shall be accomplished within 4 sec to 6 sec.

B. ZERO LEAKAGE DEFINITION

To accomplish the static sealing objectives, it was necessary to first arrive at an acceptable definition of "zero leakage" because actual zero leakage of hydrogen would be both an impossible goal to attain as well as an impossible flow quantity to measure. For this purpose, it was assumed that hydrogen leaking past the seal would be trapped in the air filled cavity of the turbine exit housing of the turbopump. It was considered that using the turbine exit housing as the entrapment volume would provide a conservative means of assigning a permissible hydrogen leakage rate for any size engine because it can be shown that with state-of-the-art turbine wheel speeds and bearing DN values, the

$$\text{Seal or Bearing Diameter} = f\ (\text{engine thrust})^{1/2}$$

and

$$\text{Turbine Wheel Diameter} = f\ (\text{seal diameter})$$

The turbine exhaust housing volume (entrapment volume) will be approximately;

$$V = f\ (\text{turbine wheel diameter})^3$$
$$= f\ (\text{seal diameter})^3$$
$$= f\ (\text{engine thrust})^{3/2}$$

Therefore, the total leakage permissible for a given engine or turbopump size will be;

$$Q_T = f\ (\text{turbine exit housing volume})$$
$$= f\ (\text{seal diameter})^3$$
$$= f\ (\text{engine thrust})^{3/2}$$

and the average leakage rate will be;

$$Q_L = f\ \frac{(\text{turbine exit housing volume})}{(\text{hold time})}$$
$$= f\ \frac{(\text{seal diameter})^3}{(\text{hold time})}$$
$$= f\ \frac{(\text{engine thrust})^{3/2}}{(\text{hold time})}$$

The drive unit considered for liquid hydrogen evaluation of the seals had a speed capability of approximately 20,000 rpm; therefore, the seal nominal diameter required to give the required minimum surface velocity of 500 ft/sec under steady-state conditions would be

$$D = \frac{(500\ \text{ft/sec})(60\ \text{sec/min})(12\ \text{in./ft})}{(3.14/\text{rev})(20{,}000\ \text{rev/min})} = 5.73\text{-in.}$$

which corresponded approximately to the size of the lift-off seal used in the M-1 hydrogen turbopump, which had a turbine exit housing volume of approximately 4.7 ft^3. Using a 0.041 volumetric ratio (Ref 1) of gaseous hydrogen to air (at standard conditions) for a non-hazardous mixture from a flammability standpoint, the total quantity of hydrogen which could be permitted to leak into the air-filled turbine exit housing during the hold period would be:

$$Q_T = 0.041\ V = 0.19\ ft^3 = 5410\ cc.$$

Arbitrarily assuming a 10 hour hold period after chilldown and prior to launch, the average static leakage rate would be:

$$Q_{AV} = \frac{Q_T}{\text{Time}} = \frac{5410}{(10)\ (3600)} = 0.15\ \text{std cc/sec}$$

which would represent the leakage flow where the seal cavity pressure was maintained at a constant level of 100 psia throughout the hold period. It was considered more logical to assume that the seal cavity would be maintained at a pressure of only 25 psia for the first nine hours of the hold and then raised to 100 psia for the last hour before launch. This assumption results in an approximate ratio of maximum leakage flow to minimum leakage flow for the hold period of;

$$\text{Flow Ratio} \approx \frac{(100)^2 - (14.7)^2}{(25)^2 - (14.7)^2} = 24 \text{ (approximately)}$$

therefore,

$$\left[(9 \text{ hours})(Q_{L\text{-}MAX}/24) + (1 \text{ hour})(Q_{L\text{-}MAX})\right] 3600 \text{ sec/hr} = 5410 \text{ cc}$$

and

$$Q_{L\text{-}MAX} = \frac{(5410)\ (24)}{(3600)(9 + 24)} = 1.09 \text{ std cc/sec}$$

From the above reasoning, the definition of "zero leakage" and, hence, the goal for this program was established as 1 standard cc/sec at an 85 psi pressure differential across the seal.

IV. DESIGN CONCEPTS

The lift-off seal design concepts prepared during Task I are described as follows. Particular emphasis was placed upon designs which provided high initial sealing loads to meet the "zero" static leakage requirement, rapid lift-off (disengagement of the sealing surfaces) to minimize rubbing wear, and fulfillment of the operational requirement of 10 hours life including 300 typical turbopump duty cycles.

A. DESIGN CONCEPT "A"

1. Description

The mechanical seal lifter device shown on Figures No. 1 through No. 5 is of the cam and roller type. Actuation is accomplished by a means of spring-loaded friction clutch, released at 1000 rpm by centrifugal force. Figure No. 2 displays a set of three rollers (R_1), which are equally-spaced and contained in a ring (R). These rollers move around on a circular track in the housing. Another set of three rollers (R_2), designated as cam-rollers, is located between the track rollers. The ends of the pins holding the rollers are flattened and engaged by slots in the driving ring (see Figure No. 3). The rollers are R-type flanged ball bearings (0.375 in. bore). (R6DD radial load capacity is 235 lb at 50 rpm.) The cam-face (Figure No. 2), which rests on the rollers, R_2, carries three (120 degrees apart) identical ascent and descent-ramps having a circumferential extension of approximately 60 degrees each. The cam itself is secured against rotation in the housing. However, if the roller carrier ring is rotated, the cam will move axially in the housing with a 60 degree turn corresponding to the full lift of the seal. Another 60 degree turn brings the cam down again. At rest, a small gap (set for nosepiece material and wear) separates the lifting shoulder of the cam from the nosepiece holder, as shown on Figure No. 4. Springs and pressure acting upon unbalanced areas force the nosepiece against the running ring to seal the cavity containing liquid hydrogen at 100 psia against the leakage cavity at 0 psig. The secondary seal (between the housing and nosepiece) is

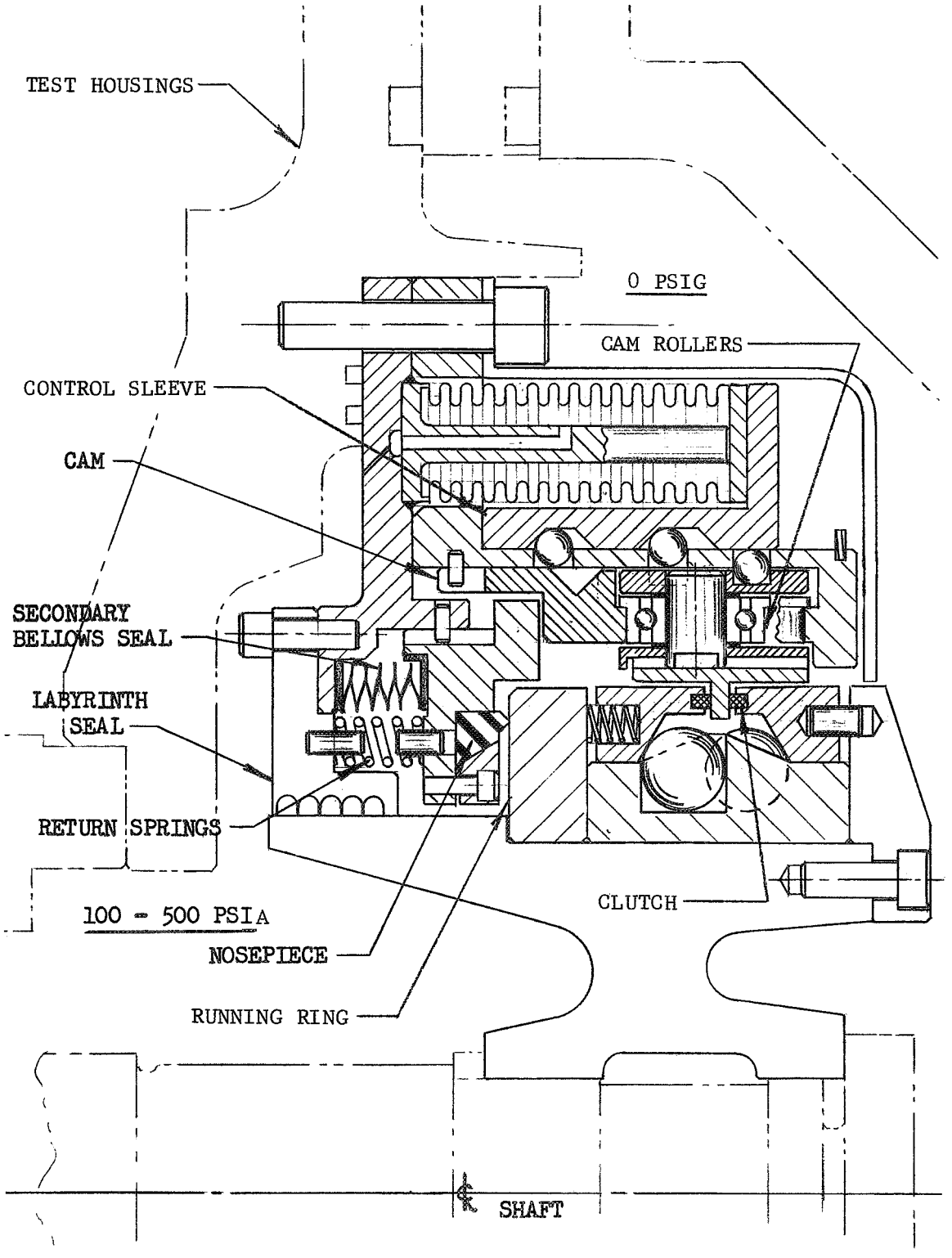

Figure 1. Lift-Off Seal Concept - Design "A"

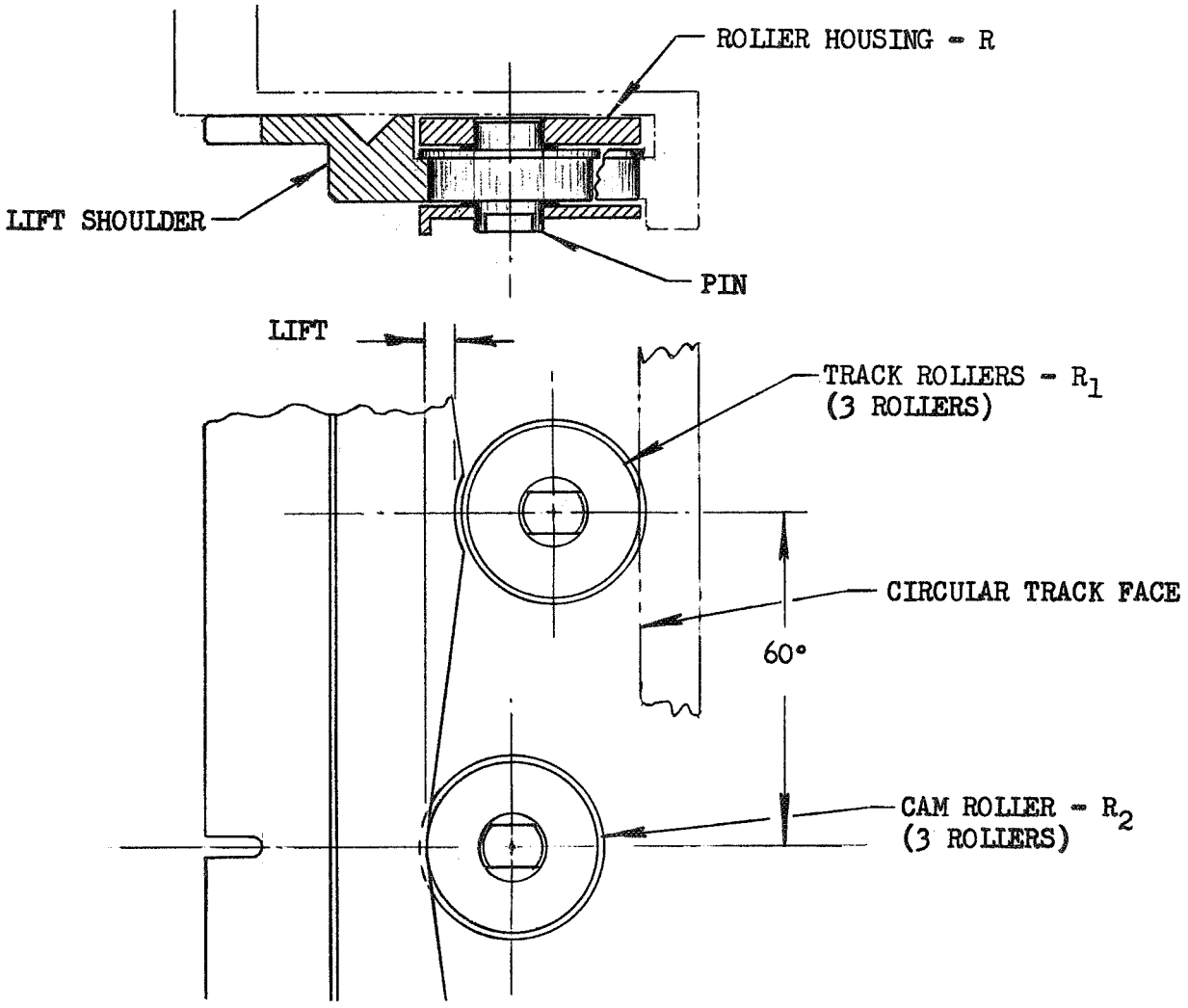

Figure 2. Lift-Off Seal Design Concept "A"

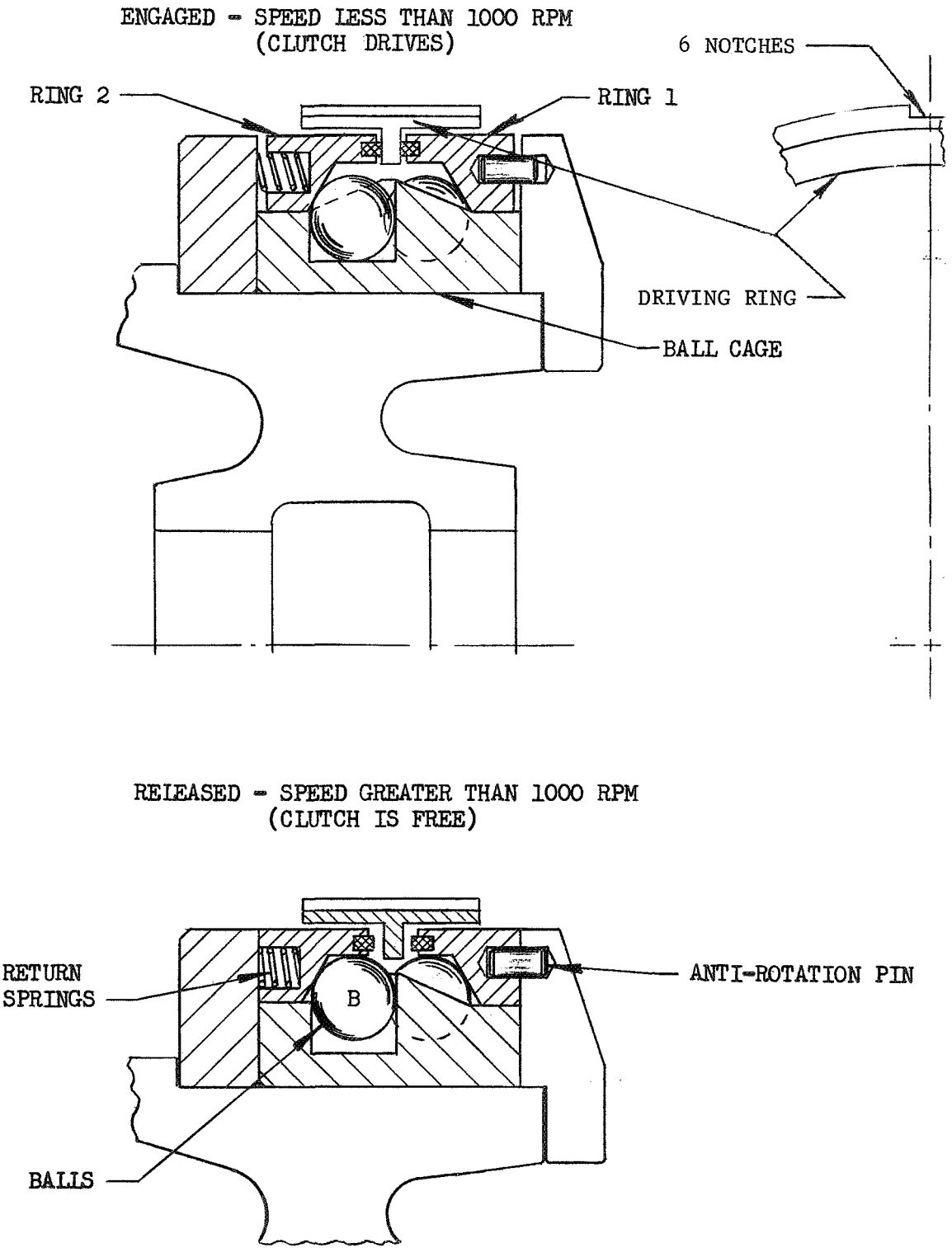

Figure 3. Lift-Off Seal Concept - Design "A"

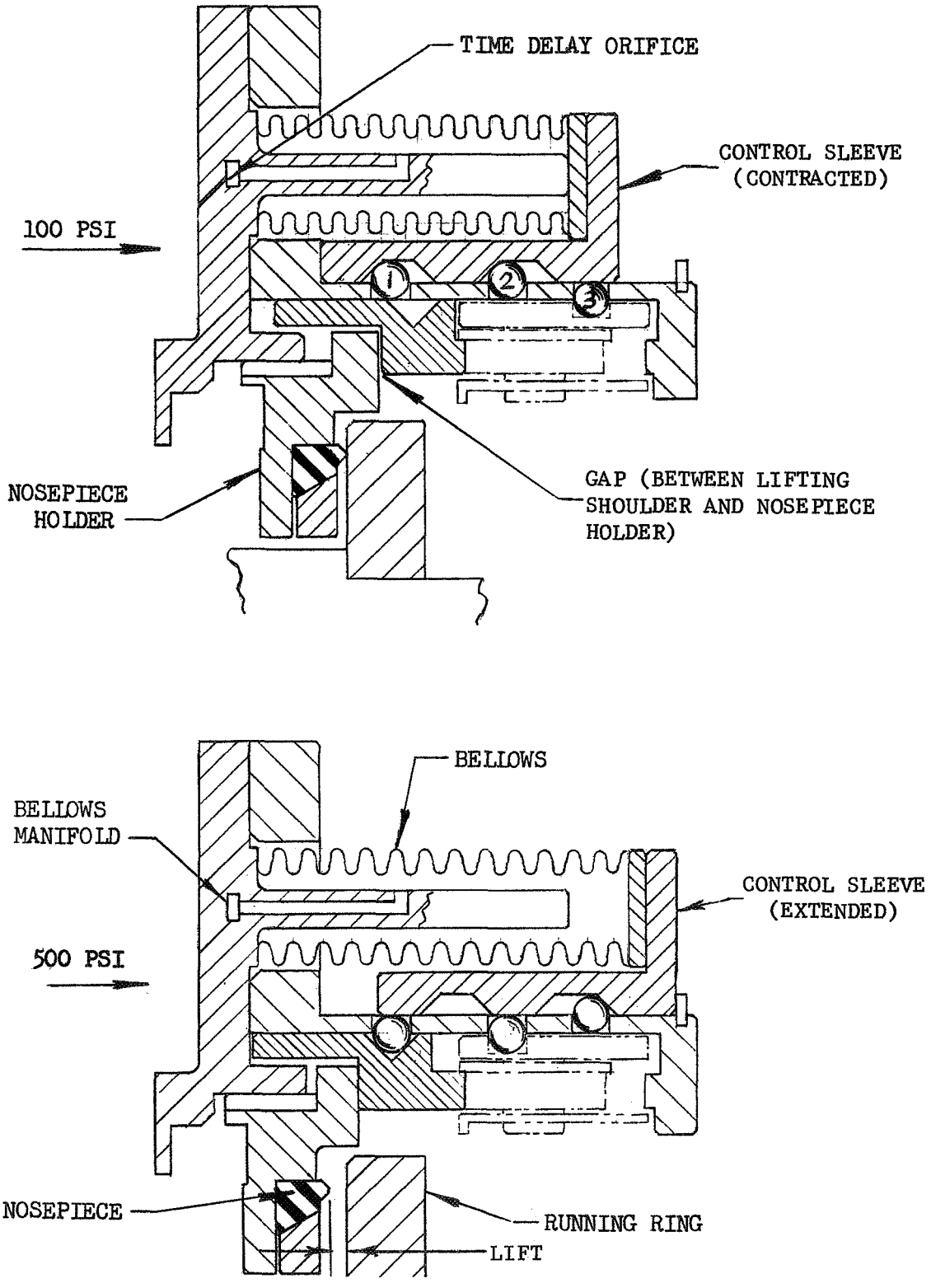

Figure 4. Lift-Off Seal Concept - Design "A"

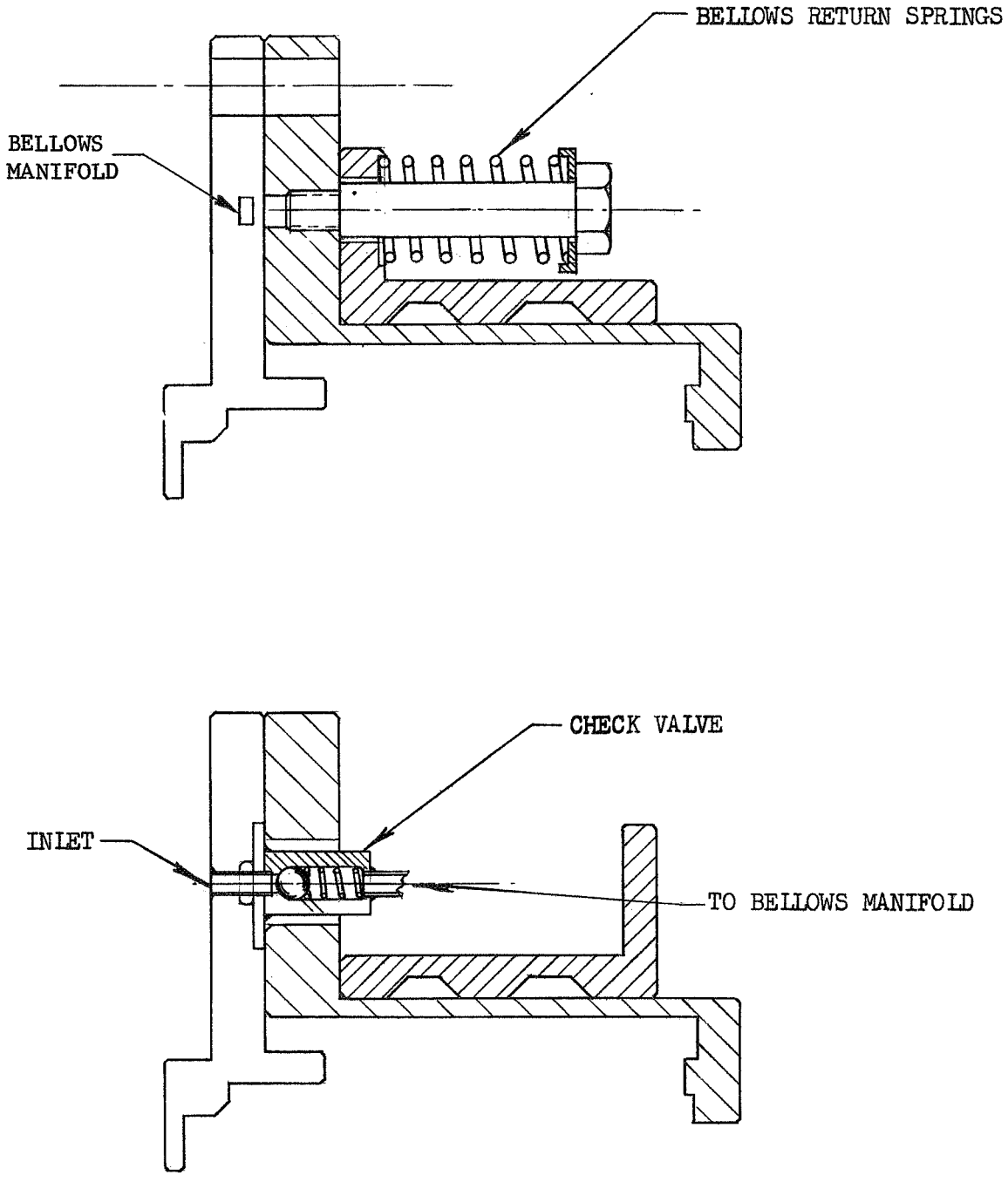

Figure 5. Lift-Off Seal Concept - Design "A"

a metal bellows welded to the corresponding components. The force required to lift the nosepiece against a cavity pressure of 100 psia is approximately 500 lb in this design. This force is obtained from the shaft by means of a spring-loaded clutch (see Figure No. 3). The driving ring is clamped between Ring 1 and Ring 2 by a number of springs. Friction between these rings and the driving ring transmits shaft torque into the lift device. If the shaft speed increases, centrifugal force on the balls, B, overcome the spring force and move Rings 1 and 2 away from the driving ring. No mechanical connection between shaft and the lift device exists at speeds greater than 1000 rpm. Above this speed, the balls rest against the cylindrical inner surface of the rings, which retain the balls against the centrifugal force.

2. Control

A set of bellows and a control sleeve are provided to achieve the desired sequence of motions (see Figure No. 4). The interior of the bellows is connected to the pressure side of the seal by means of a small, time-delay orifice. The initial pressure of 100 psia is balanced by springs, with the top of the bellows resting against a stop. Pressure build-up expands the bellows and forces the control sleeve toward the right side. A check valve (see Figure No. 5) permits the control sleeve bellows to expand freely during this pressure build-up. Conical surfaces of the control sleeve retain and free small balls which are guided in the housing bores. These balls perform the following functions:

Ball (1) Locks the nosepiece in the open position and unlocks it (delayed) when the pressure decays.

Ball (2) Runs in a track with a stop for the second 60 degrees of rotation.

Ball (3) Runs in a track with a stop for the first 60 degrees of rotation.

3. Sequence of Operation

a. Pre-Start Condition (zero shaft speed and 100 psia cavity pressure)

(1) Clutch is engaged

(2) Bellows is contracted

(3) Ball (1) is out

(4) Ball (2) is out

(5) Ball (3) is in at the start of a 60 degree track

b. Initial Start Conditions (shaft speed less than 1000 rpm and cavity slightly greater than 100 psia)

Shaft torque turns the driving ring and rollers while the cam face lifts the seal. Movement of the rollers is stopped after 60 degrees of rotation by a stop in the track of ball (3) and the clutch slips. After a shaft speed of 1000 rpm has been reached (less than one revolution of the shaft), the clutch is disengaged as indicated on Figure No. 3.

c. Start and Steady-State Conditions (shaft speed $\geq$ 1000 rpm and cavity pressure between 100 and 500 psia)

As the cavity pressure builds up, the bellows expands and the control sleeve moves toward the right, as shown on Figure No. 4. Ball (1) is locked into the "in." position and the seal is lifted. Ball (2) is pushed into the start of its 60 degree track and ball (3) is free.

Speed variations have no influence upon the seal function because the drive is disengaged above 1000 rpm. Pressure variations will have no effect because the cam and rollers are in the full-lift position and the lifter (ball (1)) is locked at pressures above 100 psia.

The labyrinth seal shown on Figure No. 1 is provided to limit the leakage during the period when the primary seal is in the lifted position.

d. Shutdown Condition (shaft speed less than 1000 rpm and cavity pressure approaching 100 psia)

At shaft speeds less than 100 rpm, the clutch engages slowly. If friction is sufficiently high, the driving ring and rollers will move 60 degrees. This movement is stopped by Ball (2) in its track and the clutch continues to slip until the shaft rpm reaches zero. The face cam and rollers now are in position to allow the seal to reseat. As the pressure in the bellows decays (pressure decay is retarded by the timing orifice), the control sleeve moves toward the left. Ball (1) becomes free and the cam is unlocked. The seal reseats under spring force and the additional force from the 100 psia cavity pressure. At the same time that Ball (1) is in the unlocked position, Balls (2) and (3) shift position in readiness for the next cycle.

B. DESIGN CONCEPT "B"

The lift-off seal concept illustrated on Figure No. 6 is somewhat similar to Design "A" with the major exception being a differential ball screw arrangement that is utilized for actuating the seal into the open position.

For a right hand thread, as viewed from X, a clockwise turn of component (B) advances (B) (essentially a bolt) toward the left, where component (A) (essentially a nut) is stationary. One complete revolution of (B)

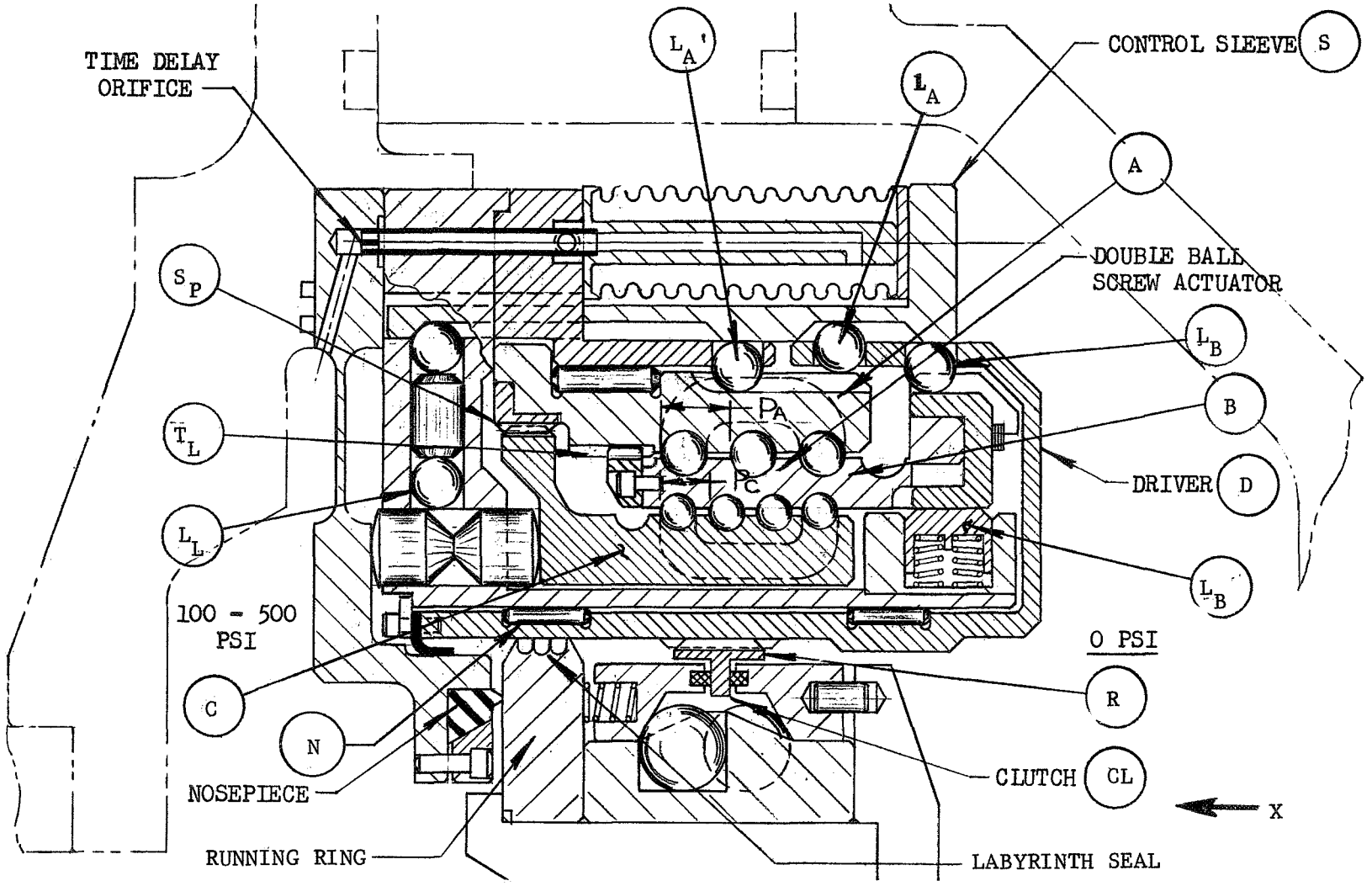

Figure 6. Lift-Off Seal Concept - Design "B"

produces an axial movement equal to the pitch, (P_A). Component (B) also acts as a nut for sleeve (C) and one revolution of (B) produces a relative axial motion of (C) to the right equal to the pitch (P_C). The resulting movement for the lift of the nosepiece away from the running ring will be (P_A) minus (P_C). In example, 180 degrees of rotation will produce a net seal opening of 0.10-in., where (P_A) = 0.5-in. and (P_C) = 0.3-in. Sleeves (A) and (C) are torsionally locked together, but are axially free to move relative to each other at spline (S_P). A reverse movement to the right is required to reposition the seal in the closed position. To achieve this motion with the same direction of rotation of driver (D), the bolt (B) is held stationary and the nut (A) is turned. This shift of locks is achieved by balls and the control sleeve (S), actuated by a bellows which is contracted by a spring acting against the 100 psia cavity pressure. As the cavity rises above the 100 psia level, the bellows expands and shifts the locks. Ball (L_B) couples or uncouples sleeve (B) to the driver (D), ball (L_A) couples or uncouples sleeve (B) to the driver (D), and ball (L_A) couples or uncouples sleeve (A) to the driver (D) while locking (A) to the housing. Component (L_B) prevents rotation of sleeve (B) where sleeve (A) is driven as would occur if the seal is still seated. Ball (L_L) locks the seal in the open position and permits the device to return to the starting position without load. During the shutdown transient and at speeds below 1000 rpm, the bellows remains expanded as a result of the retarding action of the time delay orifice. Contact with the sealing surfaces is prevented until the seal relative velocities have reached an acceptable level. The relative motion between sleeves (B) and (A) is limited to 180 degrees by a stop, (T_L). Support for the rotating members is provided by needle bearings (N). The driving force for (D) is obtained from the friction clutch (CL) which is released through centrifugal action of the balls shown when a speed of 1000 rpm has been attained; ball (L_L) has dropped into the stop and the seal is in the lifted position.

C. DESIGN CONCEPT "C"

The lift-off seal illustrated on Figures No. 7 through No. 9 relies upon a ball and ramp actuation system for rapidly separating the sealing surfaces during the start transient. Complete lift-off occurs with this device during the first 60 degrees of shaft rotation by the action of the three balls following a ramp as shown on Figure No. 9. In addition to the ball-ramp device, a control bellows is provided to augment the lifting action. As the system pressure increases from 100 psia to 500 psia, the control bellows expands and relieves the load on the ball and the ramp. The seal will remain in the lifted position despite minor system pressure and shaft speed variations during steady-state operation because of the locking ball action and corresponding groove (see Figure No. 8). Reseating of the seal during the shutdown transient is retarded until relative seal velocities have reached an acceptable level by the combined action of a timing orifice in the control bellows feed system and the locking ball.

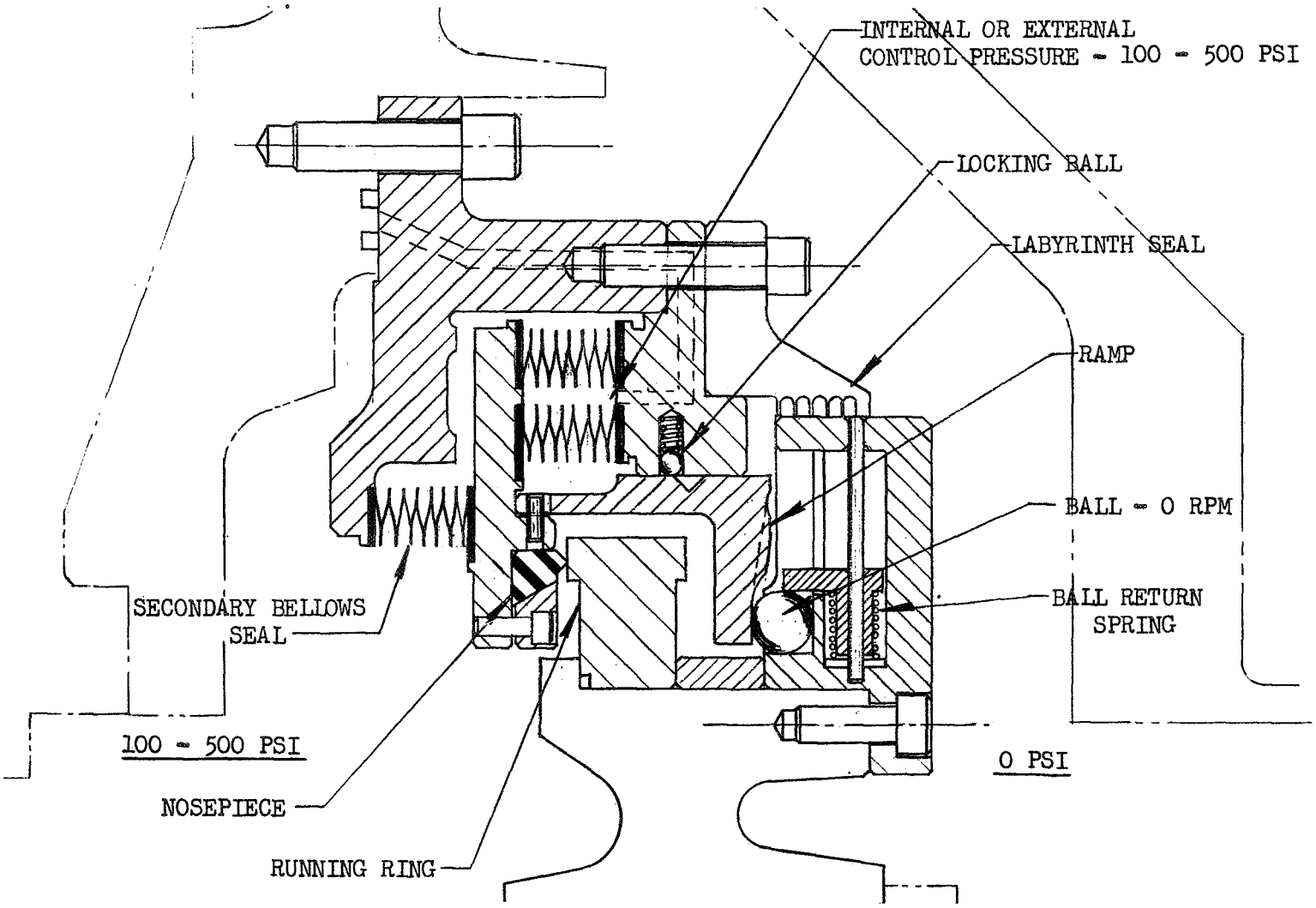

Figure 7. Lift-Off Seal Concept - Design "C"

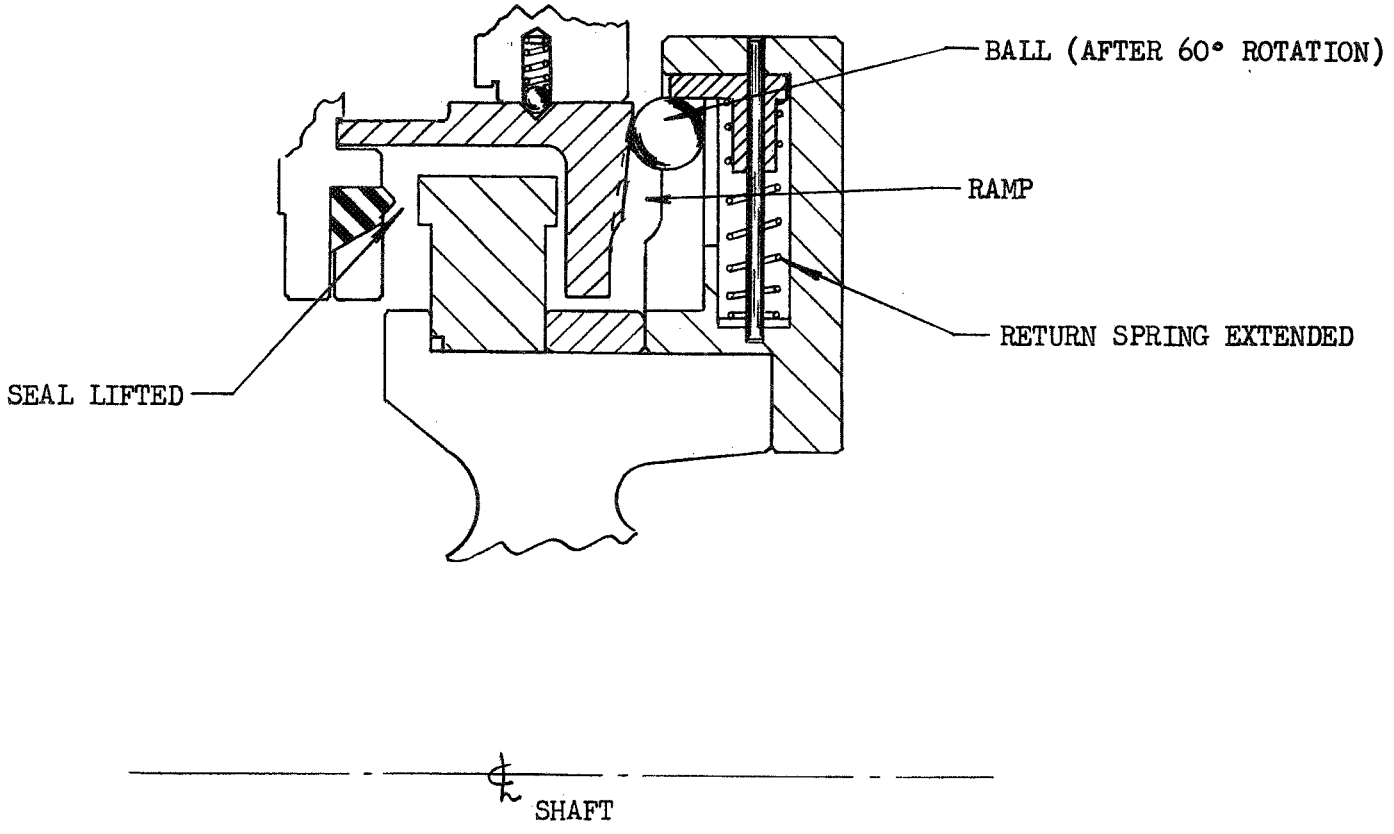

Figure 8. Lift-Off Seal Design Concept "C"

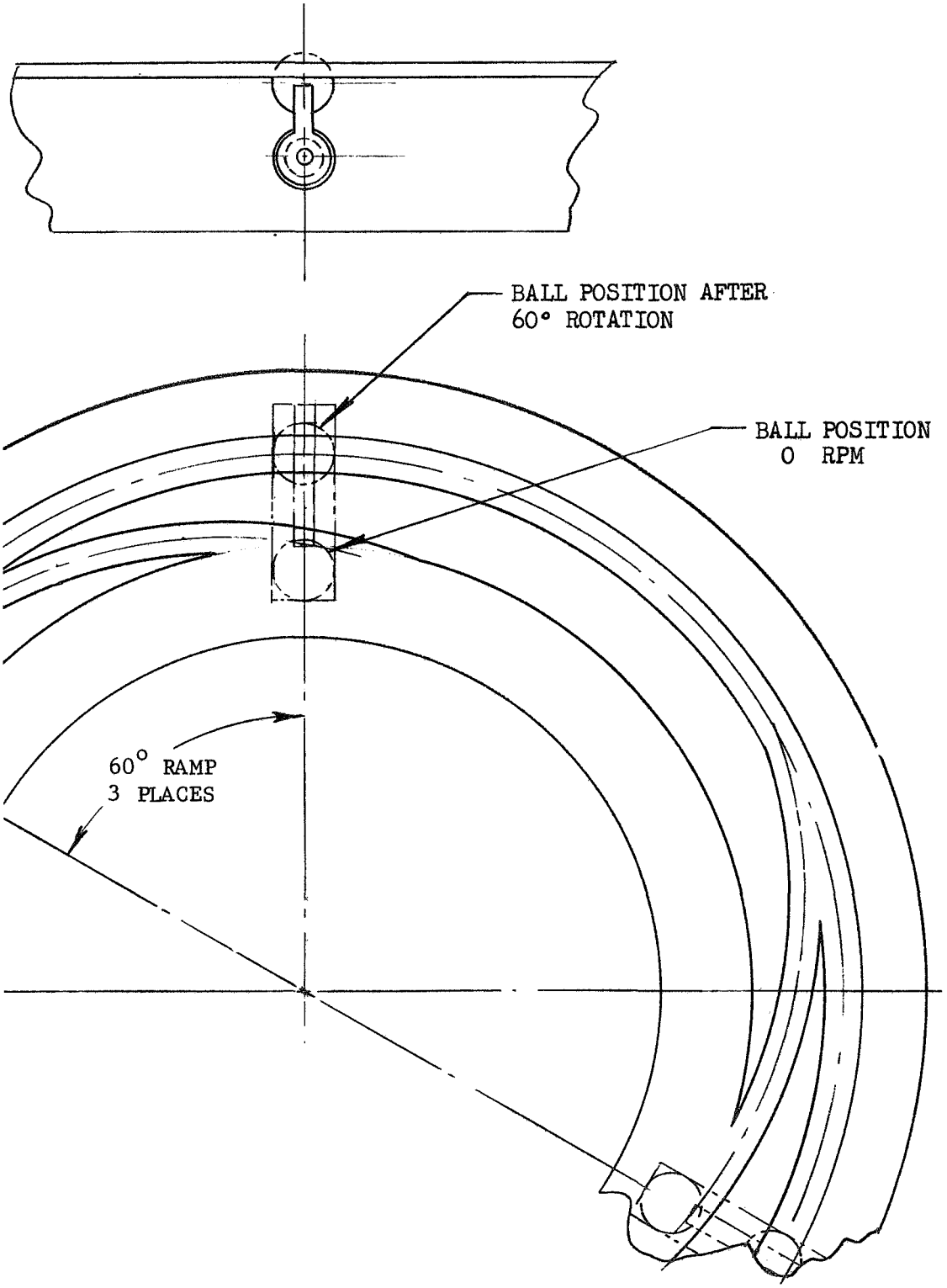

Figure 9. Lift-Off Seal Concept - Design "C"

D. DESIGN CONCEPT "D"

Figure No. 10 illustrates a seal which is lifted by differential pressure acting on bellows. Prior to rotation, the seal cavity pressure (P_c) is 100 psia, the cavity pressure upstream of the labyrinth (P_u) is 0 psig, and the downstream cavity pressure (P_d) is 0 psig. The seal cavity is isolated from the other cavities by the nosepiece seating against the running ring and by the spring-loaded ball valves shown on the figure. When shaft rotation reaches 1000 rpm during the start transient, the centrifugal force on the balls is sufficient to unseat the valve and permit P_u pressure to approach the P_c pressure of 100 psia, which will cause the nosepiece to lift away from the running ring. Reseating of the seal is retarded during the shutdown transient by the action of the ball valves at speeds above 1000 rpm and by the bellows check valve as the system pressure decays.

E. DESIGN CONCEPT "E"

The hydrostatic lift-off seal configuration shown on Figure No. 11 utilizes an externally-pressurized control bellows chamber. Pressurization of the bellows provides the initial closing force required for static sealing as well as for balancing the hydrostatic forces on the seal faces during dynamic operation. The inherently simple design offers a means for obtaining sealing loads that are sufficiently high to meet the established "zero" leakage limits while permitting rapid lift-off without wear of the seal interfaces.

F. DESIGN CONCEPT "F"

The lift-off seal design of Figure No. 12 is a pressure-actuated unit consisting of a radial piston pump arrangement providing pressure to expand a bellows which separates the nosepiece from the running-ring. Initial closing force for static sealing is accomplished by a Belleville spring assembly. The piston is driven by a cam and centrifugal clutch system which disengages at a shaft speed where the cavity pressure has risen to a level that is sufficient to maintain the seal in the open position. The seal is retained in the open position during the shutdown transient by retaining the pressure in the bellows until seal relative velocities have reached an acceptable level.

G. DESIGN CONCEPT "G"

Figures No. 13 and No. 14 depict a pressure actuated seal configuration similar to the "F" design. The bellows pressurization pistons for this design are driven by a cam arrangement which disengages by the action of pressure-sensing bellows at cavity pressures exceeding 120 psia (corresponding to a shaft speed of approximately 2000 rpm). Seal face contact during the shutdown transient is prevented by re-establishment of the piston pumping action when the cavity pressure drops below 120 psia as well as by virtue of the time delay orifice which retards the actuating bellows pressure decay until shaft speeds reach an acceptable level.

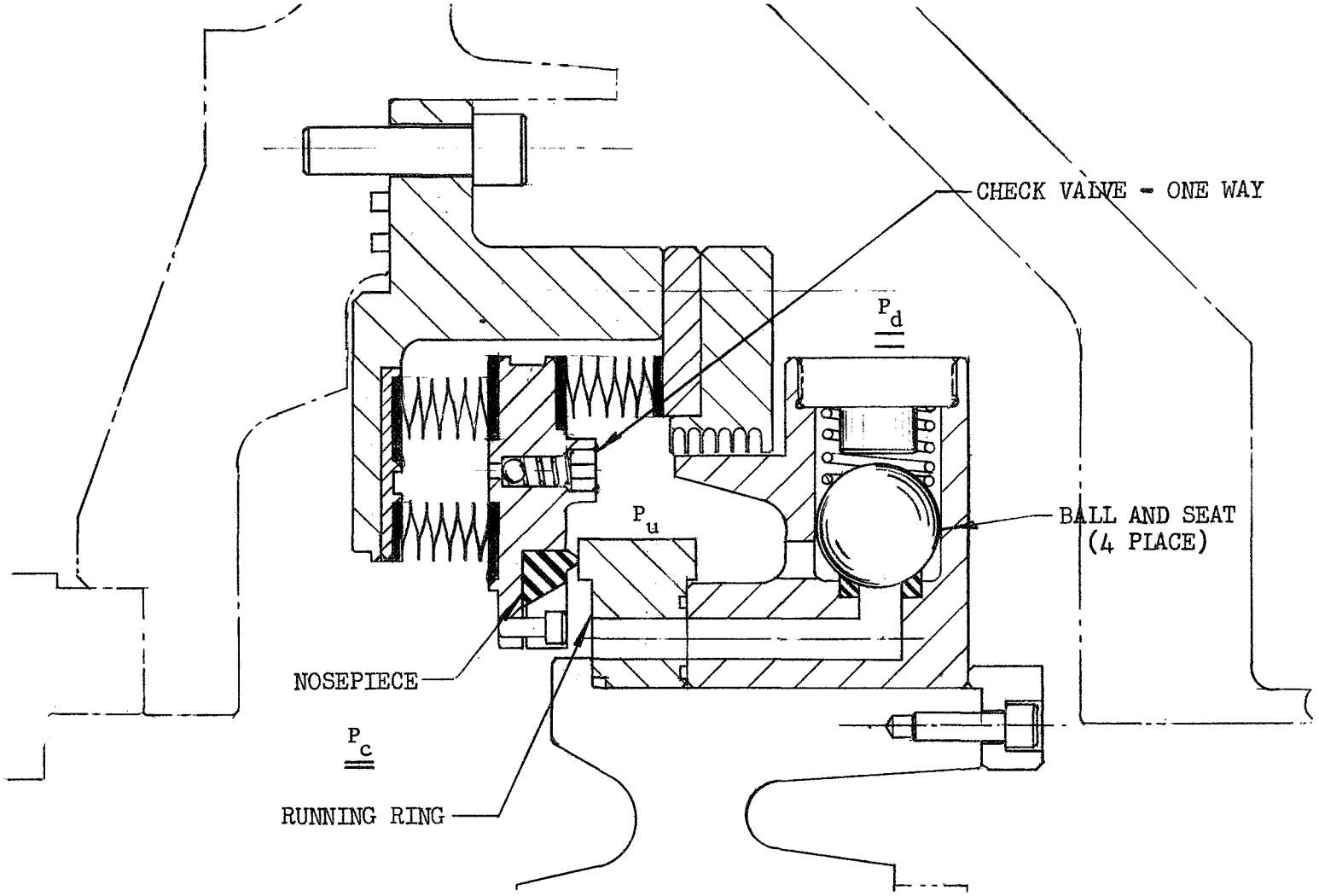

Figure 10. Lift-Off Seal Concept - Design "D"

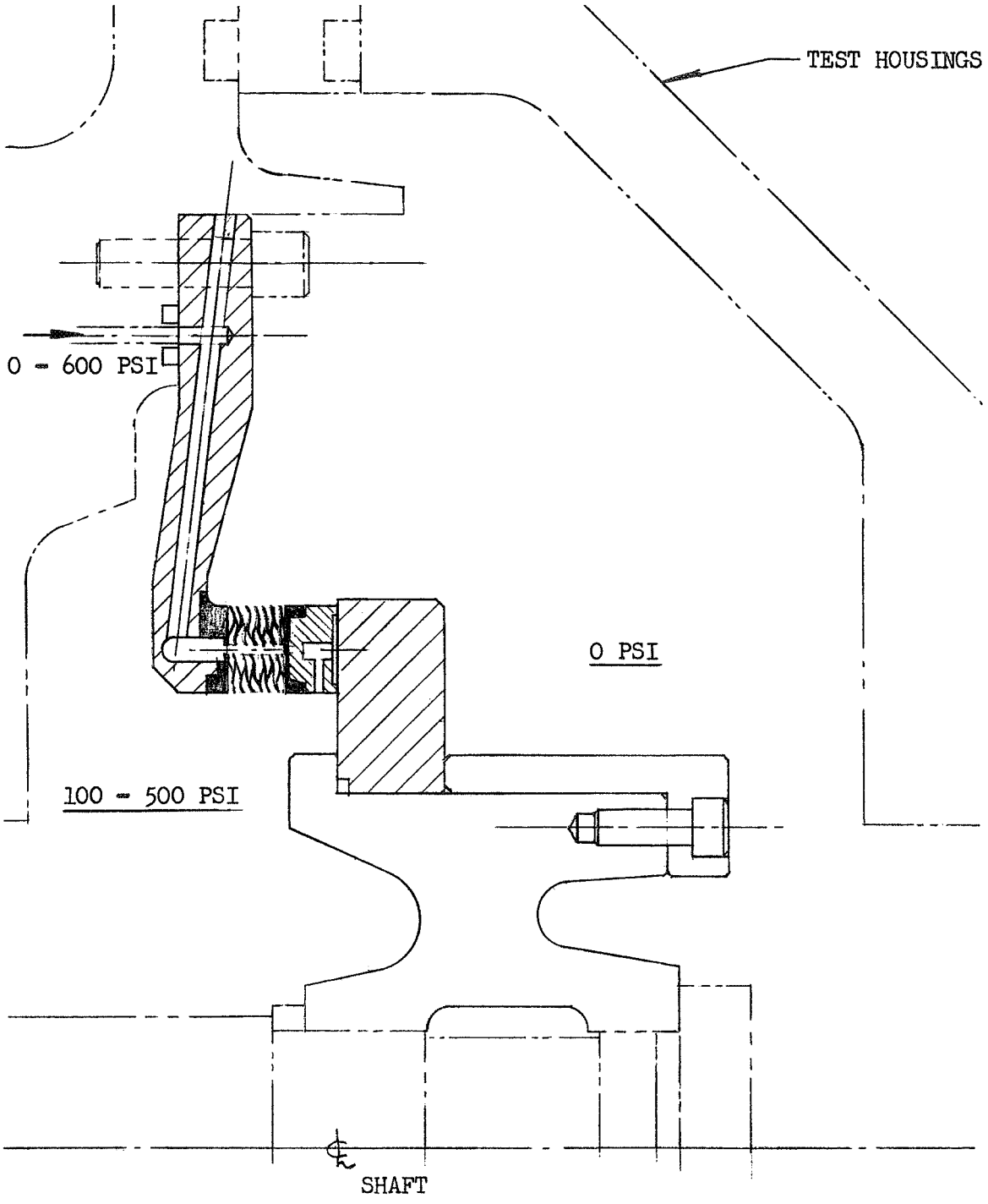

Figure 11. Lift-Off Seal Concept - Design "E"

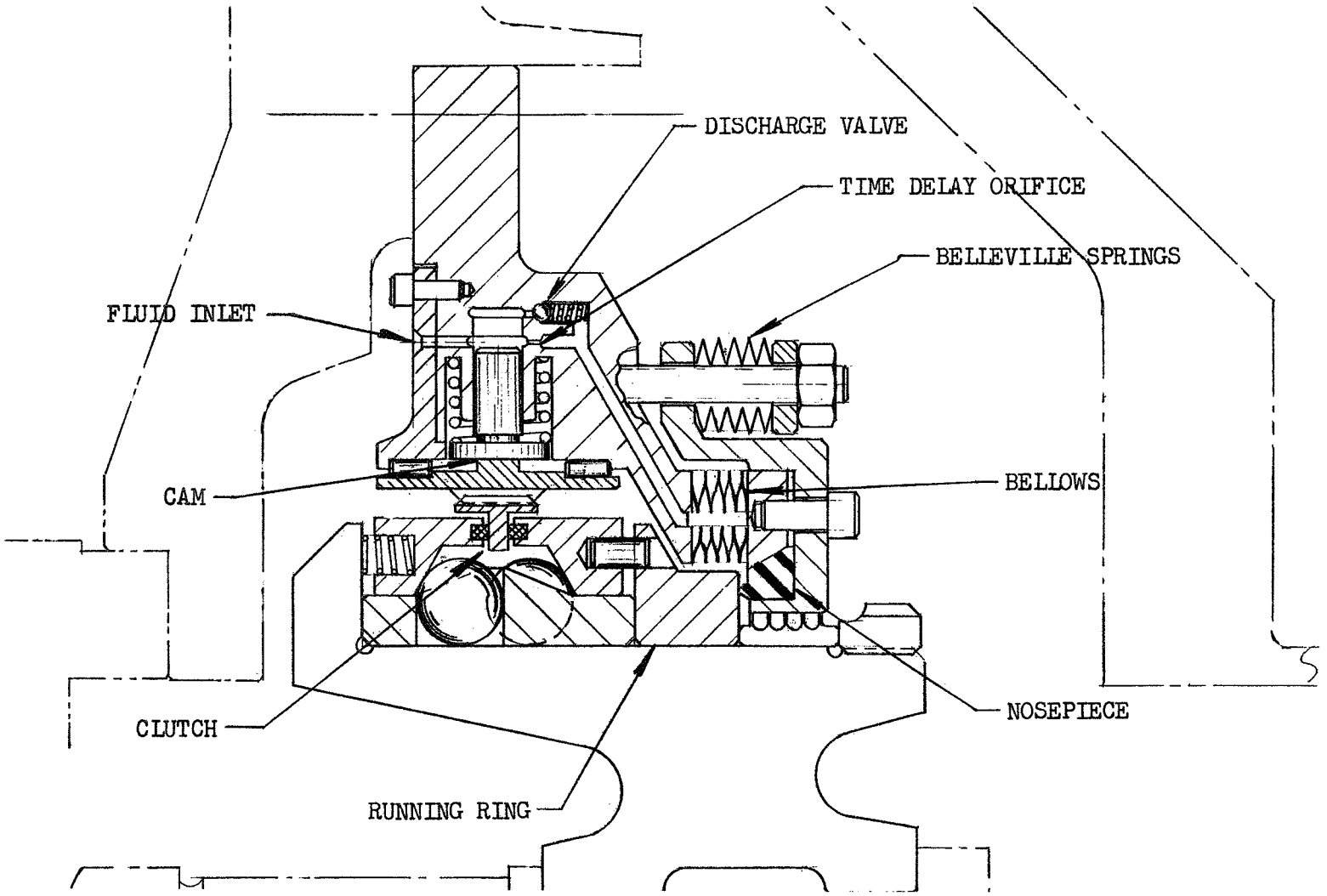

Figure 12. Lift-Off Seal Concept - Design "F"

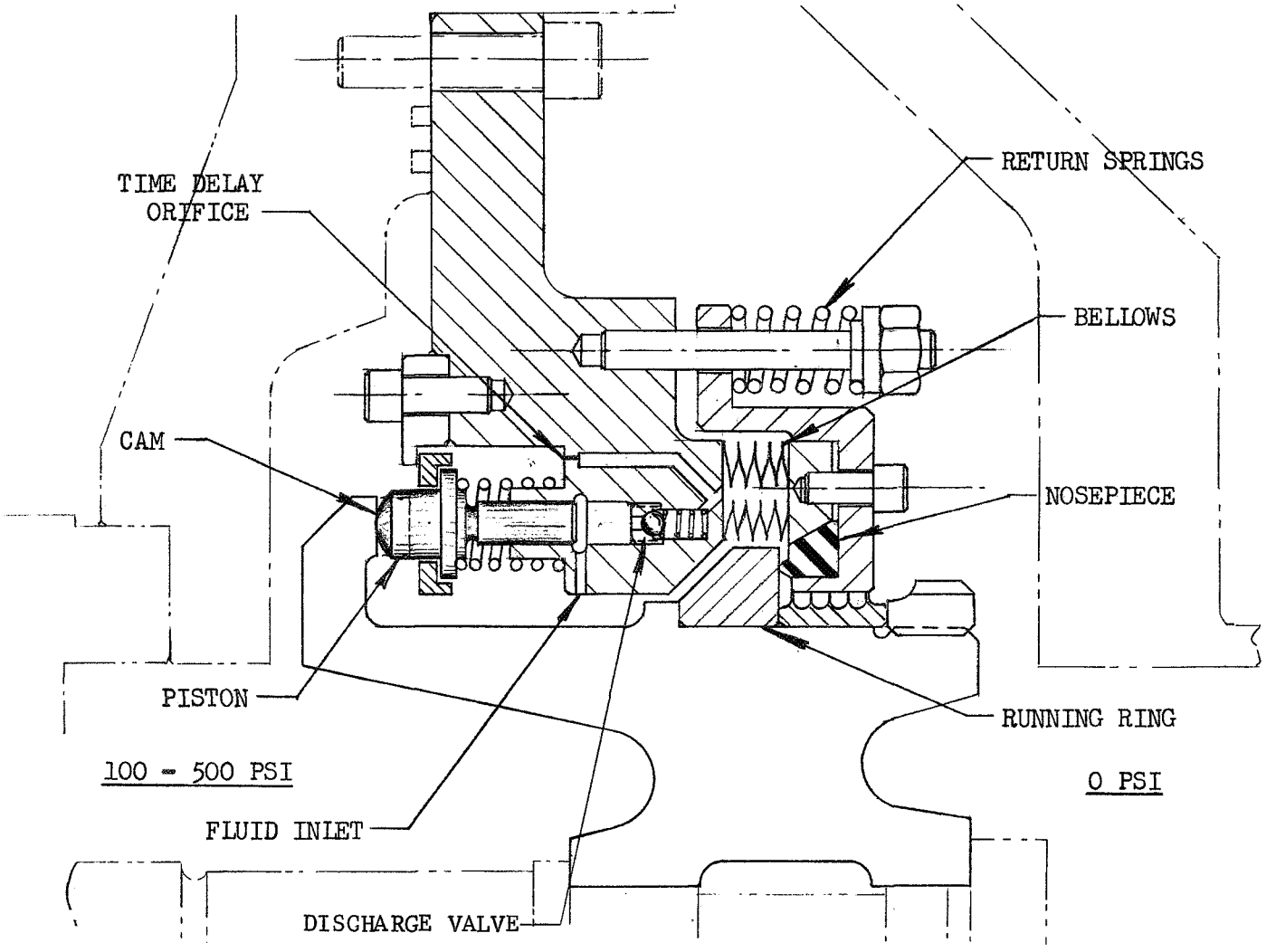

Figure 13. Lift-Off Seal Concept - Design "G"

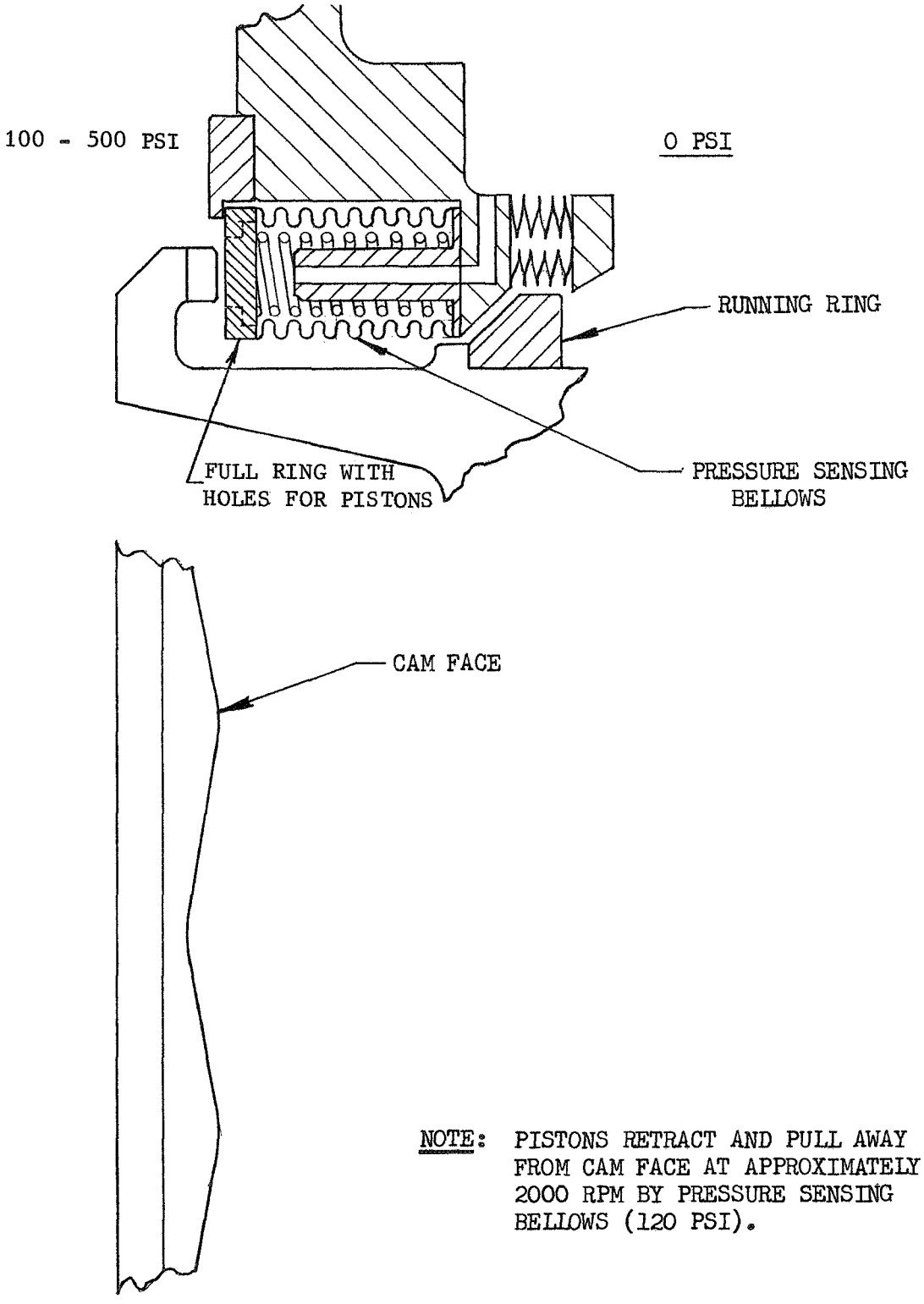

Figure 14. Lift-Off Seal Concept - Design "G"

H. DESIGN CONCEPT "H"

The design shown on Figures No. 15 and No. 16 is a modification of the "G" design, with a cam-driven piston pump providing the pressure for initial lift-off during the start transient. Again, a pressure sensing bellows is used to prevent contact between the piston follower and the cam at seal cavity pressures above 120 psia, when the nosepiece is in the lifted and locked position. A mechanical locking device is used to retain the nosepiece in the lifted position. During the shutdown transient, the mechanical lock is disengaged at pressures below 120 psia, the piston pumping action is initiated, and the seal remains lifted until acceptably low surface speeds are again established.

I. DESIGN CONCEPT "J"

This design, as represented by Figure No. 17, is a self-acting, pocketed, hydrostatic lift-off seal. The combined forces of the compressed bellows, the spring, and the pressure-area forces provide the necessary sealing load for "zero" leakage under static conditions. For steady-state operating conditions, the seal faces will be separated as a result of a balance between the pressure-area forces, the spring forces, and the hydrostatic forces at the seal face. In this design, seal interface rubbing will occur during the start and shutdown transient periods of operation. Consequently, particular emphasis must be placed upon the selection of materials with good liquid hydrogen wear characteristics.

V. LOAD LEAKAGE LIFE RELATIONSHIPS

Prior to the actual design of the lift-off seal for this program, a parametric study was conducted to determine the relationships between factors influencing both the static sealing capability and the wear resistance of seal interface components. In general, conditions optimum for static sealing (i.e., plastic deformation of the sealing lip) result in excessive wear during rubbing operation; conversely, the conditions optimum for long rubbing life (i.e., low seal element contact stress) result in poor static sealing capability.

The results of the parametric study described in this section provide a method for selecting seal interface material combinations, geometries, and face loadings which will satisfy the "zero leakage" and the operational life requirements for a specific seal application.

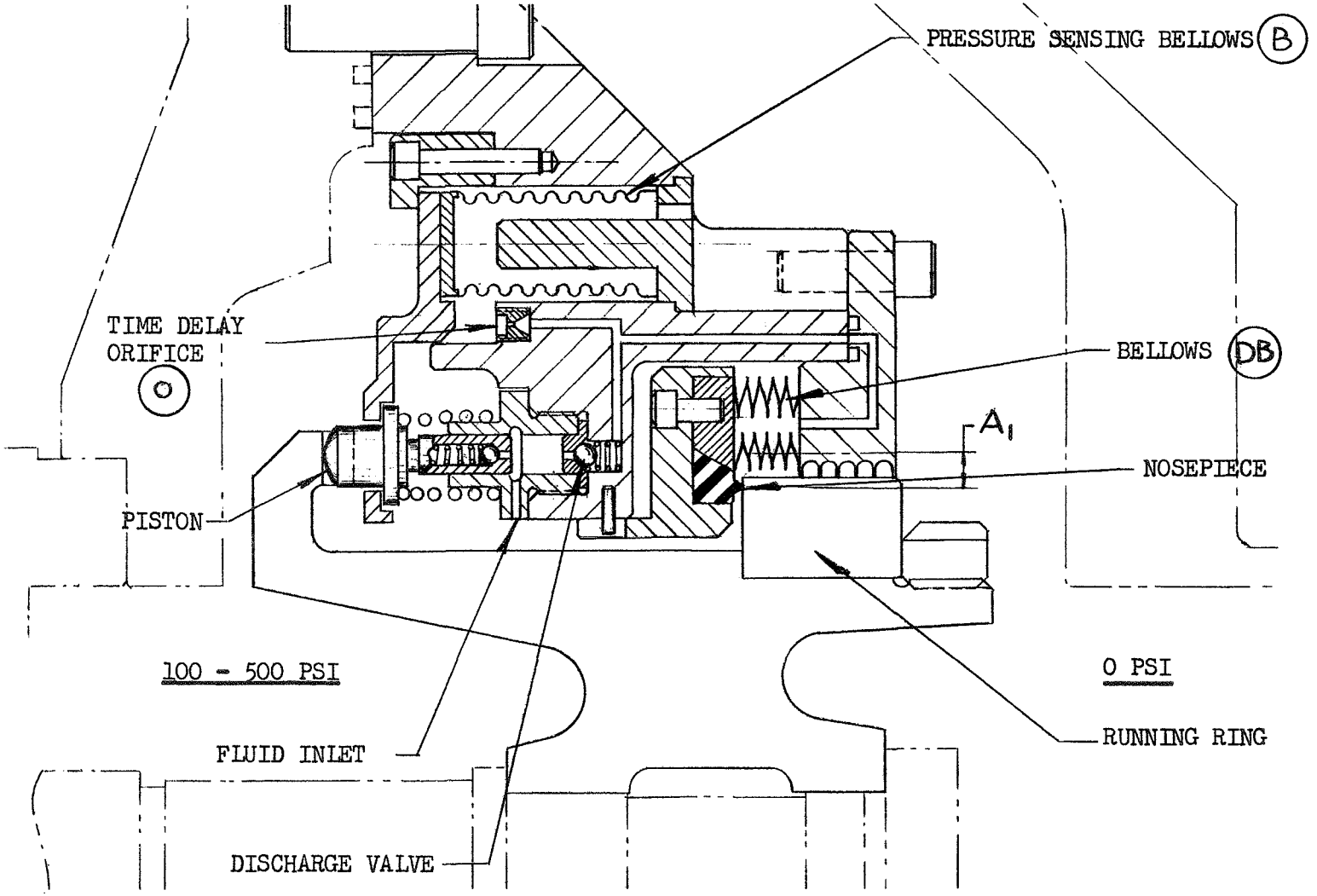

Figure 15. Lift-Off Seal Concept - Design "H"

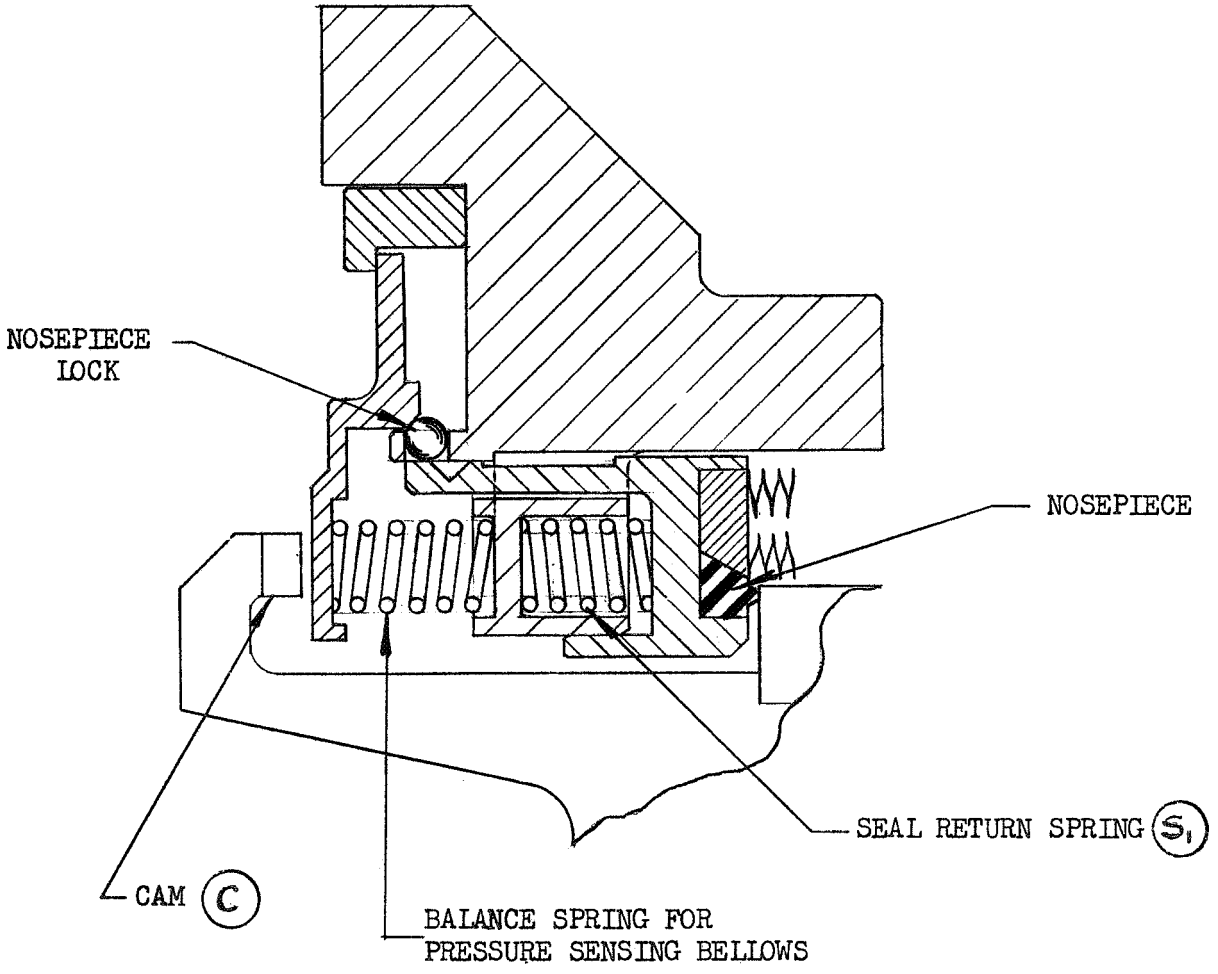

Figure 16. Lift-Off Seal Concept - Design "H"

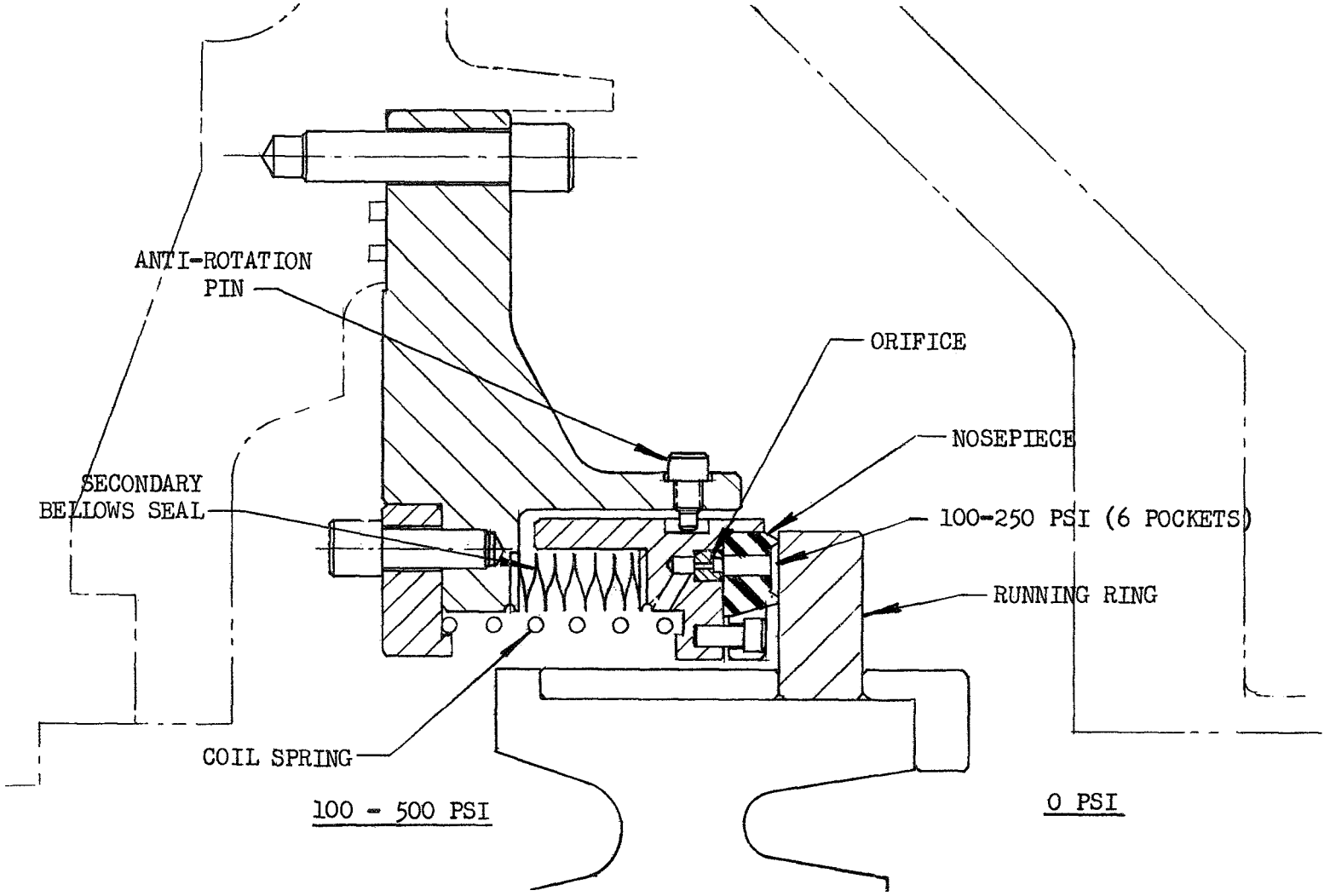

Figure 17. Lift-Off Seal Concept - Design "J"

A. STATIC SEAL LEAKAGE CRITERIA

As a result of Aerojet experience in the design of static seals for "zero leakage," the most practical "zero leakage" criteria for statically-sealed joints of helium and hydrogen systems have been established at approximately 1.0×10^{-6} std cc/sec/in. of seal interface length. However, this requirement is applicable only to statically-sealed joints. The metal or plastic gasket must be compressed plastically to ensure intimate conformity with the mating surface asperities and this results in permanent deformation with an accompanying work-hardening of the metal gaskets. No attempt is made to reuse the metal or plastic gaskets because each reuse would require a higher preload to gain the same initial conformity and the same leakage rate capability at the interface.

When reseating of the interface is required, such as in the proposed application, interface stress levels must be lowered dependent upon the number of reseating cycles required, the amount of rubbing expected at the interface, and the materials to be used. In view of the leakage rate being primarily dependent upon the interface stresses, permissible leakage necessarily will be greater than for the strictly static seal interface designed for only one compression cycle. If no rubbing exists at the interface (e.g., the seal is lifted from the seat before rotation occurs), permissible interface stresses can exceed the elastic limit and some plastic deformation would be acceptable. If rubbing exists (e.g., the seal is lifted from the seat after rotation starts), the interface stress levels must be below the elastic limit and the permissible stress levels further depend upon the amount of rubbing that occurs during the desired life of the seal.

Aerojet has extensive test experience with poppet seals, which are similar to the lift-off seal but without the rubbing. It has been demonstrated that by exercising a judicious selection of the seal and seat materials, the permissible stress levels for 300 to 500 duty cycles can be sufficient to maintain leakage rates below 1.0×10^{-3} cc/sec/in. of interface length. This represents an attainable "zero leakage" value for the non-rubbing, externally-actuated, lift-off seal designs.

The permissible interface stress levels for self-energized lift-off seal designs with some rubbing are limited by the wear characteristics of the selected seat and seal materials; therefore, leakage will be somewhat predetermined. This is discussed in greater detail in subsequent sections. Preliminary predicted values range from 1.0×10^{-3} cc/sec/in. of circumference to as high as 20 cc/sec/in. of circumference depending upon the nosepiece configuration and the materials used. The leakage value of 1.0 std cc/sec (approximately 0.06 cc/sec/in. of circumference for the seal size under consideration) established during Task I as the program goal (see Section III,A) would appear to be attainable by selecting the proper nosepiece material, geometry, loading and the over-all seal configuration.

B. NOSEPIECE DESIGN CRITERIA

1. Non-Rubbing Static Seals

The basic requirement for a static seal is plastic flow of the gasket material to fill the asperities of the mating surfaces to the extent necessary to satisfy the allowable leakage of the system fluid at all operating and environmental conditions. These requirements differ significantly from those of the elastic loading required for rubbing seals. Absolute "zero leakage" across the interface can be attained only when plastic flow of the gasket has occurred to provide complete conformity with the mating surface asperities. If this conformity of the mating surfaces is not disturbed during operation, "zero leakage" will be maintained. However, from a practical aspect, perfect conformity at the interface is nearly impossible to attain initially and is even more difficult to maintain during operation. This is subsequently amplified. If the gasket must be reused, as required in the proposed application, either the mating surfaces must seat precisely in the same position each time or the load must be increased to reform the gasket to an essentially new interface.

Investigations (Ref. 2) wherein various shaped wedges were impressed against a flat plate established that the best combination of load interface contact area and deformation as well as the lowest leakage is obtained with a soft 60 degree angle wedge against a hard plate (see Figure No. 18). Data obtained during these investigations are shown on Figures No. 19, No. 20, and No. 21.

An angular or cylindrically-shaped nosepiece mated against a flat plate has an inherent advantage over a flat nosepiece shape. The flat nosepiece requires perfect axial and angular alignment (parallelism) between the two interfaces to obtain a deformed interface equal to the length of the flat. Conversely, wedge or cylindrially-shaped nosepieces tend to form the interface parallel to the flat plate without perfect axial alignment and result in less perfect angular alignment depending upon the stiffness of the nosepiece. The interface stresses of the angular wedge are extremely high. Also, they are usually equal to the compressive strength in the plastic range. Thus, the radial width of the interface (contact area/in.) is a function of the load. The same advantages result from the use of a small radius cylindrical wedge; however, as the radius increases, elastic stresses become more predominant because the stress concentration factor decreases and the load/area relationship becomes less linear. When the radius becomes infinite (flat nosepiece), the area remains constant with load and the stress increases from zero until the compressive elastic limit is reached. At this point, the material flows normal to the load and the contact area increases nonlinearly.

Aerojet experience in the design of static seals has shown that the practical limit for the seal interface width is approximately 0.020-in. Other investigators (Ref. 2) have reported that a minimum width as low as 0.012-in. was practical for good sealing. Studies undertaken during

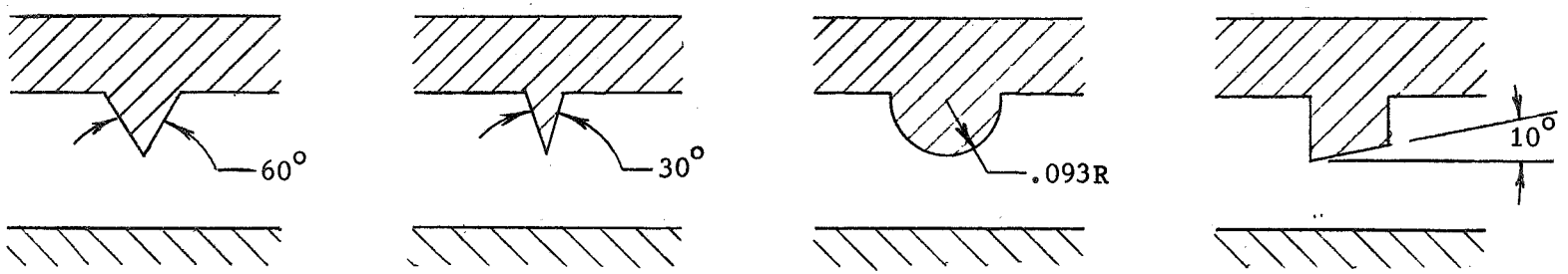

INITIAL SHAPE

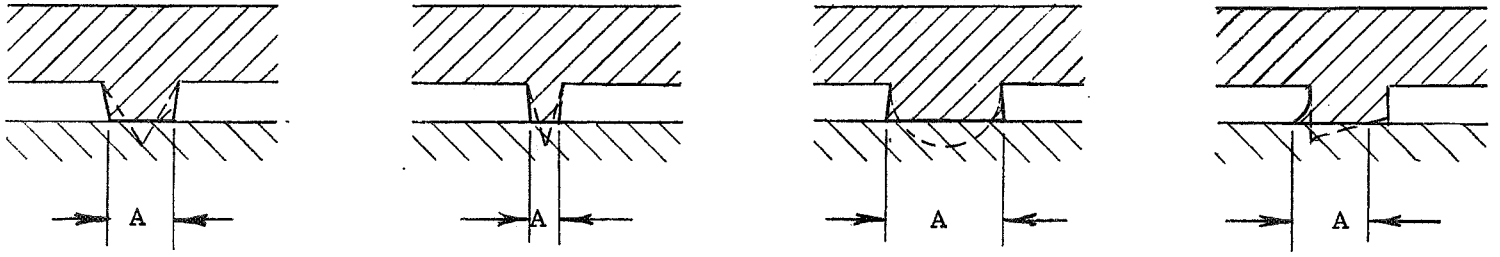

DEFORMED SHAPE

Figure 18. Wedge Configurations

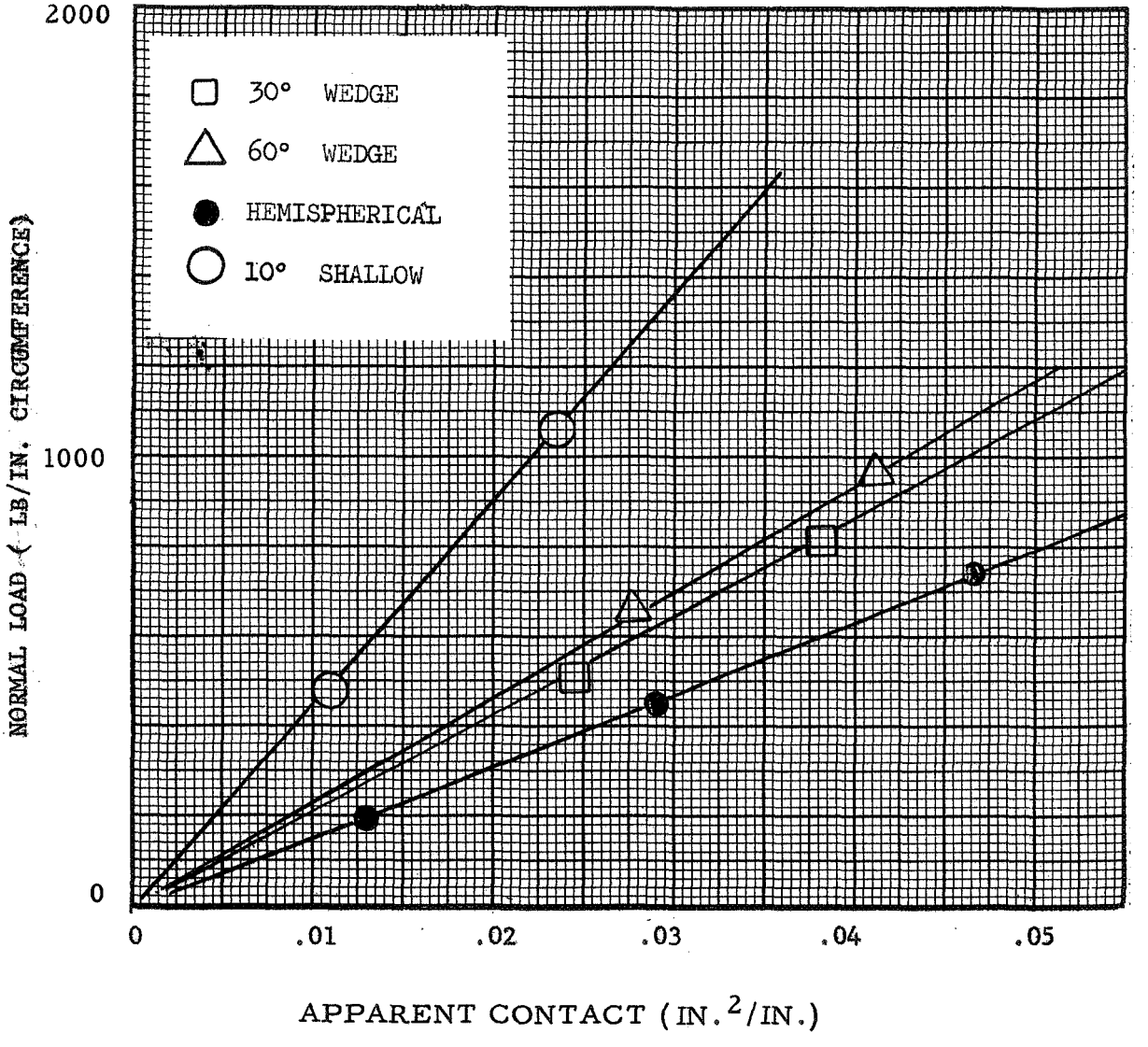

Figure 19. Apparent Area-Load Relationship for an 1100-0 Aluminum Wedge on an 1141 Flat Steel Surface (Plastic Wedge Case)

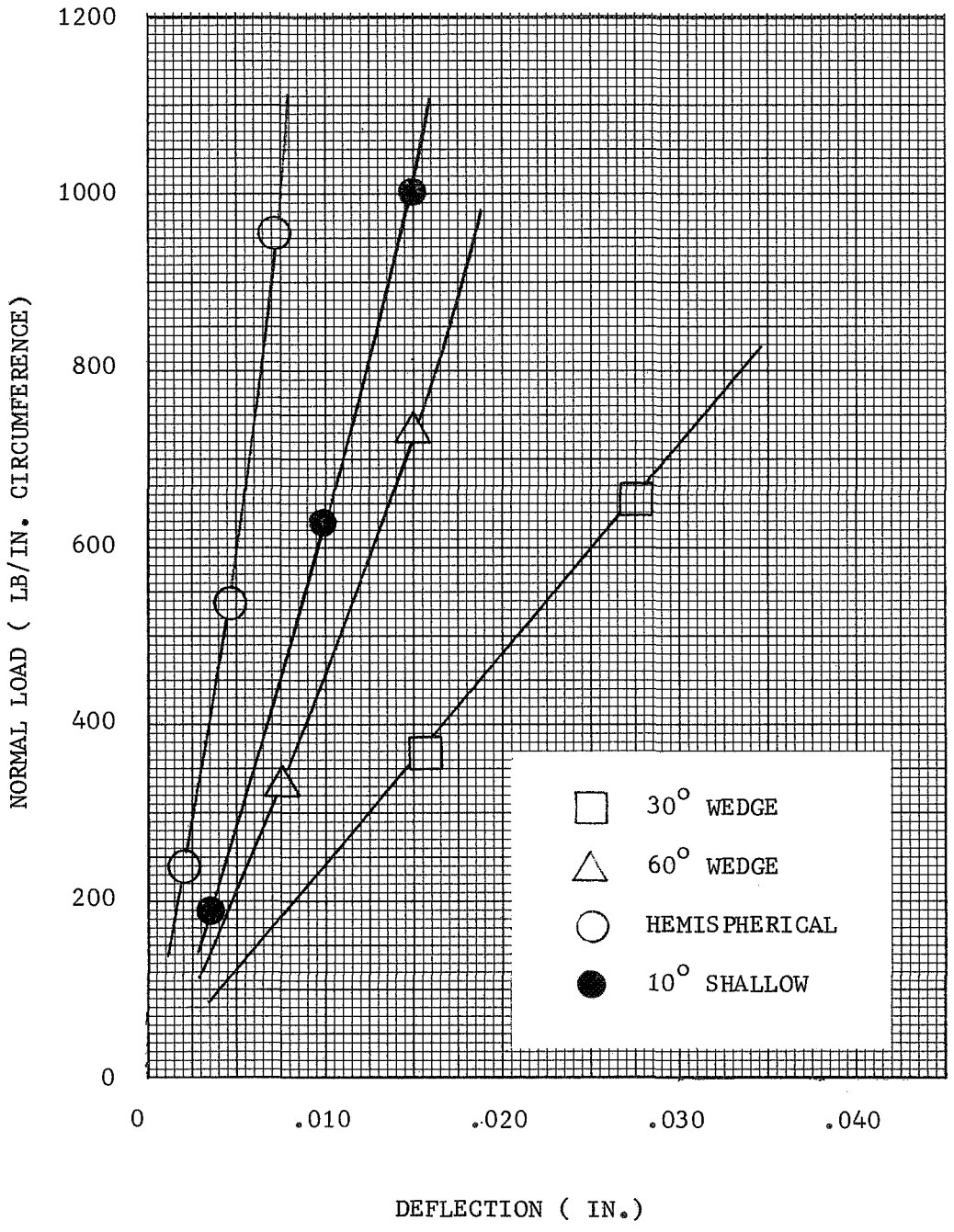

Figure 20. Load-Deflection Characteristics of an 1100-0 Aluminum Wedge on an 1141 Flat Steel Surface (Plastic Wedge Case) (Ref 2)

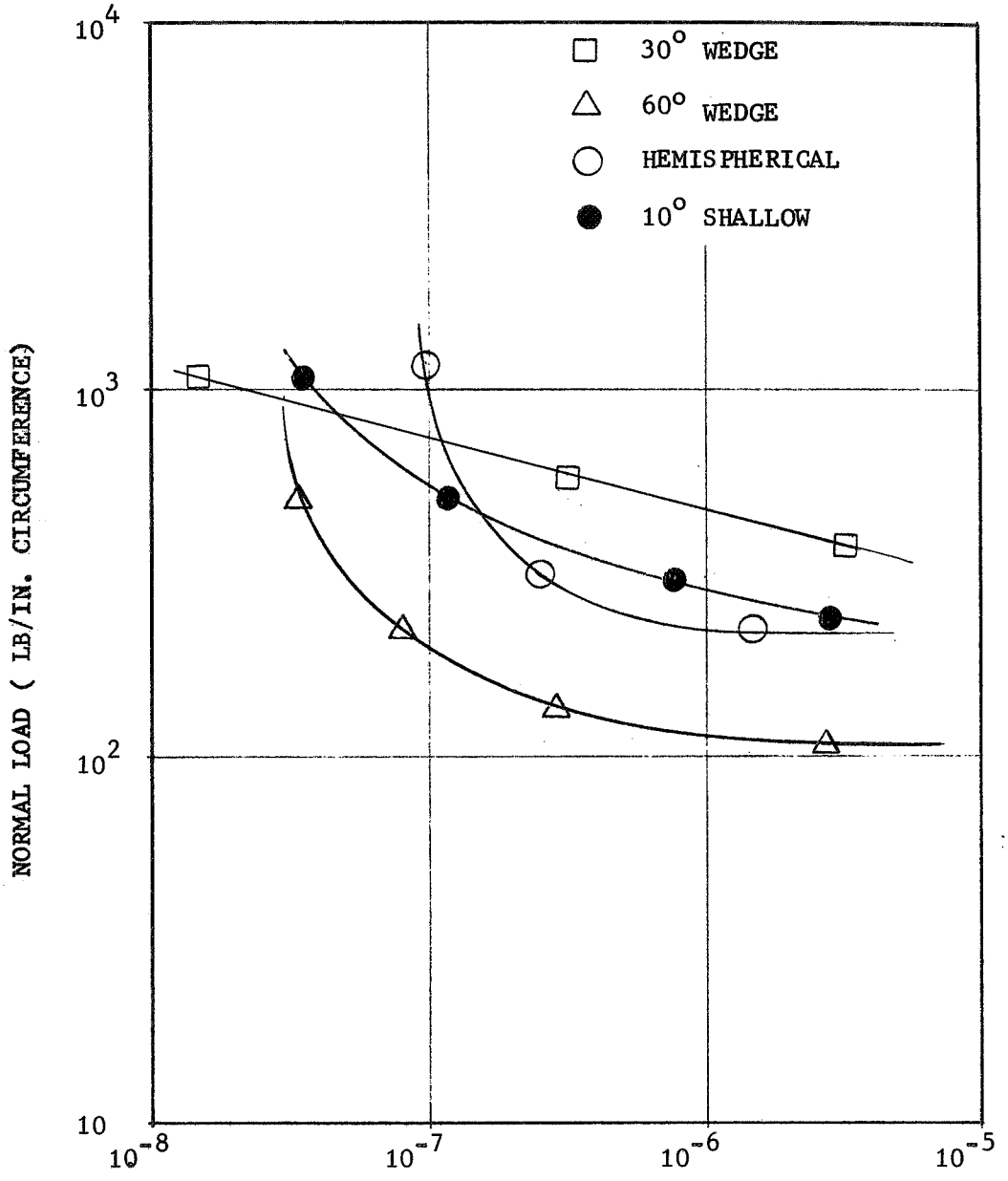

Figure 21. Leakage-Load Characteristics for the Plastic Wedge Case (Ref 2)

the conceptual design phase, Task I, established 0.040-in. as a desirable seal interface width for this specific application. The load required to gain this width with the wedge shapes shown on Figure No. 18 is a function of the compressive yield (hardness) of the wedge material.

The best material for obtaining initial static sealing would be one that provides the largest deformed contact area with the smallest load. However, other considerations eliminate many of the prospective materials. While elastomers would provide the best conformation at ambient temperature, they become brittle at low temperatures and would shatter during lift-off cycling. In addition, elastomers shrink more rapidly during cooling than the metallic seal holder and severe thermal hoop stresses are induced. Plastic materials (i.e., Teflon and Kel-F) also are relatively brittle at liquid hydrogen temperatures. Although differential contractions remain a problem with the plastics, generally they are not as severe as those characteristic of elastomers. Plastic flow (creep) under load at ambient temperature (cold flow) has been used to advantage for some seal designs utilizing the plastics. Various types and particle sizes of filler materials also have been molded into the plastics to reduce the cold flow problem. Glass fabric and particles are the most commonly used filler materials, but metal-filled and graphite-filled Teflon also have been manufactured for some applications.

The selection of metallic materials for the nosepiece is limited by the hardness of the mating surface. Good static sealing requires that the hardness of the seal material be less than one-half the hardness of the mating surface (Ref. 2) to eliminate significant deformation of the mating surface. In addition, some metals creep under load while others work-harden with deformation. Any advantage to be derived from creep in this application is questionable because the sealing load can be held constant over a relatively large deformation range with some designs. However, work hardening is definitely a disadvantage because it requires an increase in load at each reseating cycle to maintain the same interface conformity and leakage rate. If the reseating load remains constant, there is increased leakage with each cycle. The greater the work-hardening tendency of a material, the greater is the leakage.

Transfer characteristics between metal-to-metal interface materials as a result of galling during cycling or seating is another important parameter to be considered. Although this condition more appropriately applies when rubbing occurs at the interface, transfer can take place without rubbing if interface stresses are high. This implies that the nosepiece also should have a low susceptibility of material transfer with the mating (running ring) surface (Ref. 3). Assuming that no transfer of material takes place with each reseating cycle, the leakage would decrease with each cycle and become relatively constant after the material stabilizes.

Candidate nosepiece materials are shown on Table I. This selection provides a broad range of seal material hardness (Meyer hardness from $\sim$4000 psi to 420,000 psi) and strain hardening characteristics (Meyer

TABLE I

CANDIDATE NOSEPIECE AND RUNNING-RING MATERIALS

LEGEND:

		Nosepiece Configuration			Running Ring Configuration			
F	Q_L	Material	Microharness (K_g/mm^2)	Modulus (x 10^6 psi) *	Mat'l	Hardness	Modulus	Surface Finish
(1)	[1]	65% Bronze filled TFE	42	.1	347 CRES Annealed	H_m = 150 K_g/mm^2	27 x 10^6 psi	All flat circular rings with 5/8-in PTV surface finish.
(2)	[2]	Zytel 101 Nylon	76	.47				
(3)	[3]	25% Glass fibre filled TFE	20	.08				
(4)	[4]	TFE-7 Teflon	16	.06				
(5)	[5]	FEP-100	16	.06				
6								
7								
8								
(9)	[9]	ETP Copper (as rolled)	76	17	347 CRES Work Hardened (Rc-20)	Hm=252 K_g/mm^2	27 x 10^6 psi	
(10)	[10]	Hard Silver	93	10				
(11)	[11]	Hard Platinum	92	24				
(12)	[12]	Zirconium (Annealed)	68	14				
(13)	[13]	Zinc(Rolled)	44	13				
(14)	[14]	Hard Gold	72	12				
(15)	[15]	Lead Base Babbit	21	4.2				
(16)	[16]	1100-0 Alum	23	10.6				
17								
18								
19								
(20)	[20]	Ti-6Al-4V Annealed	296	16	Sintered Carbide (K60A)	Hm= 750 K_g/mm^2	88 x 10^6 psi	
(21)	[21]	Berrylium Copper-Hard	199	19				
(22)	[22]	Zirconium (Hard)	158	14				
(23)	[23]	Phosphor Bronze (1/2 Hd)	128	16				
(24)	[24]	Molybdenum	191	47				
(25)	[25]	ZK60A-F Magnesium	77	6.5				
(26)	[26]	7075-T6 Alum	160	10.3				
(27)	[27]	Tantalum (Annealed)	103	27				
(28)	[28]	A-Nickel (Rolled)	110	30				
(29)	[29]	Monel (Rolled)	150	24.5				
(30)	[30]	6061-T6 Alum	97	9.9				
(31)	[31]	347 CRES Annealed	150	27				
(32)	[32]	304L CRES Annealed	124	27				

* Modulus of elasticity in compression.

Index ∿2.1 to 2.8) for investigation. The required seal loading varies because of the hardness of the material and leakage should vary with cycling depending upon the strain hardening and cold flow or creep characteristics. All of the materials shown are less than one-half the hardness of the mating ring surface. The susceptibility to transfer material with the interface varies from very low with the Teflon to relatively high with 300 Series CRES (based upon room temperature property data).

Two different basic nosepiece shapes were considered for investigation; a 60-degree angular wedge and a large radius cylindrical wedge. The 60-degree wedge was considered to have the best sealing potential, but the wear rate might be greater for this configuration. The large radius wedge offered better wear characteristics, but would permit higher leakage flow for a given load. These configurations are shown on Figure No. 22.

Calculated load-contact area relationships for several nosepiece shapes are shown on Figure No. 23, using phosphor bronze as the wedge material. The curve for the 60-degree wedge and the small radius (0.050-in. diameter) cylindrical wedge are based upon the assumption that a condition of constant average stress occurs at the interface as the wedge is deformed (Ref. 2). This implies plastic flow of the seal material or

$$P/A' = S_n = \text{constant for a given material} \qquad \text{Eq. (1)}$$

where:

P = Applied load (lb/in.)

A' = Apparent contact area ($in.^2/in.$)

S_n = Average normal stress (psi)

The average normal stress is related to Meyer hardness, σ_m, by:

$$S_n = C\sigma_m,$$

where C is a constant that depends upon the wedge geometry and is approximately 0.5 for the 60-degree wedge and approximately 0.8 for the small radius wedge.

The Hertz formula for the maximum stress imposed by pressing a cylinder against a flat plate was used in calculating the maximum stress in the wedge, up to the compressive yield strength of the wedge material:

$$(S_c)_{max} = 0.798 \sqrt{\frac{P}{D\left[\frac{1-v_1^2}{E_1} + \frac{1-v_2^2}{E_2}\right]}} \qquad \text{Eq. (2)}$$

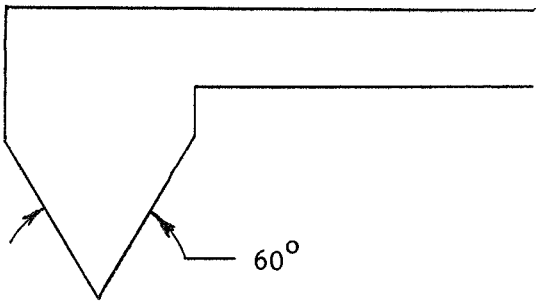

60° ANGLE WEDGE

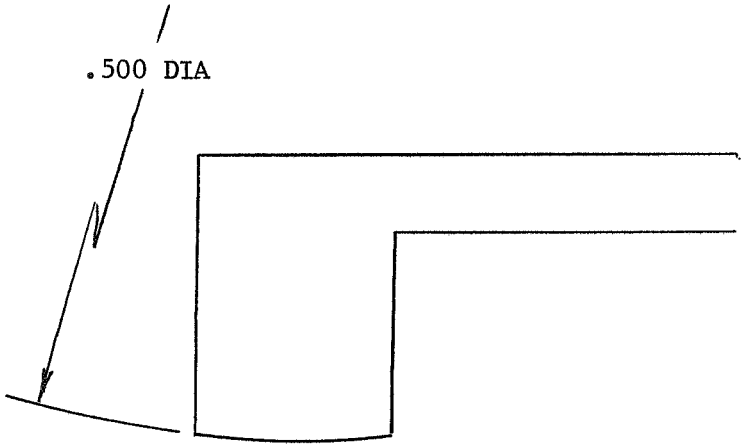

LARGE RADIUS CYLINDRICAL WEDGE

Figure 22. Nosepiece Configurations Selected for Investigation

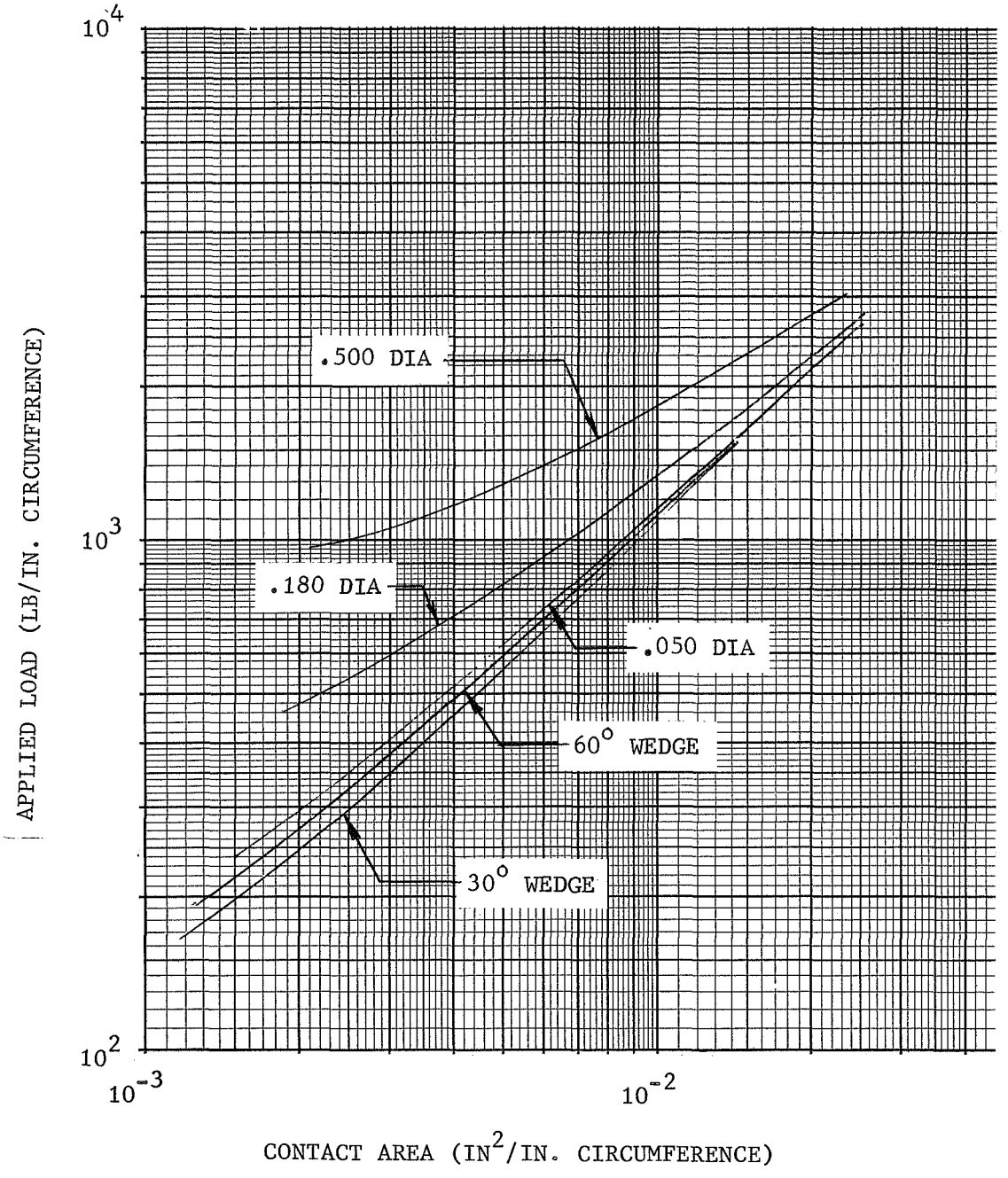

Figure 23. Calculated Load-Area Relationships for Phosphor Bronze Wedges

where:

$(S_c)_{max}$ = Maximum compressive stress induced by pressing the cylinder against the plate ($lb/in.^2$)

D = Diameter of the cylindrical wedge (in.)

v_1 and v_2 = Poisson's ratio for the seal and running ring, respectively.

E_1 and E_2 = Young's modulus of the seal and running ring, respectively (psi)

P = Applied load per inch of seal circumference, (lb/in.)

The load at which the induced compressive stress equals the compressive strength of the seal is calculated from:

$$P_{CRIT} = \left[\frac{\sigma_m}{0.798}\right] \quad D \left[\frac{1-v_1^2}{E_1} + \frac{1-v_2^2}{E_2}\right], \qquad \text{Eq. (3)}$$

where:

σ_m = Meyer hardness of the nosepiece material (psi).

Load-area relationships were calculated using the integral:

$$P = \int_{-b}^{b} S_c \, dx. \qquad \text{Eq. (4)}$$

where:

S_c = Compressive stress at any point along the contact interface.

For an applied load (P) less than the critical load (P_{CRIT}), a parabolic stress distribution over the contact is assumed as shown on Figure No. 24(a).

$$S_c = (S_c)_{max} \left[1 - \left(\frac{x}{b}\right)\right]^2 \qquad \text{Eq. (5)}$$

Substituting Equation (5) into Equation (4), the relationship

$$P = (S_c)_{max} \int_{-b}^{b} \left[1 - \left(\frac{x}{b}\right)\right]^2 dx$$

or

$$P = \frac{2}{3} (S_c)_{max} \cdot 2b$$

is obtained.

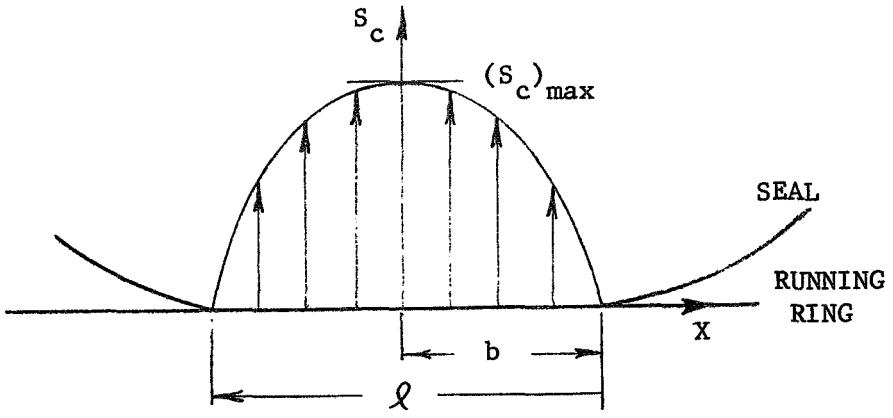

a. $P \leq P_{CRIT}$

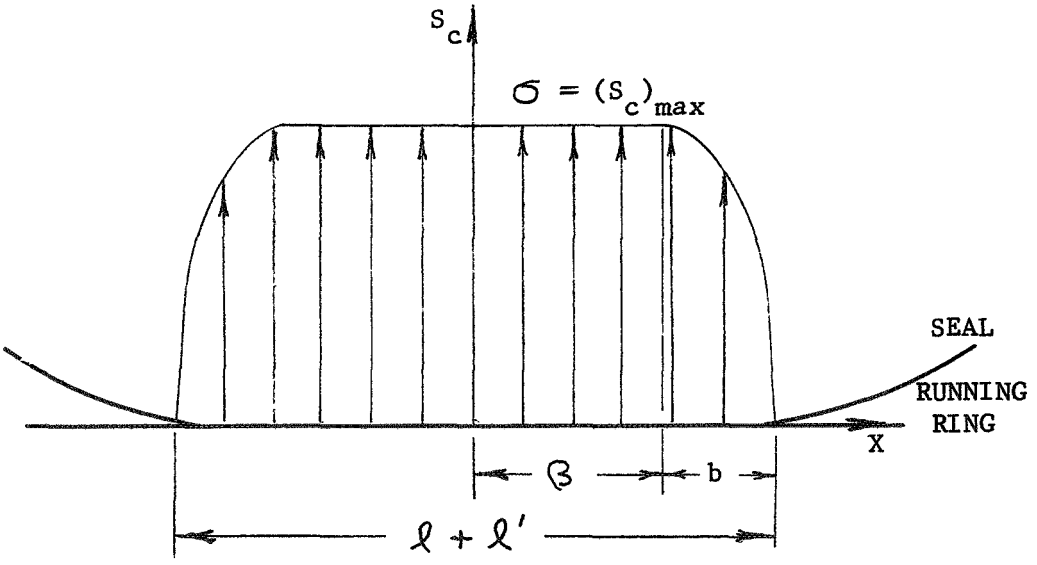

b. $P > P_{CRIT}$

Figure 24. Nosepiece Stress Distribution

Since $2b = \ell$

$$P = \frac{2}{3} (S_c)_{max} \ell \qquad \text{Eq. (6)}$$

This relationship holds for $(S_c)_{max} \leq \sigma_m$. The contact length is an elastic deformation. Then

$$P_{CRIT} = \frac{2}{3} (\sigma_m)$$

For an applied load (P) greater than the critical load (P_{CRIT}), the parabolic stress distribution flattens at the compressive yield strength of the material as shown on Figure No. 24(b). The stress parabola then is displaced outward in the x-direction.

$$P = \int_{-(b+\beta)}^{b+\beta} S_c \, d_x$$

$$P = \int_{\beta}^{\beta+b} S_c \, dx = \int_{-\beta}^{\beta} S_c \, dx + \int_{-(\beta+b)}^{-\beta} S_c \, dx$$

$$P = \frac{2}{3} \sigma_m b + \sigma_m \cdot 2\beta + \frac{2}{3} \sigma_m b$$

$$P = \frac{2}{3} \sigma_m \ell + \sigma_m \cdot 2\beta$$

$2\beta = \ell'$ and $\frac{2}{3} \sigma_c \ell = P_{CRIT}$, so

$$P = P_{CRIT} + \sigma_c \ell' \qquad \text{Eq. (7)}$$

where:

ℓ' = Plastically deformed contact width, in.

= A' = Apparent contact area, ($in.^2$/in. of seal circumference)

This plastically-deformed contact width is, in essence, the width of the leak path through which any leakage must pass. In this plastically-deformed contact area, the stress level in the seal is close to the Meyer hardness of the material. Thus, the seal flows plastically in this area and conforms to any asperities in the surface of the running ring. Also, the surface contact in this area is quite close and forms the major resistance to

fluid leakage in the eleastically-deformed region. The stress level is somewhat less than the Meyer hardness of the seal and the contact between the seal and running-ring is less intimate in this region. Therefore, there is less resistance in the leak path in this region.

To develop the load-area relationships for the various materials and configurations being considered, PCRIT was first calculated for each seal material and diameter using Equation (2). The ℓ' was calculated from Equation (7) as a function of the applied load, P.

Initial leakage rate values were estimated by a method presented by Bauer (Ref. 2), assuming a sufficient applied load to obtain a 0.012-in. and a 0.020-in. sealing width. These values are shown on Table II and the basic formula is:

$$Q_L = \frac{(Pi^2 - Po^2)a}{24\ \bar{\mu}\ po\ell'} \quad (h^3) \quad \left[1 + 6.39\ \varepsilon \frac{\bar{\lambda}}{\bar{h}}\right] \qquad \text{Eq. (8)}$$

where:

Q_L = Leakage flow across the interface (in.^{3}/sec)

Pi = Internal (or high) pressure (psia)

Po = External (or low) pressure (psia)

$\bar{\mu}$ = Viscosity of the fluid at the temperature and pressure being analyzed (Reyns - lb/sec/in.^{2})

a = Length of the interface normal to flow (in.)

ℓ' = Width of the sealing interface in the direction of flow (in.)

h^3 = Flow conductance parameter (in.^{3}) = the cube of the equivalent channel clearance between the interfaces.

ε = Correction factor for gases (0.9 for a single gas)

$\bar{h}$ = Equivalent channel clearance (or height) (in.)

$\bar{\lambda}$ = Mean molecular free path of the gas at temperature being analyzed and a mean pressure = $(P_i + P_o)/2$

Equation (8) provides for flow in the laminar, transition, and molecular flow modes. The first part of the equation is essentially the viscous flow equation and the term $(1 + 6.39\ \varepsilon\ \bar{\lambda}/h)$ is a modified molecular flow correction factor. When this term is essentially equal to 1 (i.e., $\bar{\lambda}/\bar{h} < 0.01$), viscous laminar flow predominates and will produce the largest

TABLE II. - ESTIMATED INITIAL LEAK RATES AND SEAL LOADS REQUIRED FOR PLASTICALLY DEFORMED NOSEPIECES

Nosepiece Configuration	Materials	Teflon		65% Bronze-filled Teflon		Phosphor Bronze		347 CRES	
	Contact Area, A' $In.^2/in.$	.012	.020	.012	.020	.012	.020	.012	.020
	Leak Rate, Q_L $cc/sec/in. \times 10^6$	141	8.6	141	8.6	141	8.6	141	8.6
60° Wedge 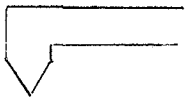	Applied Load, P Required, lb/in.	58.5	87.0	169	240	1330	2160	2850	4700
Small Radius 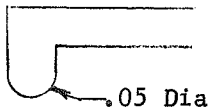		61.0	93.0	186	262	1350	2160	3000	4700
Large Radius 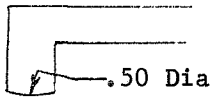		220	250	790	880	2050	2750	4800	6250

leakage flow. Between the values of approximately 1 and 7 (i.e., $\bar{\lambda}/\bar{h}$ = 0.01 to 1.0), both laminar and molecular flow (transition flow mode) exists in the channel. Values above 7 (i.e., $\bar{\lambda}/\bar{h}$ > 1.0) indicate that the predominant flow mode is molecular.

Because the fluid, fluid pressure, and fluid temperature are known, the values for the fluid properties ($\bar{\mu}$ and $\bar{\lambda}$) can be determined;

Pi = 100 psia

Po = 14.7 psia

$\bar{\mu}$ = 5.44×10^{-9} lb-sec/in.^{2} at 59°R (Ref. 4)

$\bar{\mu}$ = 1.29×10^{-9} lb-sec/in.^{2} at (530°R) (Ref. 4)

Substituting these values in the flow equation and assuming a value of 1-in. for the circumference of w, the formula reduces to:

$$\bar{Q}_L = \frac{2.1\ (10^{10})(h^3) + 1.016\ (10^5)(h^2)}{\ell'}$$

at ambient temperature (530°R) and 100 psia, and

$$\bar{Q}_L = \frac{4.99\ (10^{10})(h^3) + 2.83\ (10^4)(h^2)}{\ell'}$$

at supercooled gas temperature (59°R) and 100 psia,
where

$\bar{Q}_L$ = leakage per inch of interface length (in.^{3}/sec/in. circumference)

The values for (h^3) depend upon the net applied load, apparent contact area, the Meyer Hardness (σ_m) and Meyer Index (n') of the seal material and the peak-to-valley (PTV) surface roughness of the harder interface material. Empirical values for h^3 have been derived (Ref. 2) from tests and are shown on Figure No. 25. This figure represents the data collected for surfaces lapped and polished to the peak-to-valley roughness (PTV) heights shown on the curves. The modified stress ratio must be initially calculated using the relationship:

$$R = \frac{\left(\frac{(P)}{\ell'}\right)^{2/n'}}{\sigma_m} = \frac{\left(\frac{(W)}{Aa}\right)^{2/n'}}{\sigma_m} \qquad \text{Eq. (9)}$$

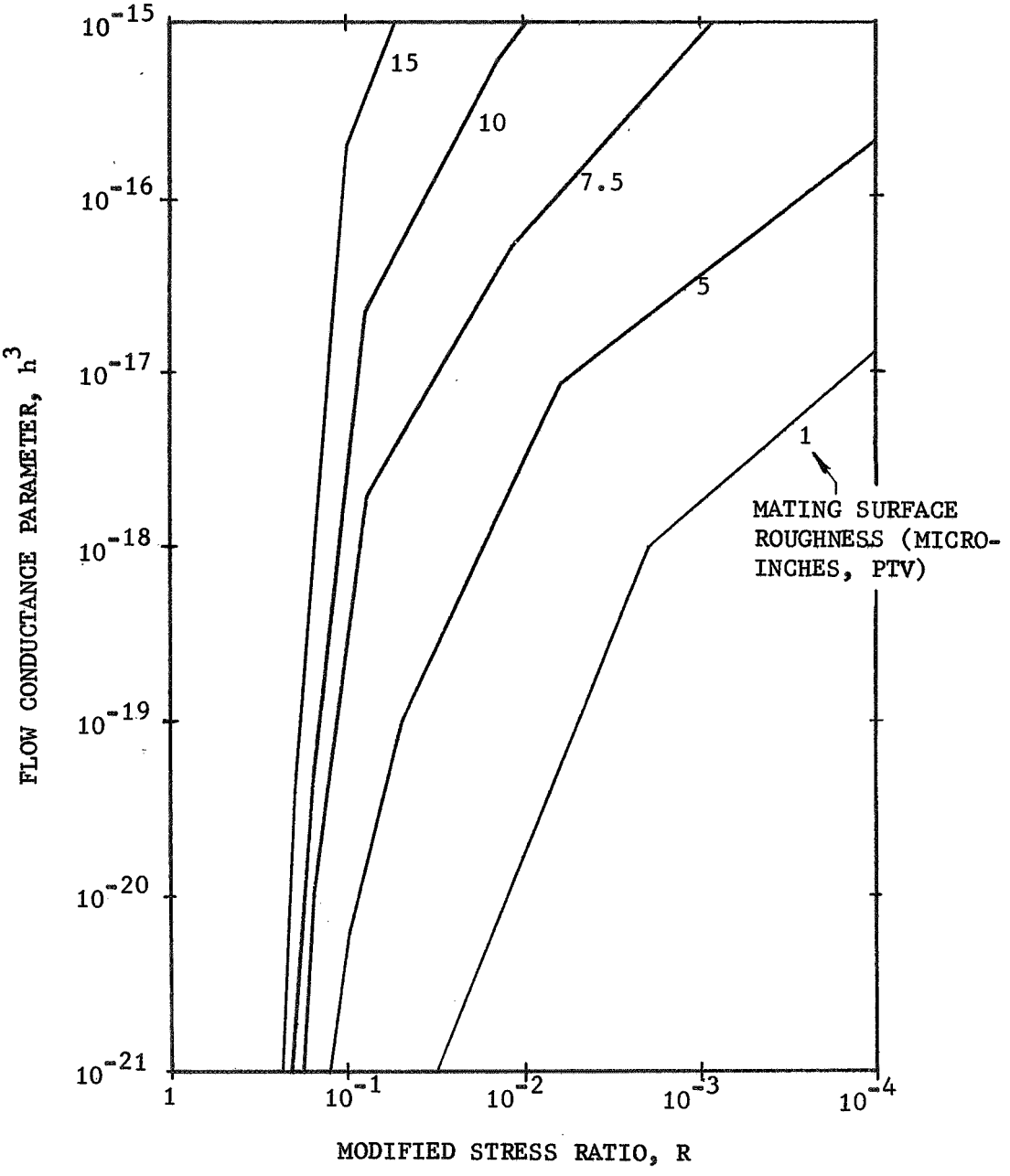

Figure 25. Design Criteria for Lapped and Polished Surfaces with Surface Roughness Shown as a Parameter (Ref 2)

where:

R = Modified stress ratio

W = The net applied load (lb)

Aa = Apparent contact area ($in.^2$)

n' = Meyer Index (hardenability) = 2.0 for most of the materials considered.

In this case, ℓ', the apparent contact width and P have been determined for the applied load per inch of seal. The selected values of ℓ' are 0.012-in. and/or 0.020-in., from which the required applied load can be determined using Figure No. 23, where phosphor bronze is the nosepiece material. Curves can be constructed in a similar manner for other candidate materials. Values for R in the plastically-deformed contact area were typically 0.3 to 0.5 for the materials considered. The larger values were obtained with the bigger diameter nosepieces. A modified stress ratio of 0.2 was conservatively selected for a PTV surface roughness of 10 microinches. It resulted in a value of 1.0×10^{-21} for h^3.

2. Static Seals with Rubbing

When rubbing occurs between the interface surfaces under load, the static sealing problem becomes highly complex. By definition, good sealing practices require that the intimate contact between mating surfaces be undisturbed to maintain the initial seal. Also, as previously explained, the best seal is attained when the gasket is compressed to a stress level above the yield (in the plastic range) of the material. However, for good wear, the interface stress levels must be in the elastic range of the materials and the permissible normal stress level is dependent upon the amount of rubbing that occurs during the desired life of the interface.

Extensive investigations (Ref. 5) have shown that the "zero-wear" life of the rubbing interfaces primarily depends upon the actual shear stress at the interface and the shear yield strength of the interface materials. The empirical relationship for "zero-wear" obtained from these investigations is:

$$S_s \leq \left[\frac{2000}{N}\right]^{1/9} GY, \qquad \text{Eq. (10)}$$

where:

S_s = The actual shear stress level at the interface (psi)

N = The number of passes experienced during the life of the interface and is related to the amount of rubbing experienced by each of the two surfaces.

G = A form of a stress concentration factor that depends upon the two materials and the lubricants used, if any, and is best determined by actual test.

Y = The yield point in shear of the materials used (psi)

For unlubricated interfaces, G can be only one of two values; 0.20 for interface material combinations with a high susceptibility to transfer, or 0.54 for interface material combinations with a low susceptibility to transfer.

The maximum permissible shear stress (S_s max) can be assumed equal to the value:

$$\left[\frac{2000}{N}\right]^{1/9} GY.$$

It can be calculated for various values of N if the value of G is known for the particular material combination. Values for "G" were taken from the referenced literature (Ref. 5), assuming the mating interface to be tungsten carbide hardfacing, while values for "Y" were either taken from the same source or estimated from the material hardness. These values are shown on Table III. The calculated maximum permissible shear stress at various values of N for a few representative candidate materials is shown on Figure No. 26.

TABLE III

VALUES USED FOR STRESS CONCENTRATION FACTOR "G" AND YIELD POINT "Y"

Nosepiece Material	G	Y (psi)
Teflon	0.54	3,000
65% Bronze-Filled Teflon	0.20	8,000
Phosphor Bronze	0.20	27,000
347 CRES	0.20	50,000

The maximum permissible normal stress, S_n, is related to the shear stress by:

$$S_{n(max)} = \frac{S_{s(max)}}{K\sqrt{1/4 + \mu^2}} \qquad \text{Eq. (11)}$$

where:

$S_{n(max)}$ = Maximum permissible normal stress (psi)

$S_{s(max)}$ = Maximum permissible shear stress previously calculated (psi)

K = Stress concentration factor

μ = Friction factor and is dependent upon the two materials in contact and the lubrication, if any.

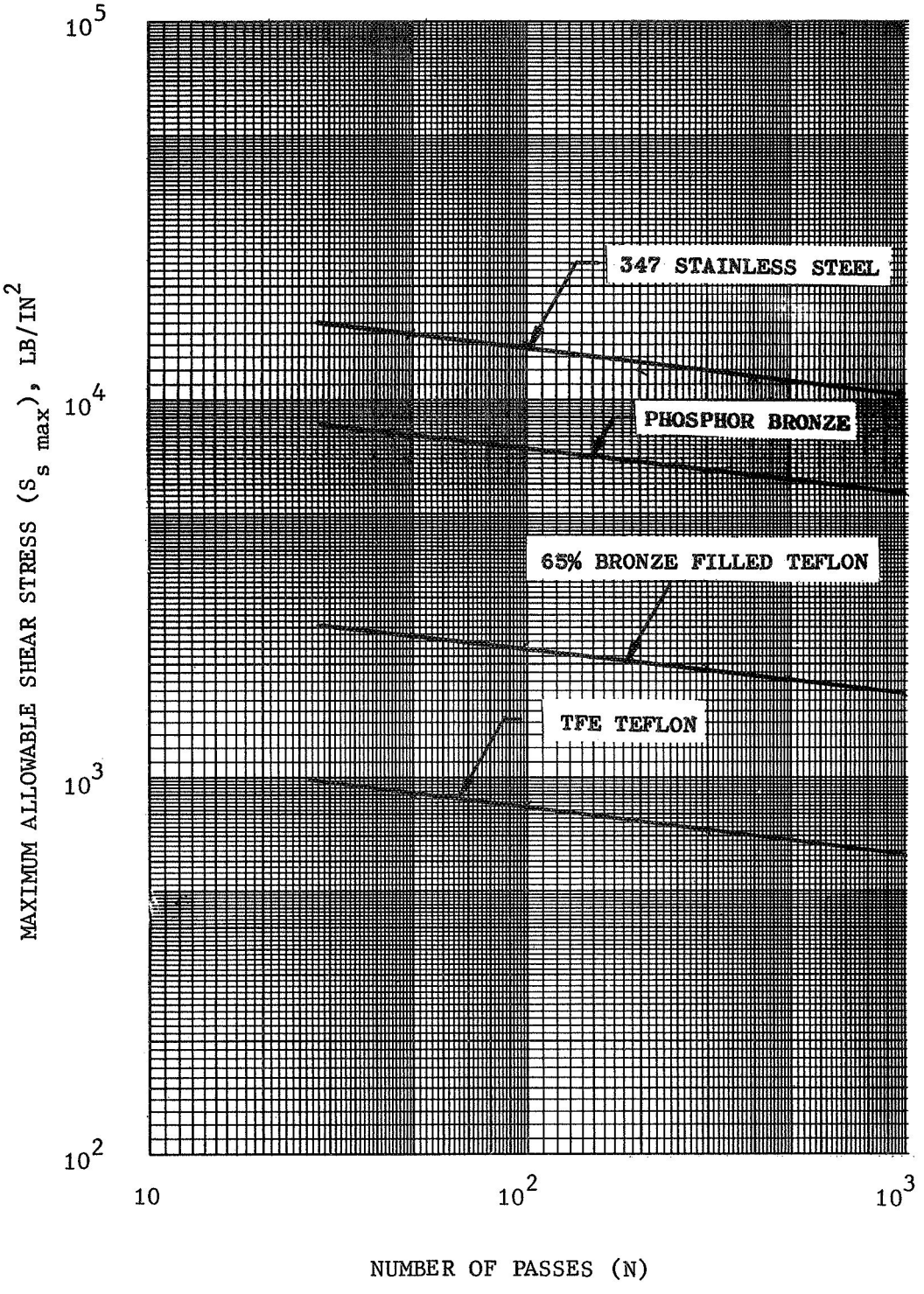

Figure 26. Calculated Maximum Allowable Shear Stress ($S_{s\ max}$) for Several Candidate Nosepiece Materials

The stress concentration factor, K, depends upon the sharpness of corners and edges in the direction of sliding (Ref. 5). For well-rounded corners, the value of K is approximately 2 while for sharp corners, it can be as high as 1000. The value of K is best determined by actual test, but preliminary estimates were made based upon data collected by McGregor (Ref. 5) and are shown on Table IV. The friction factor, μ, shown also was taken from the McGregor data.

TABLE IV

VALUES USED FOR STRESS CONCENTRATION FACTOR "K" AND FRICTION FACTOR "μ"

Nosepiece Material	Nosepiece Configuration	K	μ
Teflon	60-degree Wedge	200	0.09
	Small R Cylinder	50	
	Large R Cylinder	5	
65% Bronze-Filled Teflon	60-degree Wedge	200	0.03
	Small R Cylinder	50	
	Large R Cylinder	5	
Phosphor Bronze	60-degree Wedge	200	0.67
	Small R Cylinder	50	
	Large R Cylinder	5	
347 CRES	60-degree Wedge	200	1.00
	Small R Cylinder	50	
	Large R Cylinder	5	

The width of the interface, ℓ, is estimated from the modified Hertz stress equation (Ref. 5) for the cylinders against a flat plate using the relationship:

$$\ell = 3.56 \, (S_n)_{max} \, D \left[\frac{1-v_1^2}{E_1} + \frac{1-v_2^2}{E_2} \right] \qquad \text{Eq. (12)}$$

where:

ℓ = Sealing edge width (in.)

$(S_n)_{max}$ = Maximum normal stress ($lb/in.^2$)

D = Diameter of the cylinder (in.)

v_1 and v_2 = Poisson's ratio for the nosepiece and the running-ring material, respectively.

E_1 and E_2 = Young's modulus of the nosepiece and the running-ring, respectively (psi).

Assuming that the normal applied load, P, is controlled by the stress level so that

$$S_n = \frac{P}{\ell} \text{ , then } P = S_n \ell$$

The values of "v" and "E" were taken from various references and are shown on Table V. The value of D for the 60-degree wedge nosepiece was assumed to be approximately 0.005-in. The calculated values of contact width, ℓ, are shown on Figure No. 27 for a 0.500-in. diameter nosepice and for the different materials under consideration. Theoretically, ℓ is proportional to D; therefore, the contact widths will be reduced an order of magnitude for the 0.050-in. diameter and two orders of magnitude for the 0.005-in. diameter.

TABLE V

VALUES USED FOR POISSON'S RATIO "v" AND YOUNG'S MODULUS "E"

Material	Poisson's Ratio (v)	Young's Modulus (E) psi
Teflon	0.35	5.7×10^4
65% Bronze-Filled Teflon	0.35	1.0×10^5
Phosphor Bronze	0.34	16×10^6
347 CRES	0.30	30×10^6
Tungsten Carbide	0.30	30×10^6

The permissible stress levels and the resultant sealing edge width are preset for a particular nosepiece configuration. Additionally, the materials that can be used are dictated by the desired (or designed) "zero-wear" life as defined by the number of passes. As a consequence, the leakage can be estimated from these preset conditions for a particular design number of passes (N'). Entering the value of N in the appropriate curve (such as Figure No. 26), the maximum allowable normal stress, $S_{n(max)}$ can be determined. With this value of $S_{n(max)}$, the seal leak path length, ℓ, is determined from Figure No. 27 while the applied load P, is determined from:

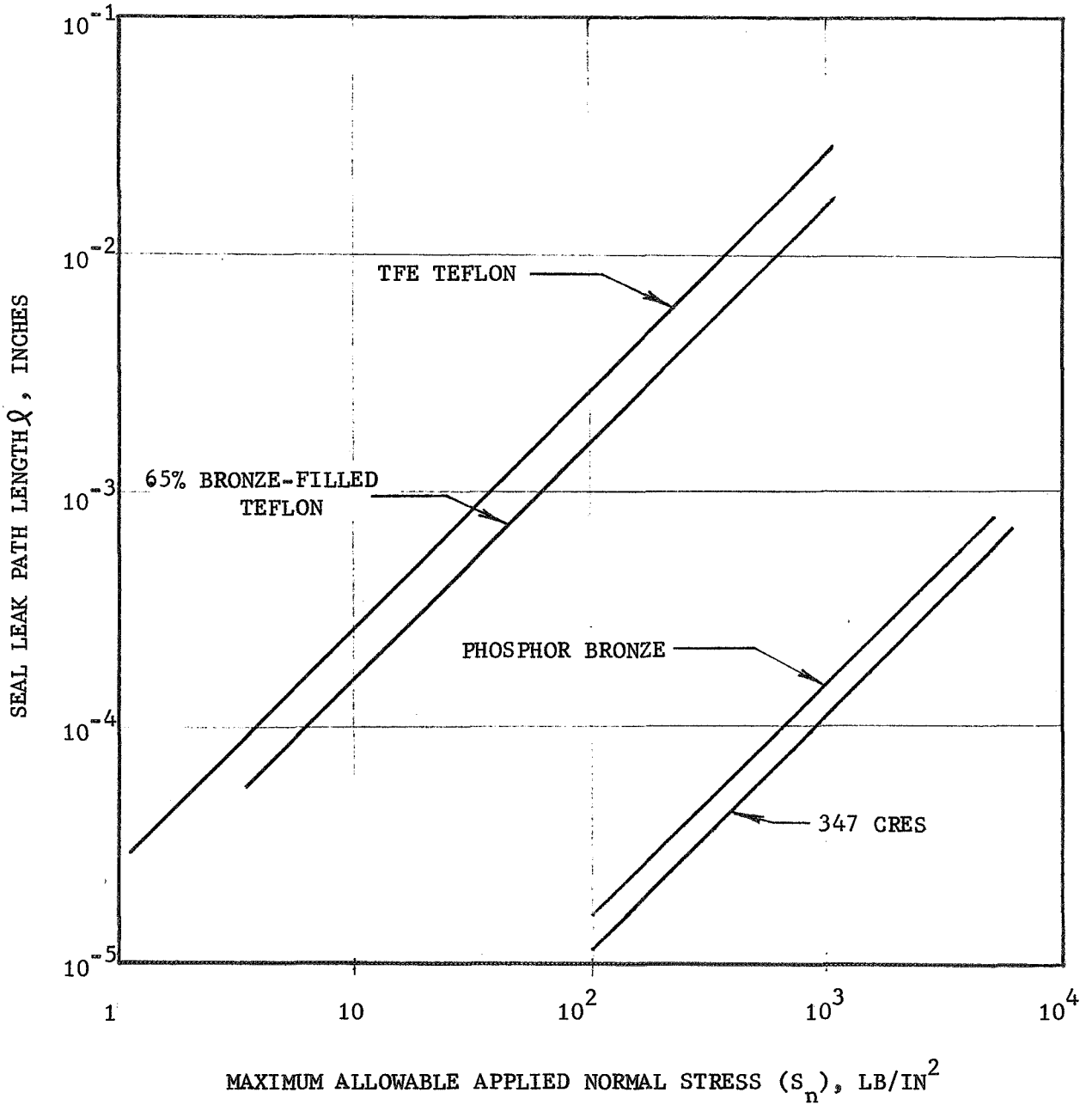

Figure 27. Calculated Seal Leak Path Length at Maximum Allowable Normal Stress for a 0.500 in. Diameter Nosepiece

$P = S_{n(max)}\ \ell$, for a particular seal life, N', and the modified stress ratio, R, as determined from Equation (9). A value for (h^3) is determined from Figure No. 25 and the leakage calculated from Equations (6) and (7). Typical leakage rate values for the large radius nosepieces which are needed to satisfy the requirements for design life (N') are plotted on Figure No. 28.

A number of conclusions can be drawn from these estimates. Firstly, the lowest leakage rates will be obtained for rubbing seals with large diameter cylindrical nosepieces because the permissible normal stresses (S_n) can be greater and, thus, the sealing edge width (ℓ) can be larger as the radius approaches infinity (i.e., two flat plates in perfect contact). Although the mating of two flat plates is not desirable from a practical aspect because such a seal presents extremely critical alignment problems, the design radius should be as large as possible within the limits of the permissible misalignment during assembly. Secondly, the Teflon (or bronze-filled Teflon) nosepiece has the best leakage rate capability, providing it will not shatter at the temperatures of liquid hydrogen. Although the permissible stress levels are much lower for the Teflon than the other materials having the same design life, the Teflon provides a wider leak path (ℓ) and a smaller equivalent interface channel height (h) at the lower normal stress and normal load values. If the cold flow and brittleness problems can be reduced within acceptable limits by utilizing fillers or applying design techniques, this material would be the best selection. This suggests the possibility of using the low modulus, low hardness metals (i.e., tin or silver), particularly in view of their susceptibility to transfer in contact with the tungsten carbide mating surface being potentially low (Ref. 6) (wear factor "G" potentially = 0.54). Also, these metals offer potential capabilities that are reasonably close to those of the Teflon without the problem of shattering.

Composite plots were made (Figures No. 29 and No. 30) of the calculated values of hydrogen leakage and "zero-wear" rubbing life to provide a more direct basis for comparing the various candidate materials and geometries considered for the lift-off seal nosepiece and running ring. These parameters were plotted as a function of the applied load for the materials listed on Table I. From these curves, it is theoretically possible to select the nosepiece material and interface geometry best suited for the application.

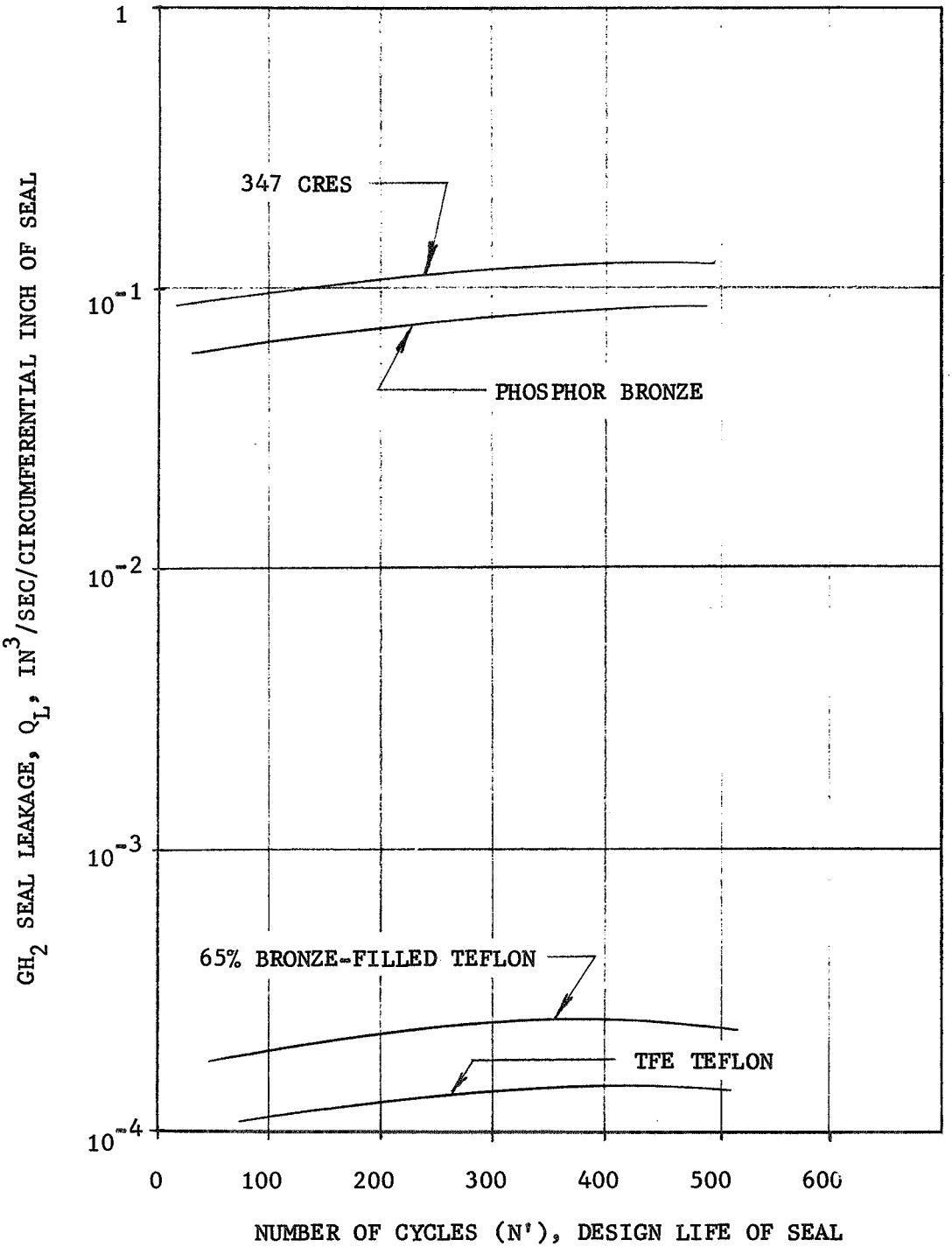

Figure 28. Calculated Leakage Rate for "Zero Wear" Design Life for a .500-in. Diameter Nosepiece

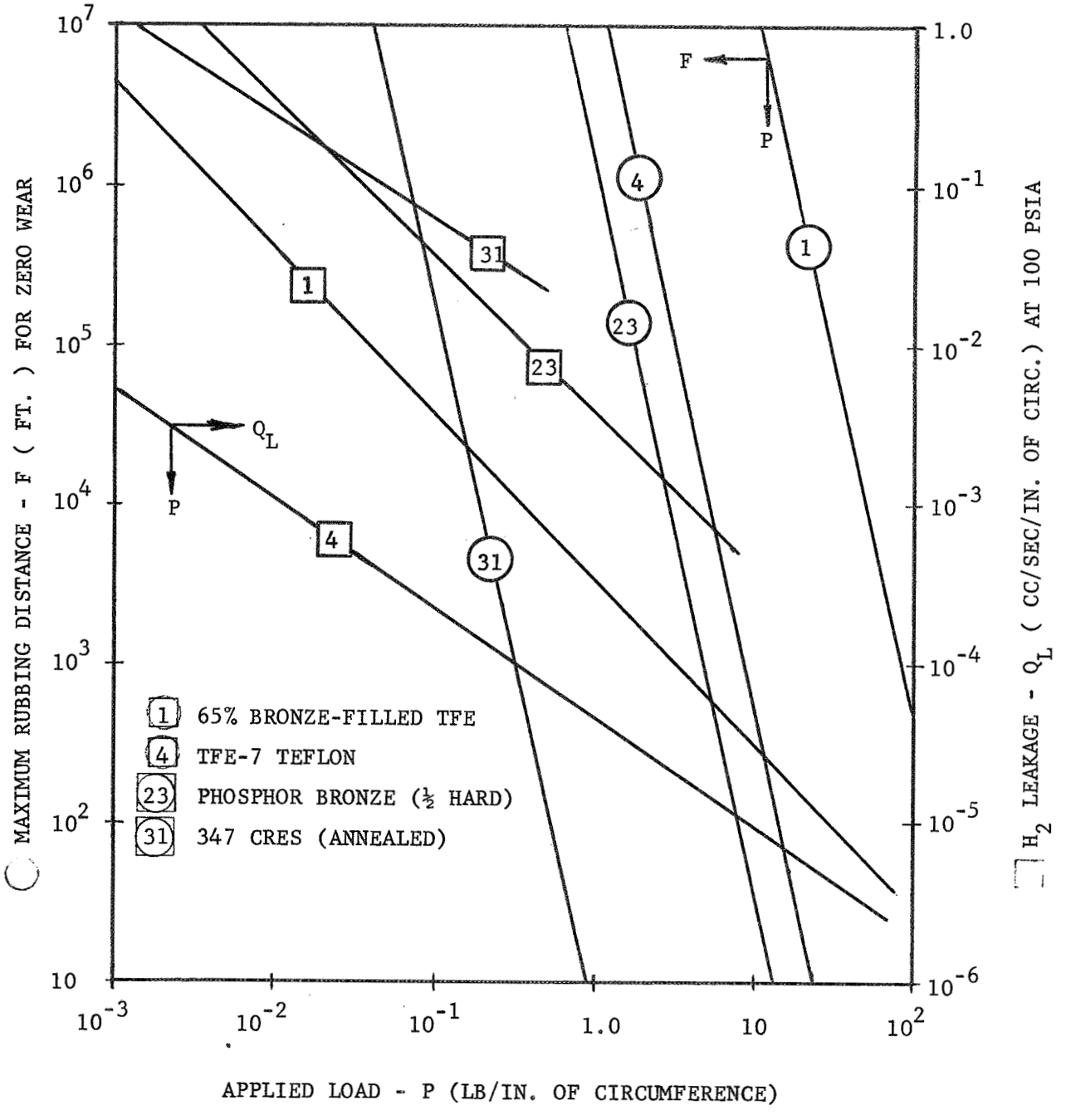

Figure 29. Load-Leakage-Life Relationships for Large Radius Nosepieces

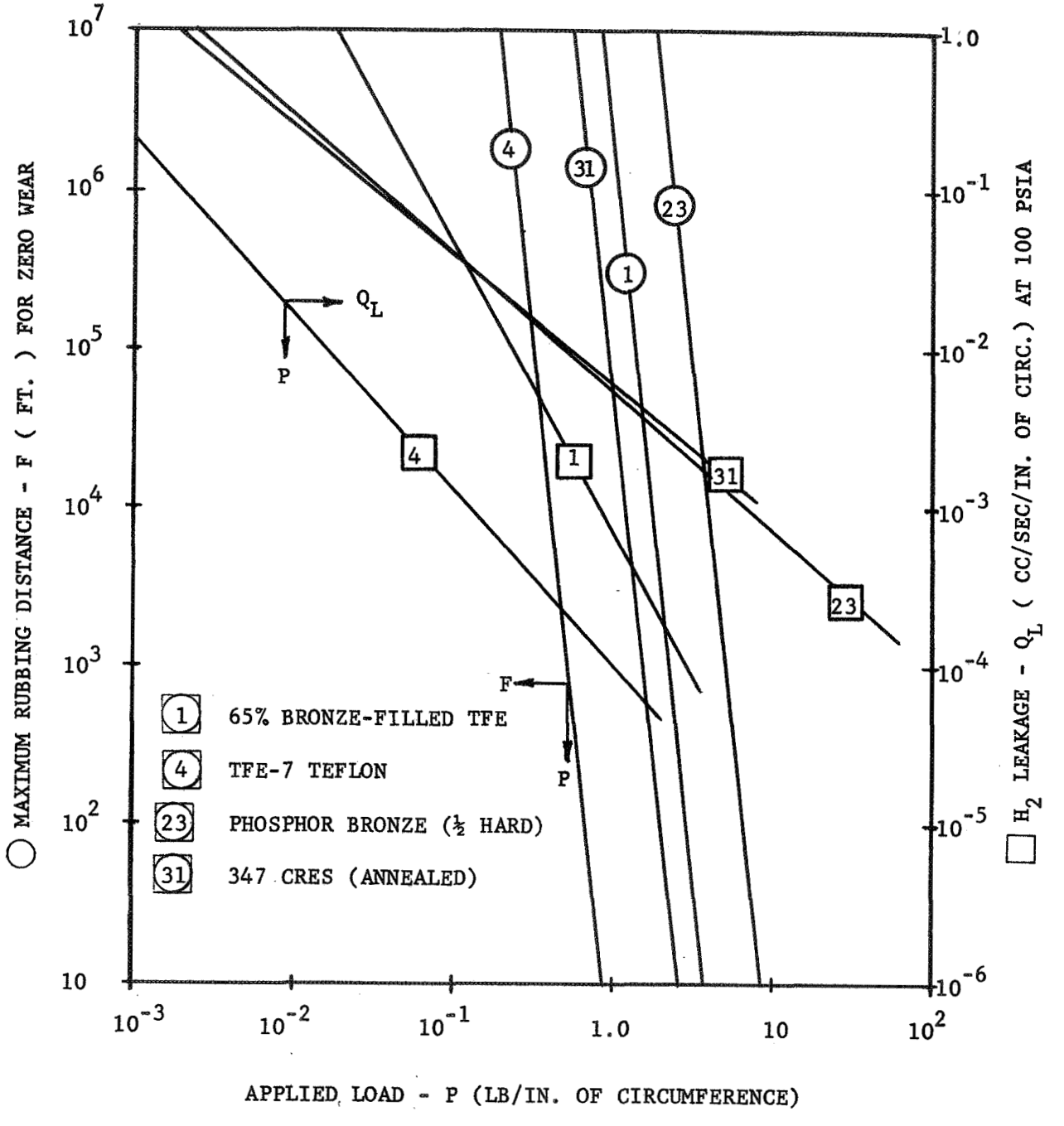

Figure 30. Load-Leakage-Life Relationships for Blunted 60 Degree Wedge Nosepieces

VI. HYDROMECHANICAL DESIGN AND FABRICATION

The original intention during Task I was to concentrate upon seal designs that would lift-off rapidly during the transient period so as to minimize or prevent rubbing of the surfaces. However, the load-leakage-life studies conducted in parallel with the preparation of the design concepts indicated that program goals ("zero" leakage and long life) could be achieved without any need for the type of complex seal actuating systems implied by the illustration on Figure No. 1.

At the conclusion of the Task I conceptual design effort, two of the lift-off seal configurations described in Section IV were selected for detail design and analysis. These concepts (Design "E", Figure No. 11, and Design "J", Figure No. 17) were pocketed hydrostatic face seals which differed primarily in the means used to achieve static sealing and to control interface rubbing during transient operation. Both of the selected concepts were subjected to rigorous hydraulic and mechanical analyses. Detail manufacturing drawings were prepared. They included all of the dimensional, material, and processing information necessary for fabricating all of the required components and assemblies.

A. EXTERNALLY-PRESSURIZED SEAL DESIGN

Initial parametric studies were conducted to determine the optimum face geometry using a hydrostatic bearing and seal computer model developed in a previous contract (Ref. 7). The 33 cases initially considered are shown on Figure No. 31. The nomenclature for these cases is described on the seal face schematic (Figure No. 32). The studies resulted in graphical presentations, similar to that of Figure No. 33, for steady-state operating load capacity, dynamic leakage flow, axial stiffness, torsional stiffness, and recess (pocket) pressures as a function of the running clearance between the seal face and the mating ring. The following final nominal face geometry was selected after successive iterations:

Number of Pockets - 12

Inner Exit Land Radius - 2.875-in.

Exit Land Width - 0.040-in.

Face Width - 0.525-in.

Orifice Diameter - 0.016-in.

Pocket Width - 0.100-in.

Inner Land Width - 0.350-in.

Inner Land Setback - 0.0003-in.

SUMMARY OF CASES

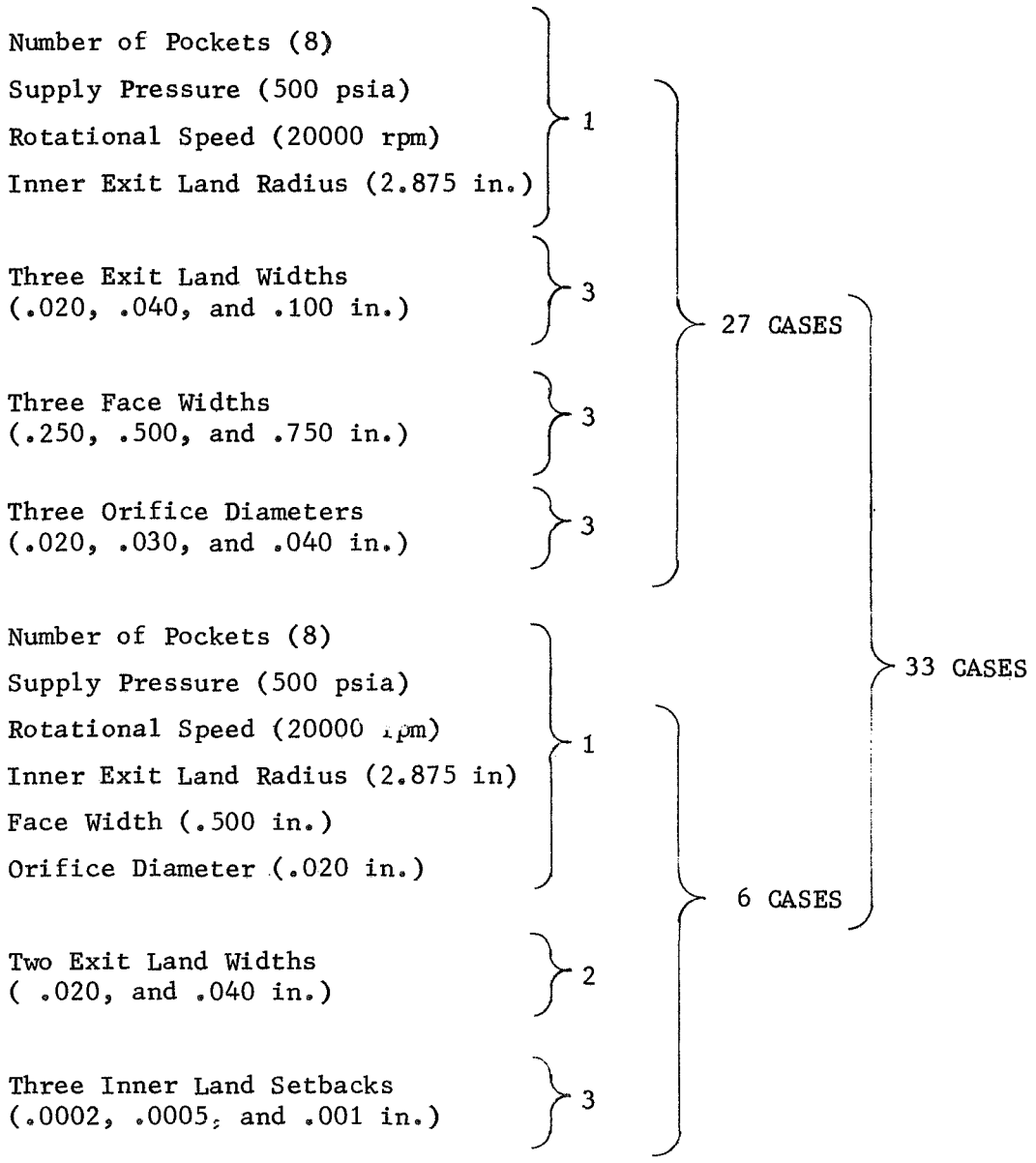

Figure 31. Externally Pressurized Lift-Off Seal Parametric Study Cases

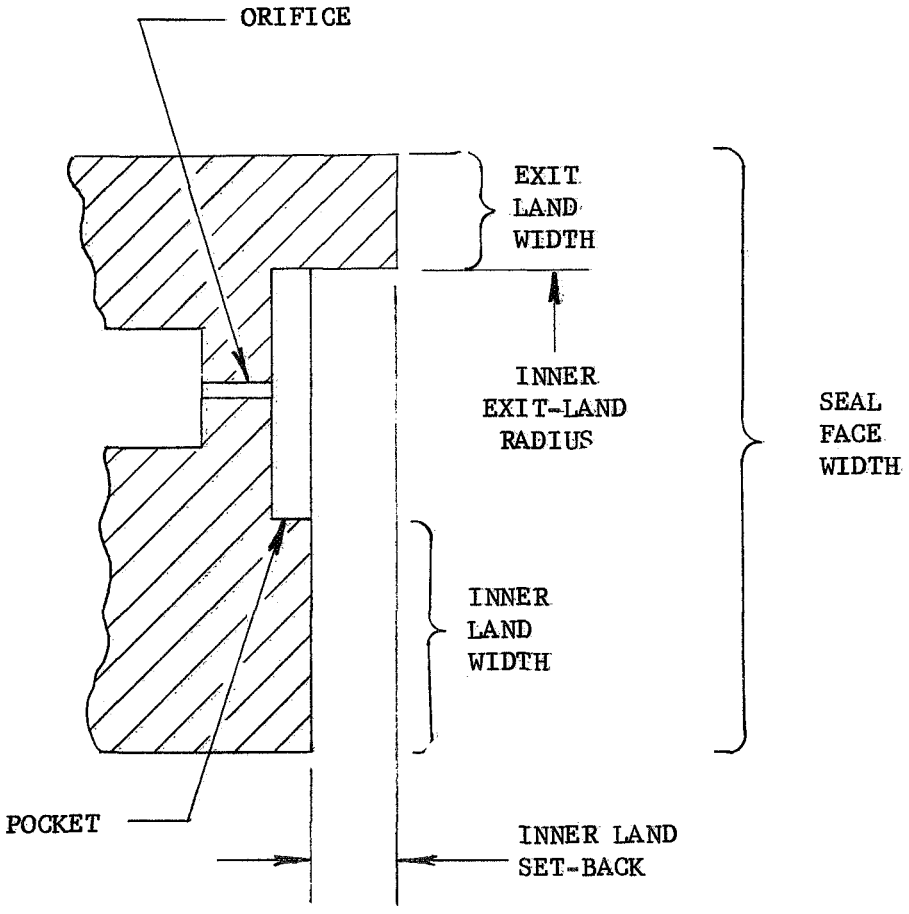

Figure 32. Seal Face Schematic

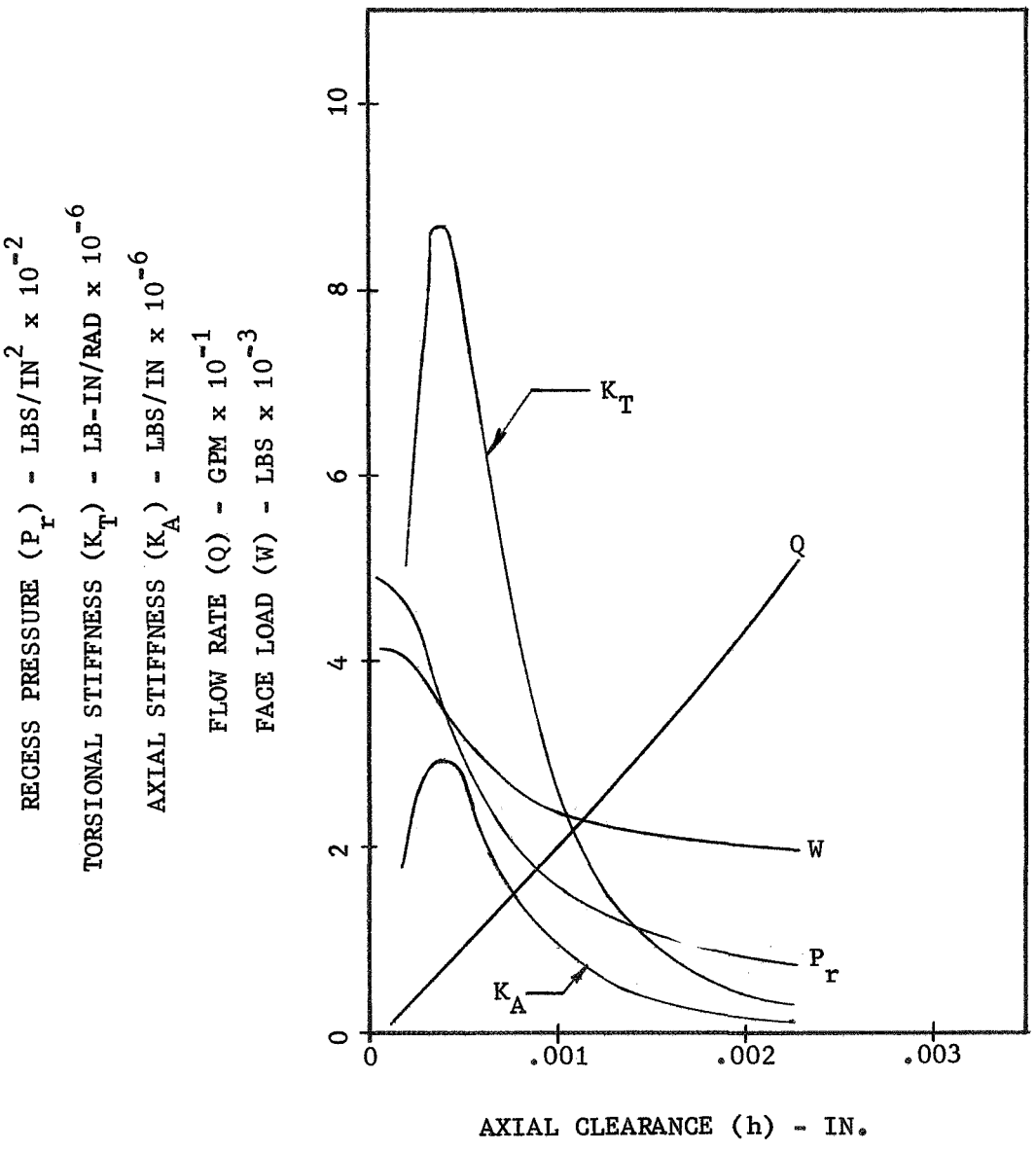

Figure 33. Estimated Seal Face Steady-State Performance Characteristics

The pockets, or recesses, for this design are 0.010-in. deep and equally-spaced on the seal face with 0.100-in. circumferential spacing between each pocket. The 0.040-in. wide exit land width and the extremely small (0.0003-in.) inner land setback was necessary to provide the required lip area for static sealing while maintaining a stable operating film between the inner land and mating ring. The design was arranged to include the sealing lip and the setback as a part of the softer mating ring to maintain a relatively uncluttered pocketed face.

Several concentric actuating bellows arrangements were considered. It was determined that a bellows chamber using a set of single convolution toroidal bellows, similar to one included on a seal for storable propellants (Ref. 7), would provide the optimum means for controlling the center of the forces on the back side of the seal face while experiencing little or no change in effective bellows area when pressurized.

The final design arrangement is shown on Figure No. 34. In this design, the stationary member of the seal is constructed entirely from age-hardened Inconel 718 with the contact face being flame-sprayed with tungsten carbide, followed by grinding and lapping to a 4 micro-inch finish. The bellows are 0.004-in. thick Inconel 718 hydroformed into the toroidal shape from a welded cylinder of sheet stock and then joined to the mating components. A bellows chamber area of approximately 4.6 $in.^2$ results from this design. The rotating ring shown, which has the 0.040-in. wide sealing nosepiece lapped to an average surface of 1 micro-inch and the 0.0003-in. setback for the seal inner land, is made of phosphor bronze (QQ-B-750, Composition A, Half-Hard). This material was selected after the material combinations shown on Figures No. 29 and No. 30 were compared for wear life and static sealing capabilities. The 0.040-in. wide flat seal sealing lip was selected to provide a contact surface which would lend itself to conventional manufacturing techniques. Lapping spherical surfaces, as would be necessary in a large radius nosepiece, and controlling the geometry of a 60 degree blunted conical nosepiece for application on a hydrostatic seal would have been extremely difficult because of the small nosepiece dictated by the inner land setback requirement.

The estimated seal operating curve of Figure No. 35, which includes the effect of running-ring rotation, shows that at the design conditions of 20,000 rpm and at a cavity pressure of 500 psia, the separation between the seal face and the nosepiece will be approximately 0.001-in. The operating line shown reflects the back side force resulting from pressurization of the bellows chamber. Under initial static conditions, the bellows chamber pressure (P_B) is greater than the 100 psia seal cavity pressure (P_C) so as to provide the sealing load needed to achieve "zero" leakage. During the start transient, when seal cavity pressure and shaft speed are increasing, the bellows chamber pressure is allowed to equalize with the seal cavity pressure and the running clearance will vary as indicated. Dynamic seal

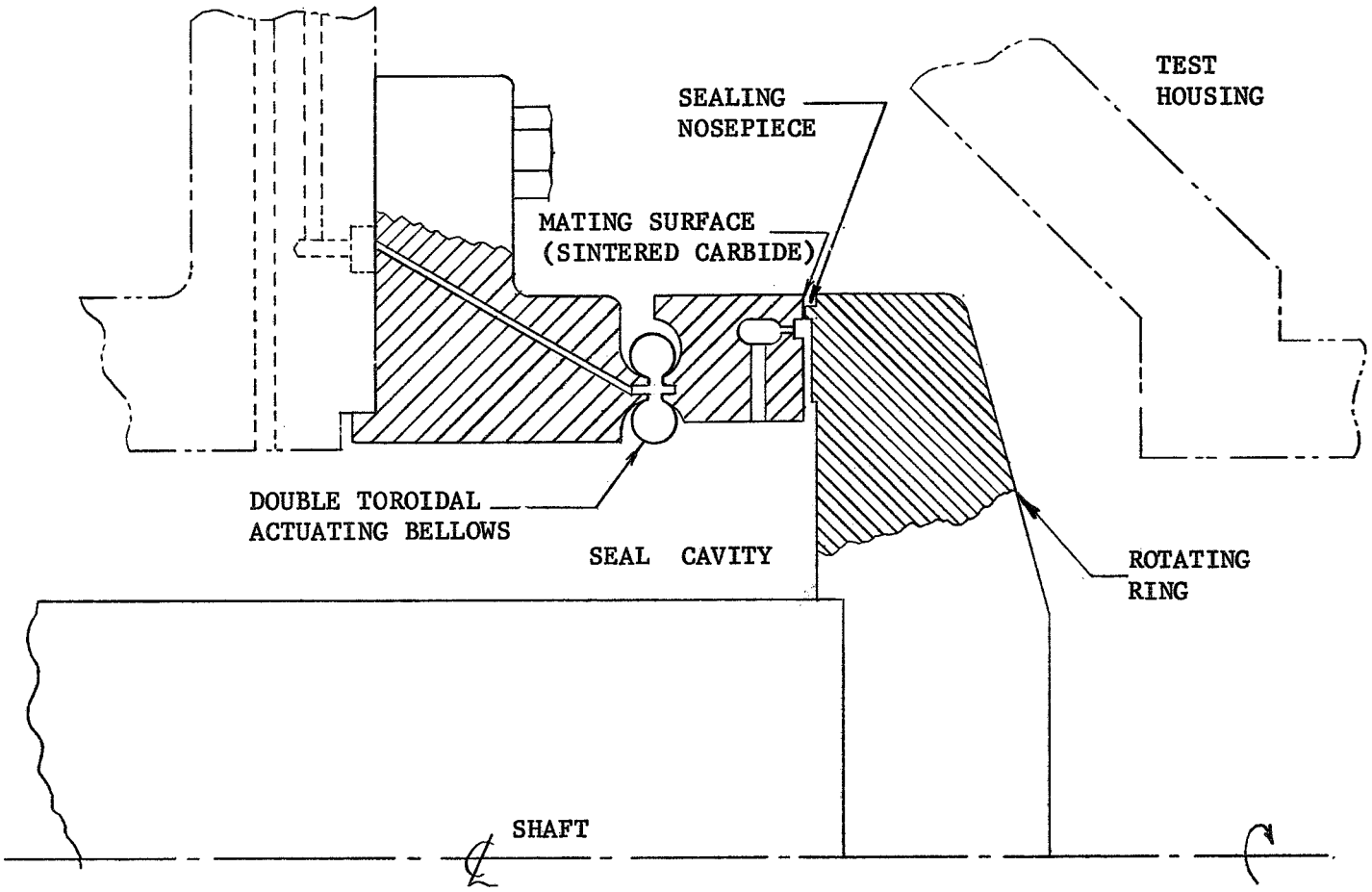

Figure 34. Externally Pressurized Hydrostatic Lift-Off Seal

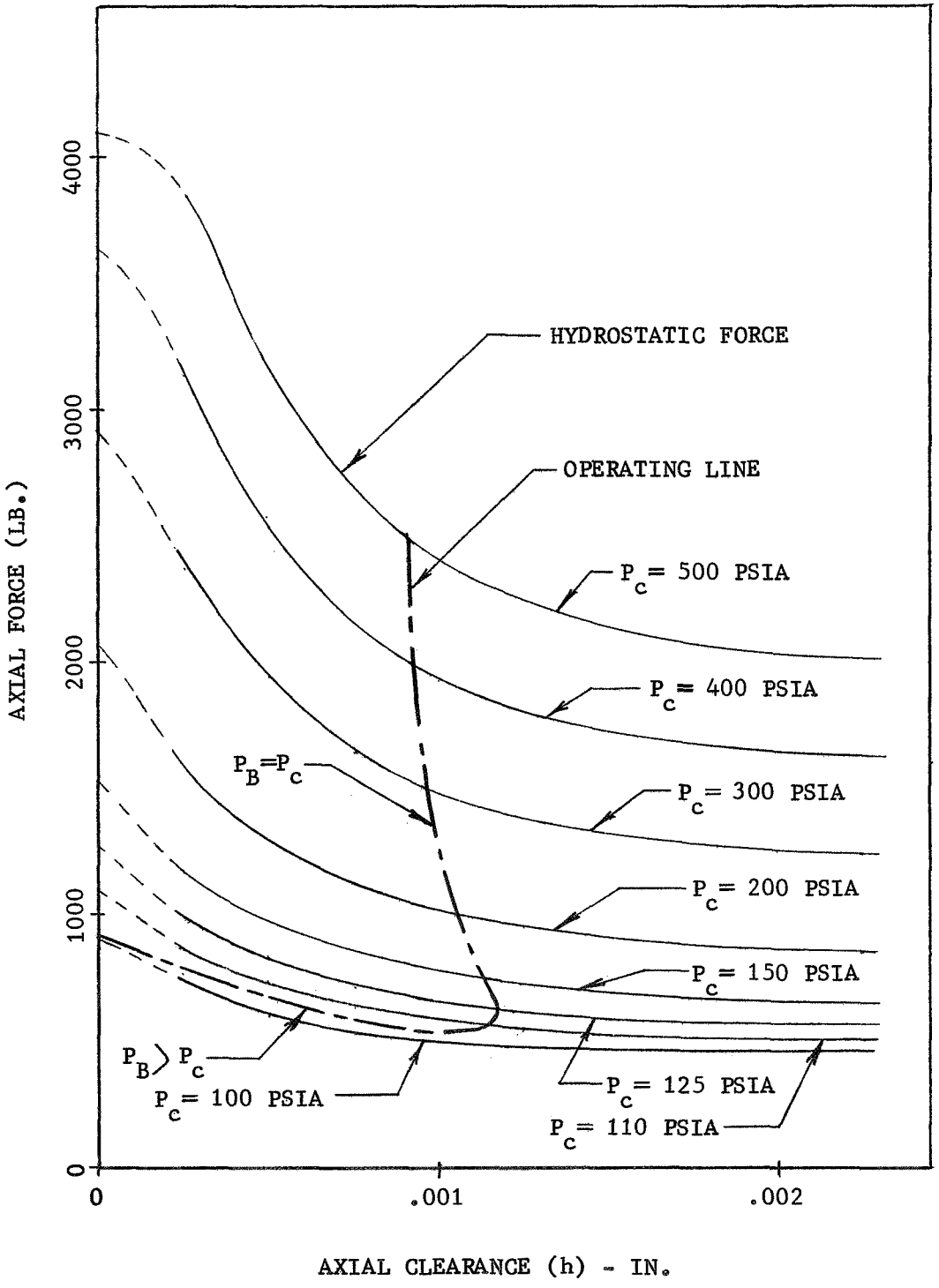

Figure 35. Externally Pressurized Hydrostatic Lift-Off Seal Estimated Operating Performance

leakage flow will vary during transient operation in a similar manner, as indicated by the curve on Figure No. 36. Maximum steady-state leakage flow at design conditions is estimated to be approximately 16 gpm.

B. SELF-ACTING SEAL DESIGN

A parametric study, similar to that discussed in Section V,A, was conducted to determine the face geometry requirements for the self-acting hydrostatic seal concept. The nominal face geometry selected for this design was:

Number of Pockets - 5

Inner Exit Land Radius - 2.875-in.

Exit Land Width - 0.040-in.

Face Width - 0.585-in.

Orifice Diameter - 0.022-in.

Pocket Width - 0.240-in.

Pocket Depth - 0.020-in.

Inner Land Width - 0.300-in.

Inner Land Setback - 0.0005-in.

This seal, as shown on Figure No. 37, was designed so that the pocketed face, the sealing lip, and the inner land setback are part of the softer stationary member, while the rotating ring is a hard-surfaced flat member. Initial static sealing for this design is achieved by pre-loading the bellows when installing the running-ring and by specifying a tight tolerance on the bellows spring rate during manufacture. The bellows spring rate and preload were dictated by the wear and sealing characteristics of the softer member, which is titanium alloyed with aluminum and vanadium (MIL-T-9047) for this design. The load-leakage-life charts (Figures No. 29 and No. 30) indicated that the titanium alloy should have a rubbing life and sealing capability comparable with the phosphor bronze selected for the design discussed in Section VI,A. The basic materials used for this seal were Inconel 750 for the mounting flange and bellows, with a Hastelloy B transition ring between the bellows and the titanium alloy seal face body. The transition ring was included to overcome fabrication problems associated with the joining of a Inconel 750 bellows to the titanium body. For this purpose, the bellows was to be welded to the transition ring, which, in turn, would be diffusion-bonded to the titanium. The running-ring is Inconel 750 with the rubbing surface flame-sprayed with tungsten carbide.

The estimated performance curve on Figure No. 38 shows that this seal design (which relies solely upon bellows pre-load, bellows spring rate,

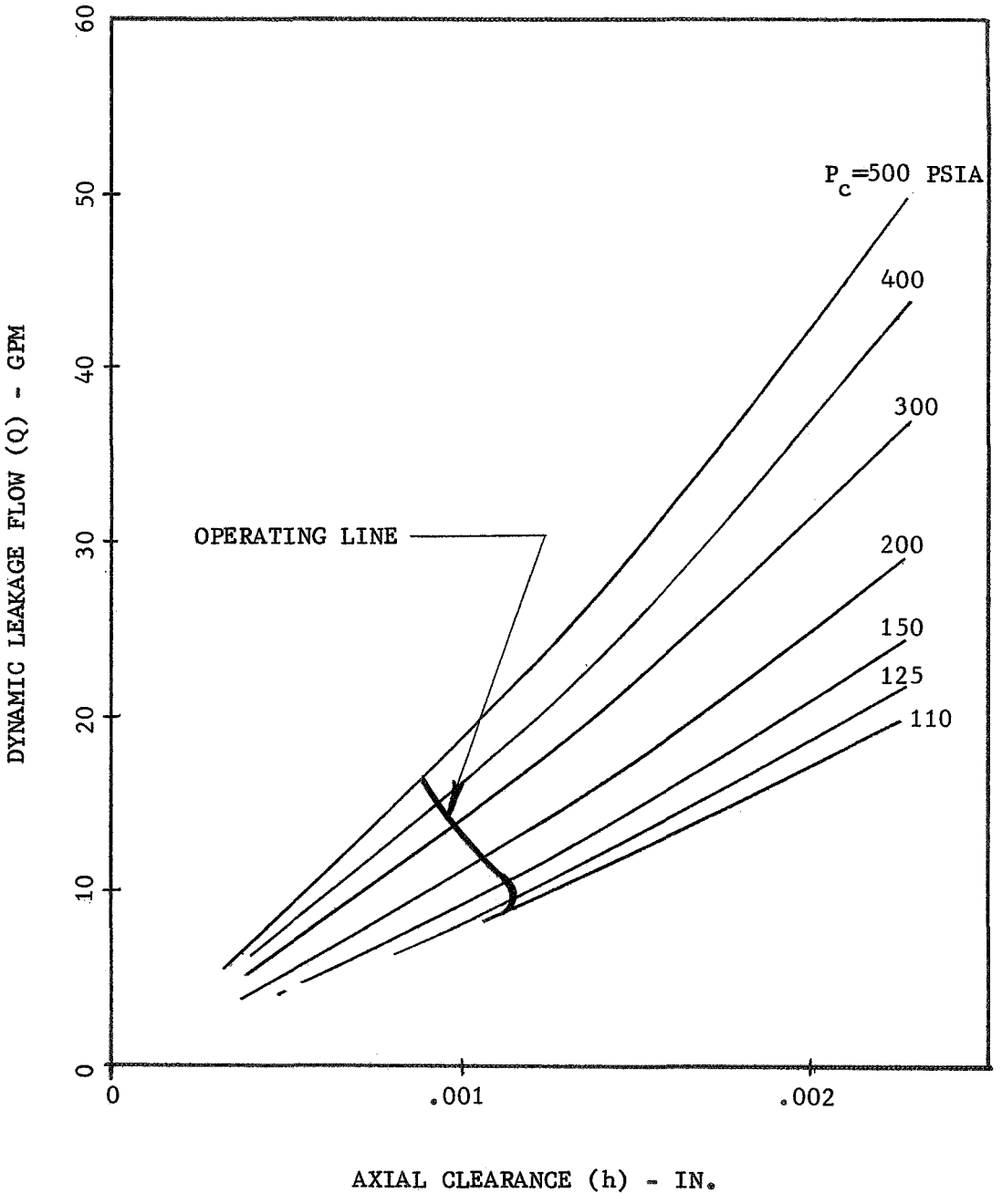

Figure 36. Externally Pressurized Hydrostatic Lift-Off Seal Estimated Dynamic Leakage Flow

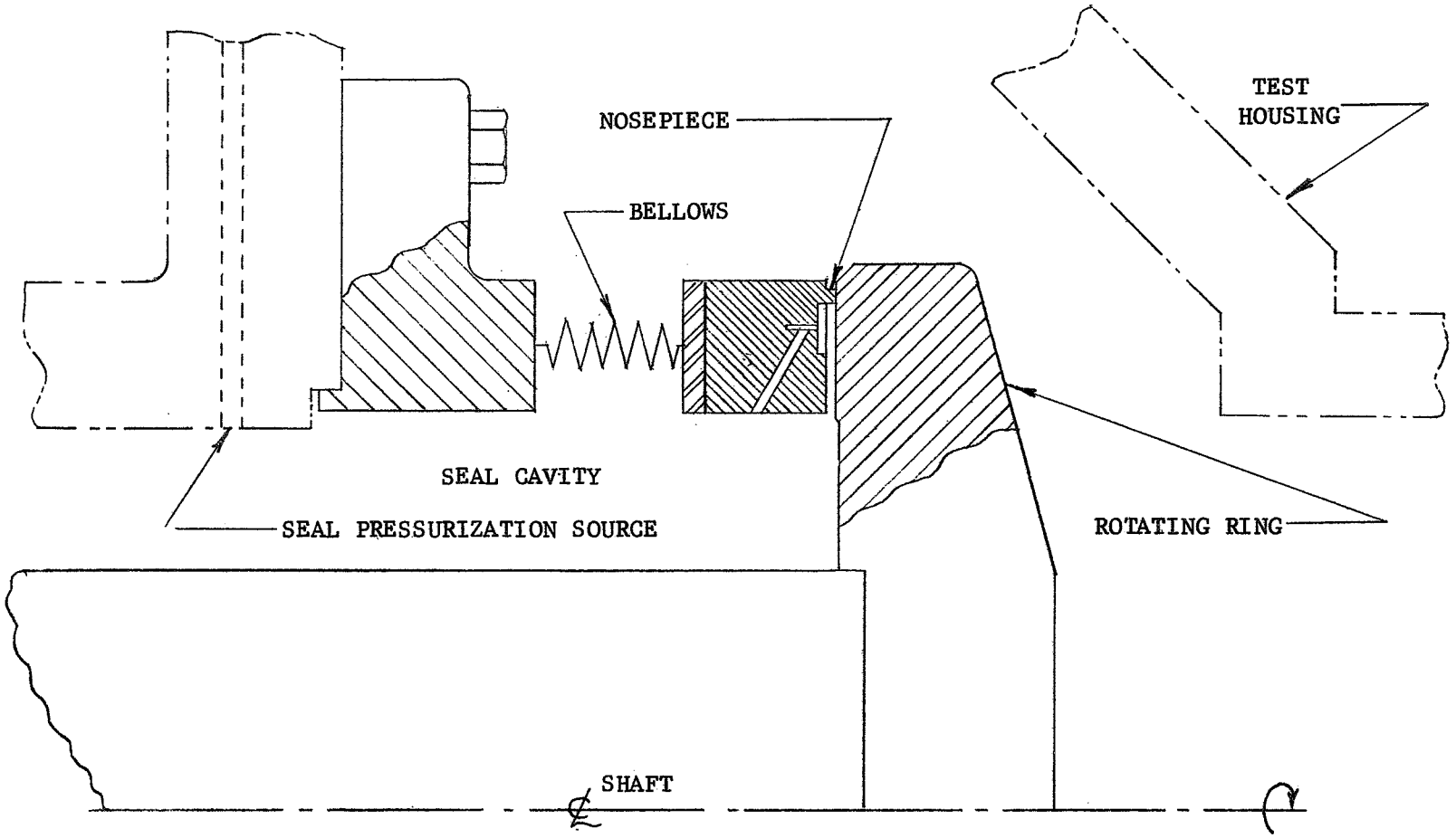

Figure 37. Self-Acting Hydrostatic Lift-Off Seal

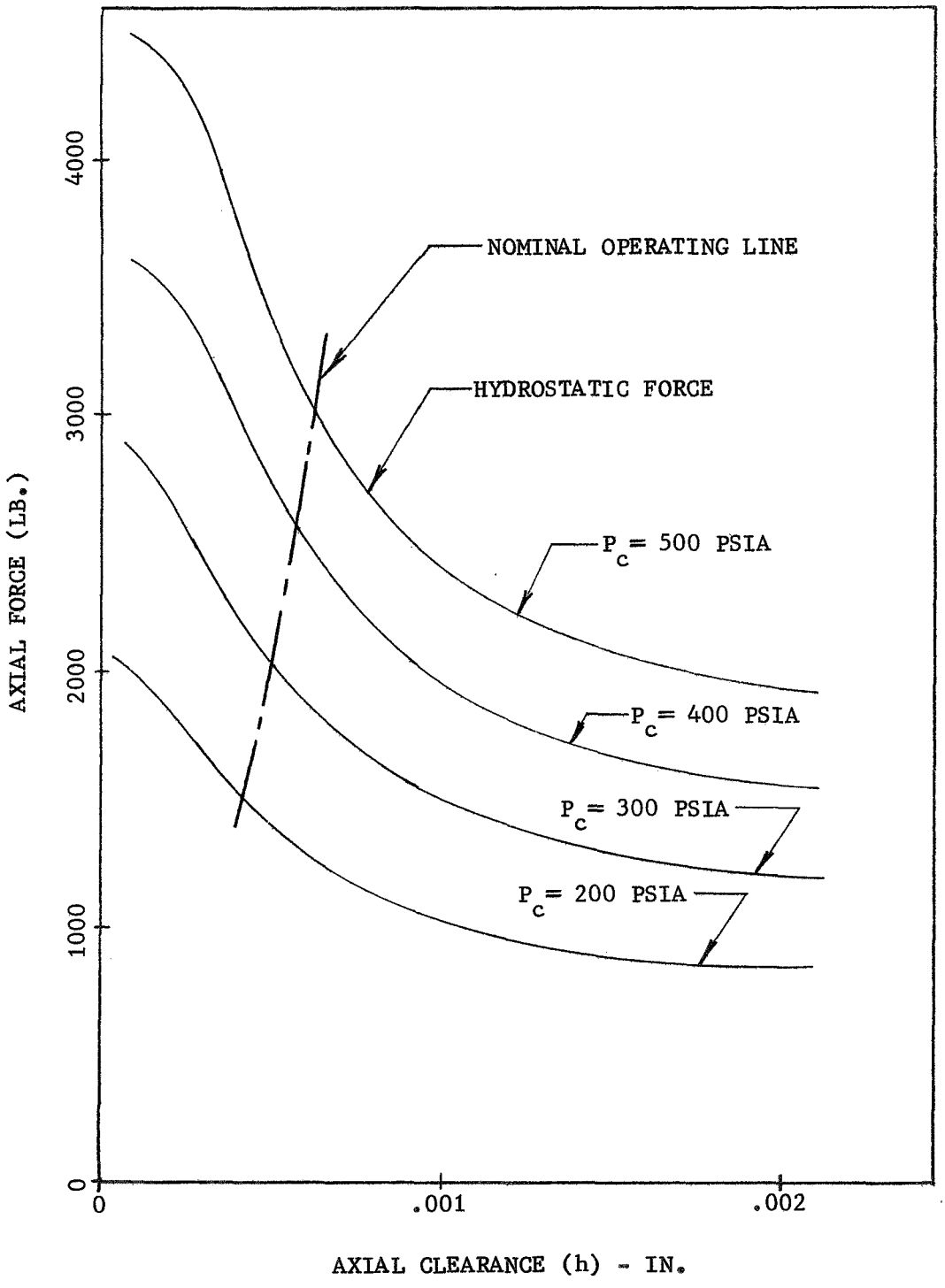

Figure 38. Self-Acting Hydrostatic Lift-Off Seal Estimated Operating Performance

and the internal seal cavity pressure for operation) will have a clearance between the running-ring and the sealing nose of approximately 0.0006-in. at the design operating point.

C. DESIGN SELECTION

At the completion of this task, the decision was made to proceed with fabrication of the externally-pressurized seal design described in Section VI,A while holding the self-acting seal design for future consideration. This decision was primarily based upon the load-leakage-life curves (Figures No. 29 and No. 30) being constructed utilizing materials properties that were estimated or extrapolated from available room temperature data in applying the equations of Section V.

Selection of the self-acting seal design would require a more precise knowledge of the specific cryogenic materials properties and, hence, the load-leakage-life characteristics. This information would be needed to select the correct bellows spring rate and pre-load essential to achieving the program goals.

The externally-pressurized seal design concept provided the means for varying or adjusting the static sealing load and controlling the face load during transient operation by regulating the pressure in the bellows chamber. Also, data collected during the testing of this design would provide an improved basis for future seal design efforts.

D. TEST UNIT DESIGN MODIFICATION

The turbine-driven test unit, depicted on Figure No. 39, was designed during the Task II effort. It provided a vehicle for liquid hydrogen test evaluation of the lift-off seal. Both the turbine drive and the power transmission for this unit were previously used for bearing and seal testing during the M-1 program (Ref. 8) and could operate at speeds in excess of 20,000 rpm. The Government-furnished seal test head used in this unit required several modifications to provide compatibility with the lift-off seal designs. This modification primarily consisted of a redesign of the sealed fluid portion of the test head to allow for installation of the seal and to provide the necessary instrumentation ports and cavity feed passages. A redesigned shaft also was included to minimize the overhung moment and reduce the radial and axial run-out. Several spacing sleeves, adapters, and mounting flanges were required to offset component manufacturing tolerances and thermal shrinkage during cryogenic operation. Provisions were made to measure and record shaft rotational speed, hydrogen pressures and temperatures in all cavities, hydrogen static and dynamic leakage flows, as well as tester slave component parameters (i.e., bearing temperatures, lubricant pressures and temperatures, and turbine pressures).

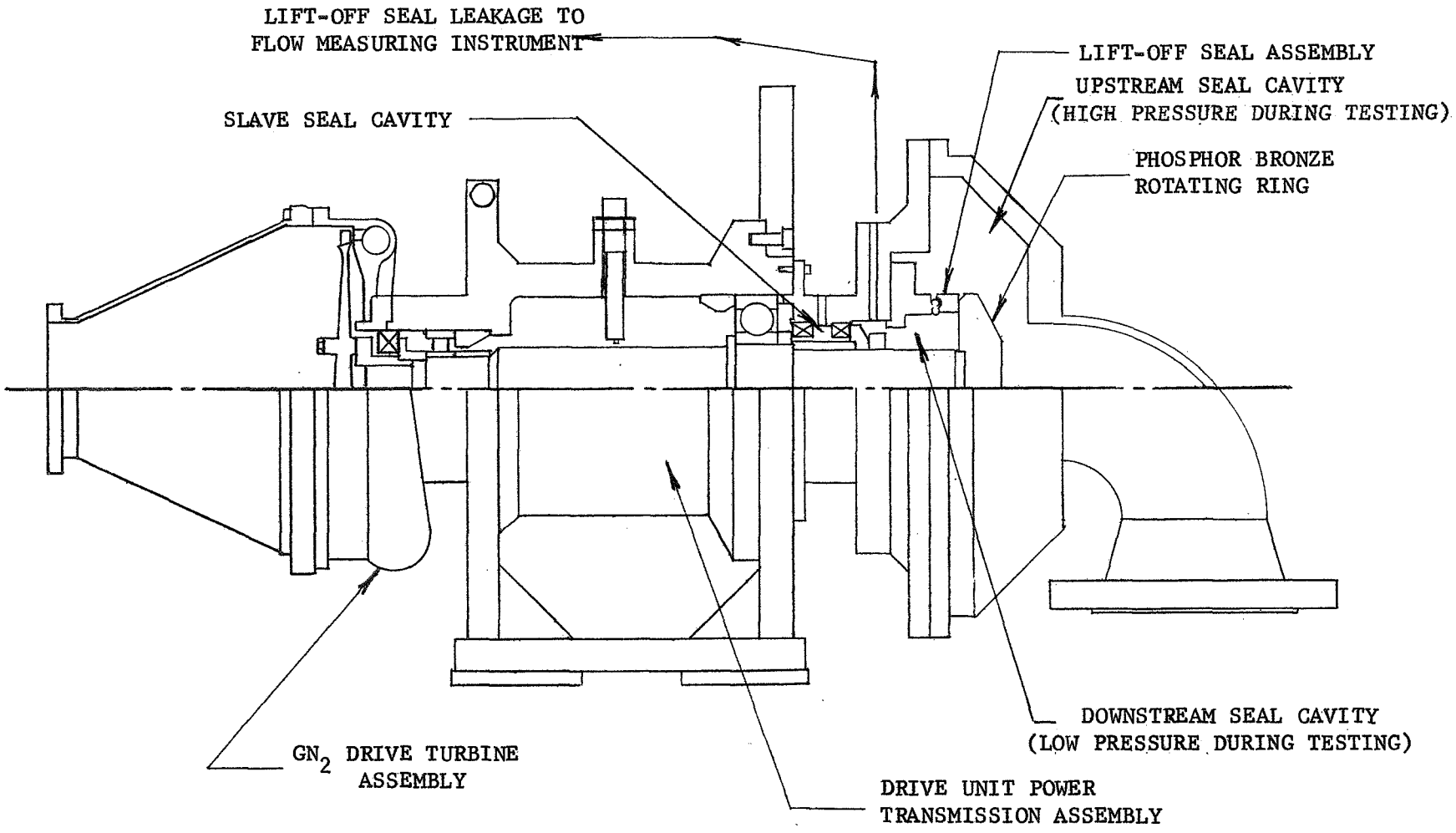

Figure 39. Lift-Off Seal Tester Assembly

Fabrication of the new components and modifications of the existing ones were accomplished concurrent with the Task III lift-off seal fabrication effort.

E. LIFT-OFF SEAL FABRICATION

Fabrication of the components for the seal test unit and the phosphor bronze running-ring was accomplished without any significant difficulties. All of these components either met or exceeded drawing requirements. The average surface finish on the sealing nose of the running ring was 1 micro-inch with a peak-to-valley (PTV) variation of 5 micro-inches. This was the desired finish and corresponded with the values used for the leakage and life calculations on Figures No. 29 and No. 30.

Problems were encountered during the fabrication of the lift-off seal in manufacturing the toroidal bellows, and in the subsequent joining of the bellows to mating components.

Fabrication methods were changed on several occasions in an attempt to circumvent these problems. Initially, it was intended that the "legs" of the bellows be electron-beam welded to the adjoining rings because this method had been successfully applied previously (Ref. 7). When the vendor experienced difficulty in producing an acceptable weld joint using this process, it was proposed that GTAW joining methods be utilized as an alternative. The "legs" were welded using this method, but it was found that there was lack of fusion in a small area. This would result in a leak between the bellows chamber and the seal cavity and an attempt was made to weld repair this small section. Additional damage (see Figure No. 40) was incurred and was sufficiently severe to require remanufacture of the attachment rings as well as the procurement of additional bellows. A change in procedure allowing the use of gold-nickel brazing of the bellows legs to the rings was authorized and subsequently implemented. During one of the finish-machining operations on the virtually completed assembly, the outer bellows was pierced by a clamping fixture (as shown on Figure No. 41) again necessitating the remanufacture of the rings and bellows.

The new bellows and other components were fabricated into the required assembly. At this point in the fabrication cycle, the assembly was subjected to a proof pressure check prior to the final hard-facing and lapping operations. The test revealed a pressure decay in the bellows chamber, which indicated the presence of significant bellows leakage. Either the bellows-leg-to-ring joint was inadequate or the material had ruptured. Closer examination pinpointed the leakage area to the zone in the vicinity of the fusion-welded joint of the outer bellows. A set-up was made to ascertain the severity of the leak, using gaseous nitrogen as the test fluid. The results of this test were as follows:

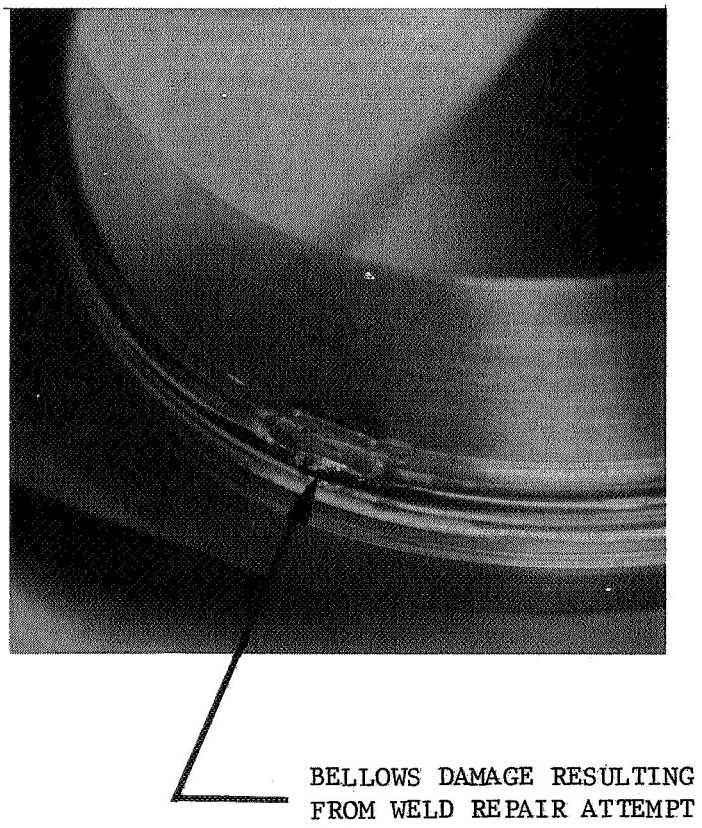

Figure 40. Bellows Weld-Repair Damage

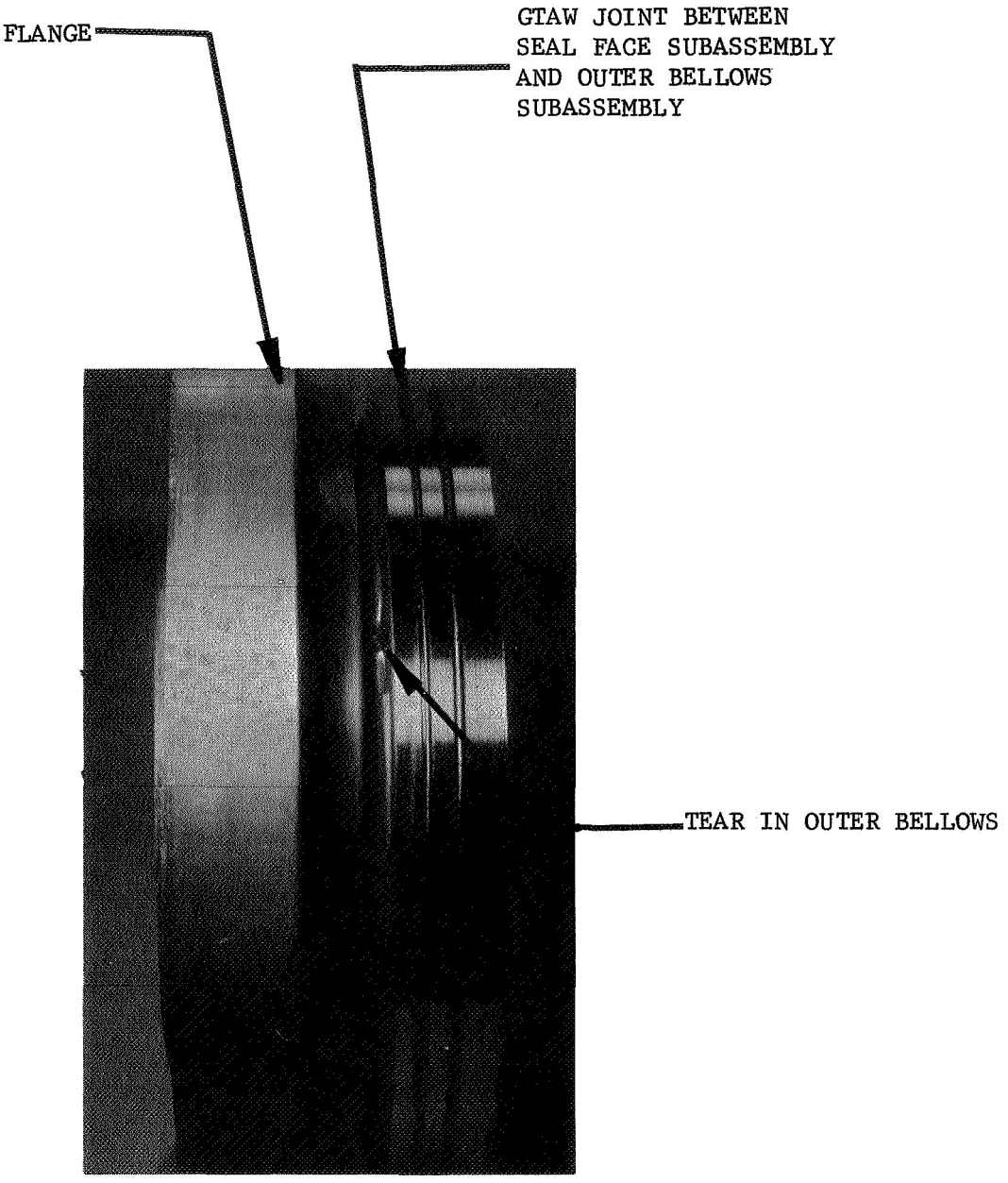

Figure 41. Bellows Damage Resulting from Fixturing

Bellows Cavity Pressure	Observed GN_2 Leakage
25 psig	15 std cc/sec
50 psig	32 std cc/sec
75 psig	49 std cc/sec

Based upon these results, it was concluded that the seal could not possibly function as originally intended because leakage of this magnitude from the outer bellows into the seal leakage cavity during static leak testing with hydrogen would preclude any reasonable accuracy in determining the leakage past the seal contact faces. The hydrogen leakage through the discrepant portion of the outer bellows would be in excess of two orders of magnitude greater than the anticipated flow past the sealing faces.

In view of the manufacturing problems experienced with the bellows, it was decided to alter program requirements by revising the liquid hydrogen testing procedures to permit the use of the seal with its outer bellows leak. This would permit the reasonable attainment of over-all objectives without incurring the risk in program delay and expenditures that continued efforts to complete the seal in accordance with the drawing requirements appeared to offer.

The seal vendor was advised to complete the remaining manufacturing operations which included flame-spraying of the seal face, electrical discharge machining (EDM) of the pockets, and final grinding and lapping of the contact surface. These were accomplished and the completed assembly (see Figure No. 42) was delivered to the test site.

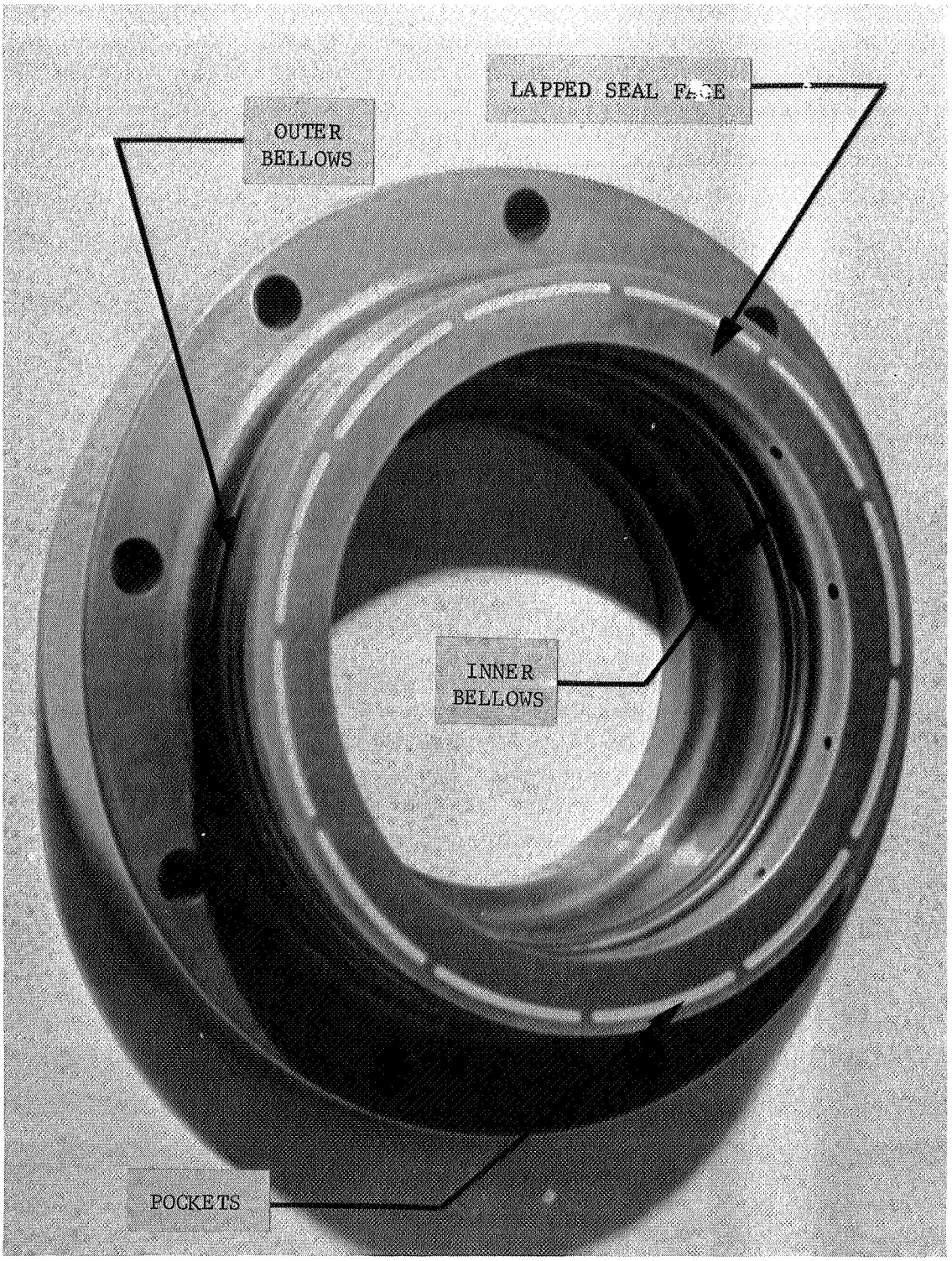

Figure 42. Completed Lift-Off Seal

VII. LIQUID HYDROGEN TESTING

The test plan originally proposed for liquid hydrogen evaluation of the lift-off seal called for dynamic operation in the manner indicated by Figure No. 35. Static sealing tests were to be conducted with 100 psia liquid hydrogen in the seal cavity, liquid hydrogen at atmospheric pressure in the leakage cavity, and with either liquid or gaseous hydrogen in the bellows cavity pressurized to the level required to achieve the "zero" leakage program goal.

The previously described excessive leakage of the outer bellows of the completed hardware necessitated a redirection of the testing plan so that the test results achieved would be meaningful. In the new test plan, a "backwards" pressurization of the seal would permit static leakage to be determined. This meant that hydrogen flowed radially inward past the sealing faces instead of flowing radially outward. To accomplish this, the upstream seal cavity is pressurized to several levels, the bellows chamber is connected to the upstream seal leakage cavity via a pressure equalizing line (see Figure No. 43), and the seal cavity is maintained at atmospheric pressure. The result of the pressure-area balance is a positive closing load between the nosepiece and the running ring. Using the curves and equations of Section V, it was estimated that hydrogen leakage flow would vary between approximately 0.015 std cc/sec, with 20 psia in the upstream cavity (as designated on Figure No. 39) to 0.045 std cc/sec with 60 psia in the upstream cavity. Rubbing tests also were conducted to simulate 300 turbopump start and shutdown transients.

A. TEST SETUP

The lift-off seal tester assembly unit shown on Figure No. 39 was installed in a liquid hydrogen test bay at Wyle Laboratories' Norco California Liquid Test Facility. Propellant lines, filters, valves, regulators, a 2000 gal liquid hydrogen storage vessel, the turbine drive-gas system, instrumentation, and other components were provided in compliance with the requirements of the flow schematic included as Figure No. 43.

A flow transducer (designated as FM-SL on Figure No. 43) was provided to measure the leakage of hydrogen under static conditions. The basic instrument had a 5.0 mv full-scale output signal and was calibrated between 0 and 10 standard cc/min of hydrogen (0 to 0.17 cc/sec). Based upon the estimated seal leakage rates of between 0.015 and 0.045 standard cc/sec (0.9 and 2.7 cc/min) for the pressure extremes, this instrument would provide an adequate range for measurement. However, as previously explained (Section VI,C), insufficient cryogenic material property data are available to accurately determine the modified stress ratio; therefore, the leakage rates calculated must be viewed with this in mind. The shunt circuit arrangement shown on Figure No. 44 was constructed to extend the flow measuring range. With the shunt valve closed, the maximum measurable flow was 10 std cc/min for a 5 millivolt output signal and with the valve open, the maximum

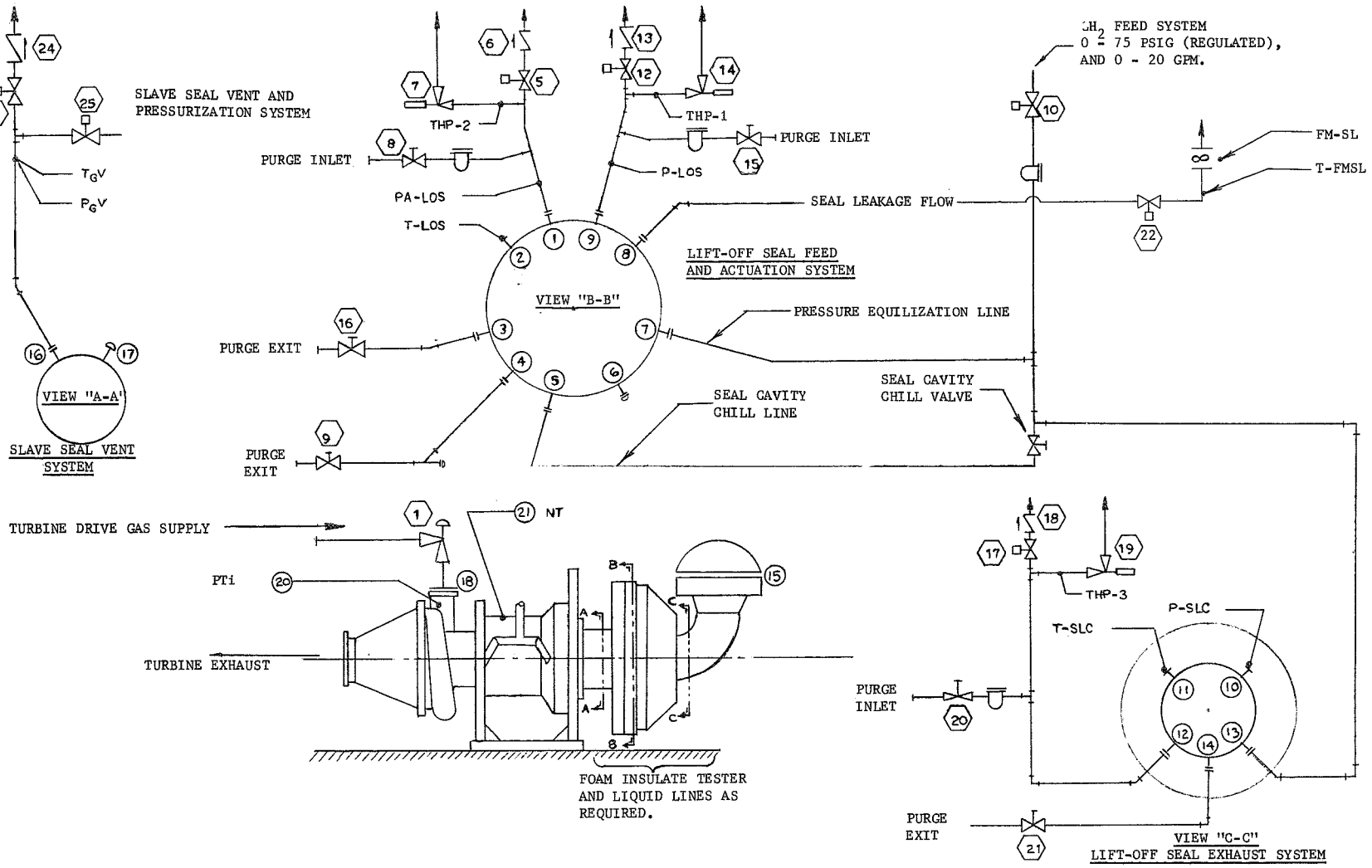

Figure 43. Test Flow Schematic

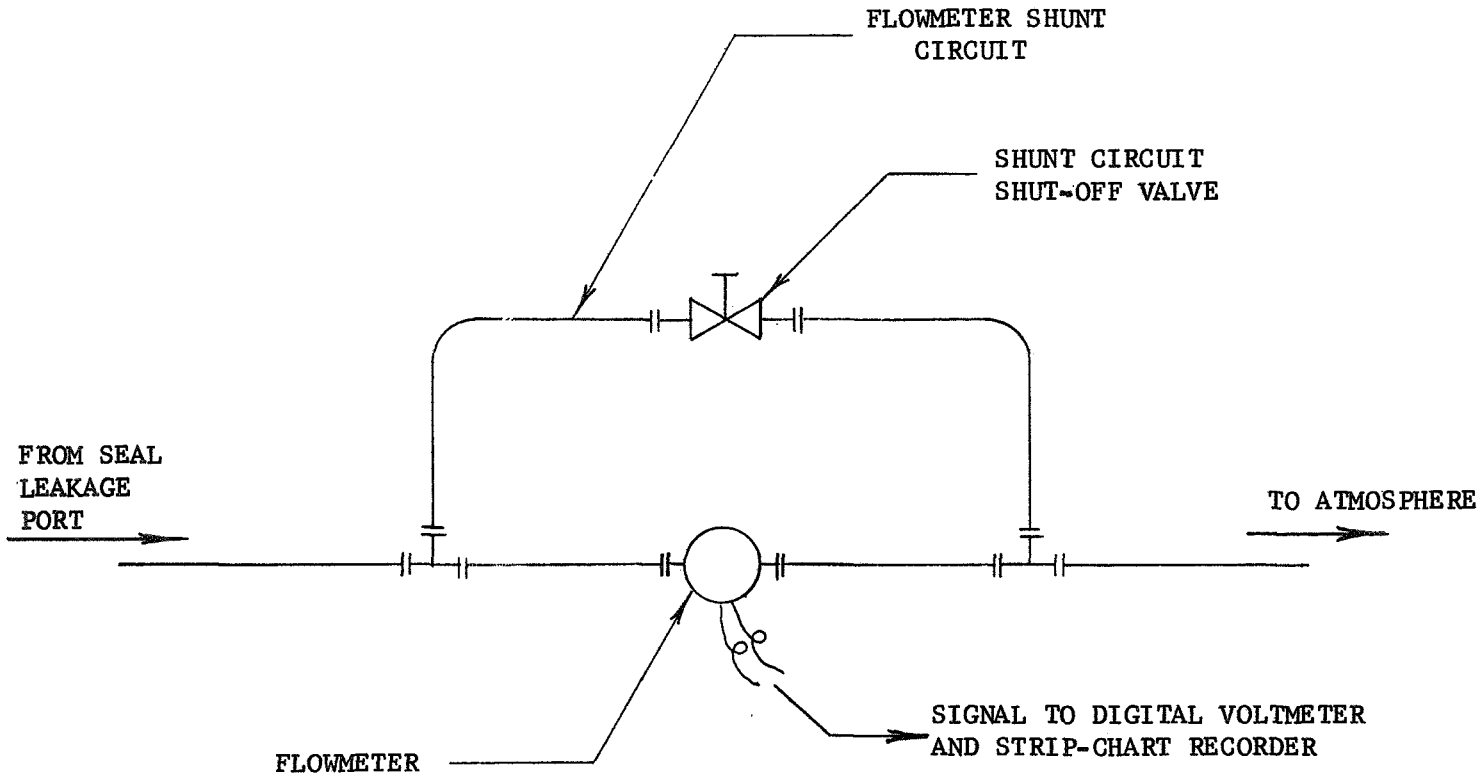

Figure 44. Hydrogen Leakage Flow Instrumentation Schematic

measurable flow range was extended to 180 std cc/min (3 cc/sec) for a 5 millivolt output signal. This system was calibrated against water displacement measurements using nitrogen, helium, and hydrogen (Figure No. 45) as the test fluids. The transducer output was connected to both a digital voltmeter as well as a strip chart recorder to monitor "zero leakage" flow rates during the subsequent testing.

The turbine drive gas system consisted of a nitrogen cascade, pressure regulators, a fast-acting turbine start valve with a shut-off timer (Figures No. 46 and No. 47), and two, series-connected, spherical nitrogen start bottles (Figure No. 47). With this system, variations of the shaft acceleration and maximum shaft speed could be provided by altering the valve shut-off timer, the supply pressure, and the system pressure decay rate.

B. TEST PROCEDURES

Before liquid hydrogen was flowed into the test unit, gaseous nitrogen was used to purge moisture and oxygen from all of the affected cavities. Then, the nitrogen was purged with gaseous helium or gaseous hydrogen.

Chilldown of the tester was accomplished by flowing hydrogen into the upstream cavity (port No. 13 on Figure No. 43) and into the downstream (seal) cavity by opening the seal cavity chill valve (see Figure No. 43). In each instance, approximately 1.5 hours were required from the opening of the supply valve to the time when liquid hydrogen temperatures were observed in the cavities.

Initial static leakage tests were accomplished at upstream cavity pressures ranging from 20 psia to 60 psia before rotation.

At the completion of the prerotational leak test, the pressure in the upstream cavity was reduced to 20 psia to lessen the seal face load. Also, the shaft was manually rotated 180 degrees from its original position. Once temperatures stabilized, an additional leakage flow check was conducted to determine what effect a change in the circumferential orientation of the nosepiece in relationship to the mating surface would have upon leakage.

The basic goal of the seal program was to achieve "zero" leakage for a 10 hour life, including 300 turbopump duty cycles. Consequently, a rubbing wear test was devised to approximate the rubbing which would be experienced during 300 turbopump start and shutdown transients. Based upon the self-acting seal performance analysis (Section VI,B), separation of the sealing faces would occur at a shaft speed of approximately 2500 rpm and the average nosepiece load up to the point of lift-off would be approximately 50 lb. Consequently, a series of three cyclic rubbing tests was conducted. The curve on Figure No. 48 represents one shaft rotational speed cycle with 20 psia maintained in the upstream cavity to impose a constant 50 lb to 60 lb loading on the seal face. The first rubbing test consisted of 57 cycles, the

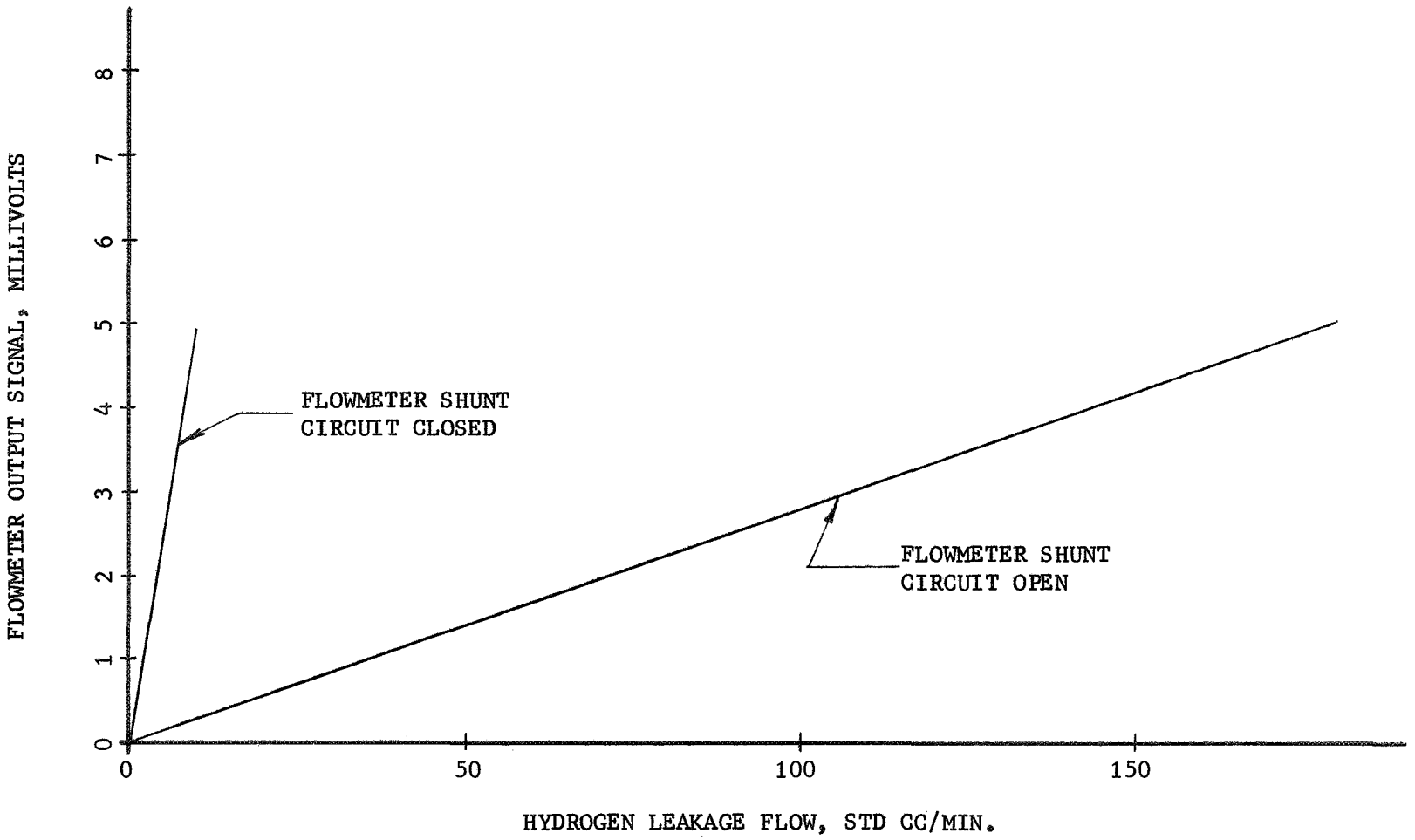

Figure 45. Hydrogen Leakage Flow Loop Calibration

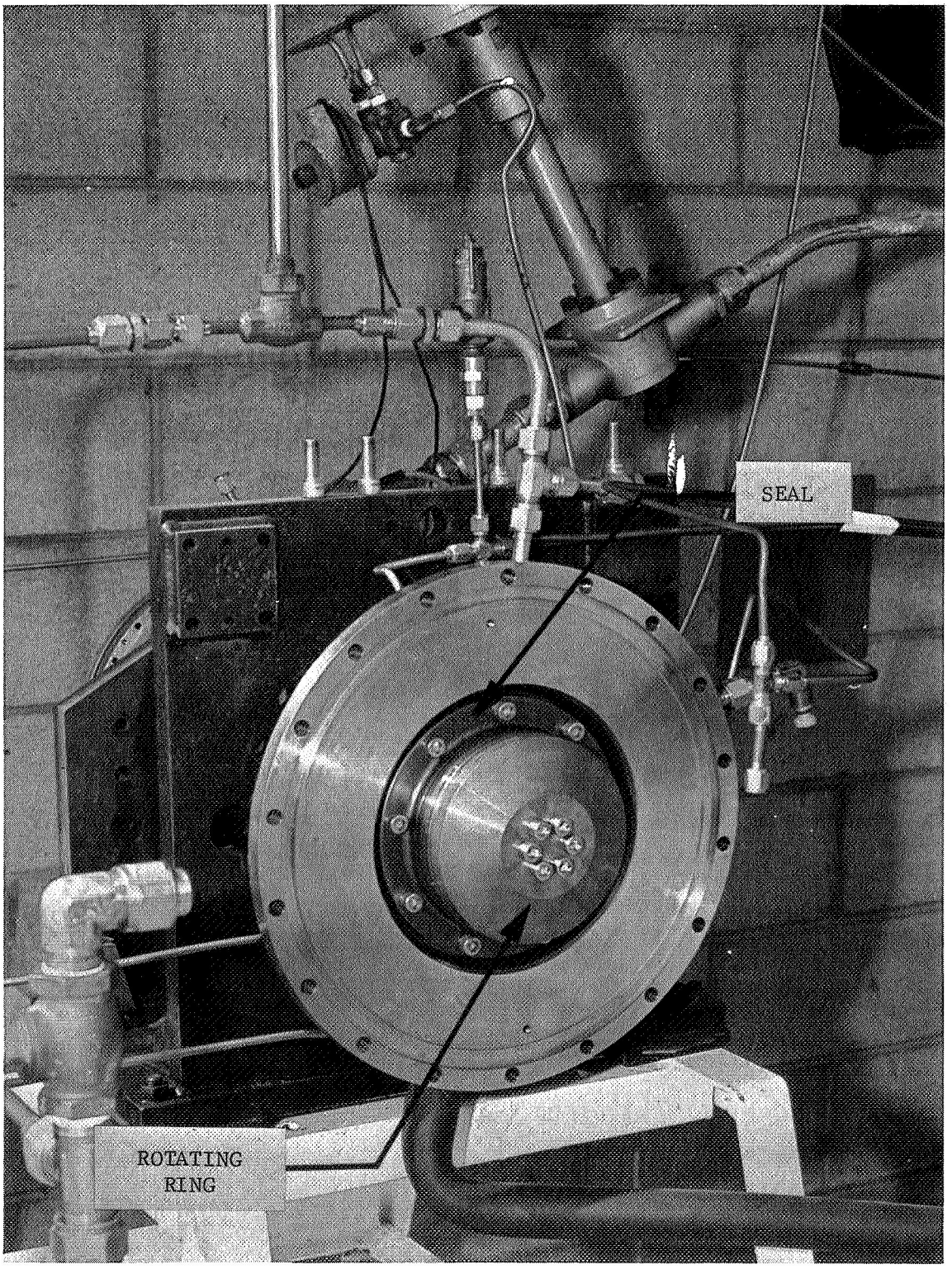

Figure 46. Lift-Off Seal and Rotating Ring Installed in Test Unit

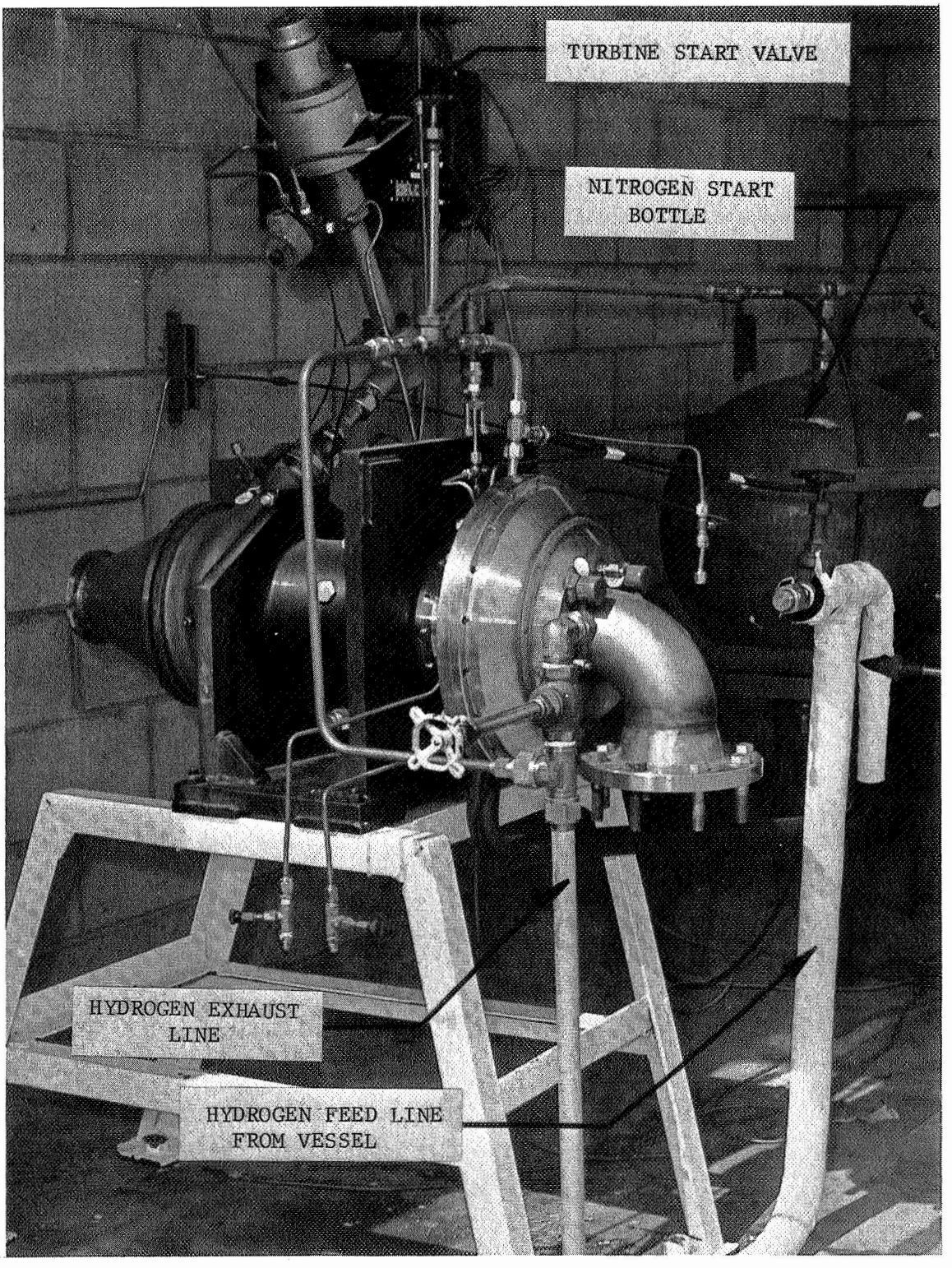

Figure 47. Installation of Assembly in Test Bay

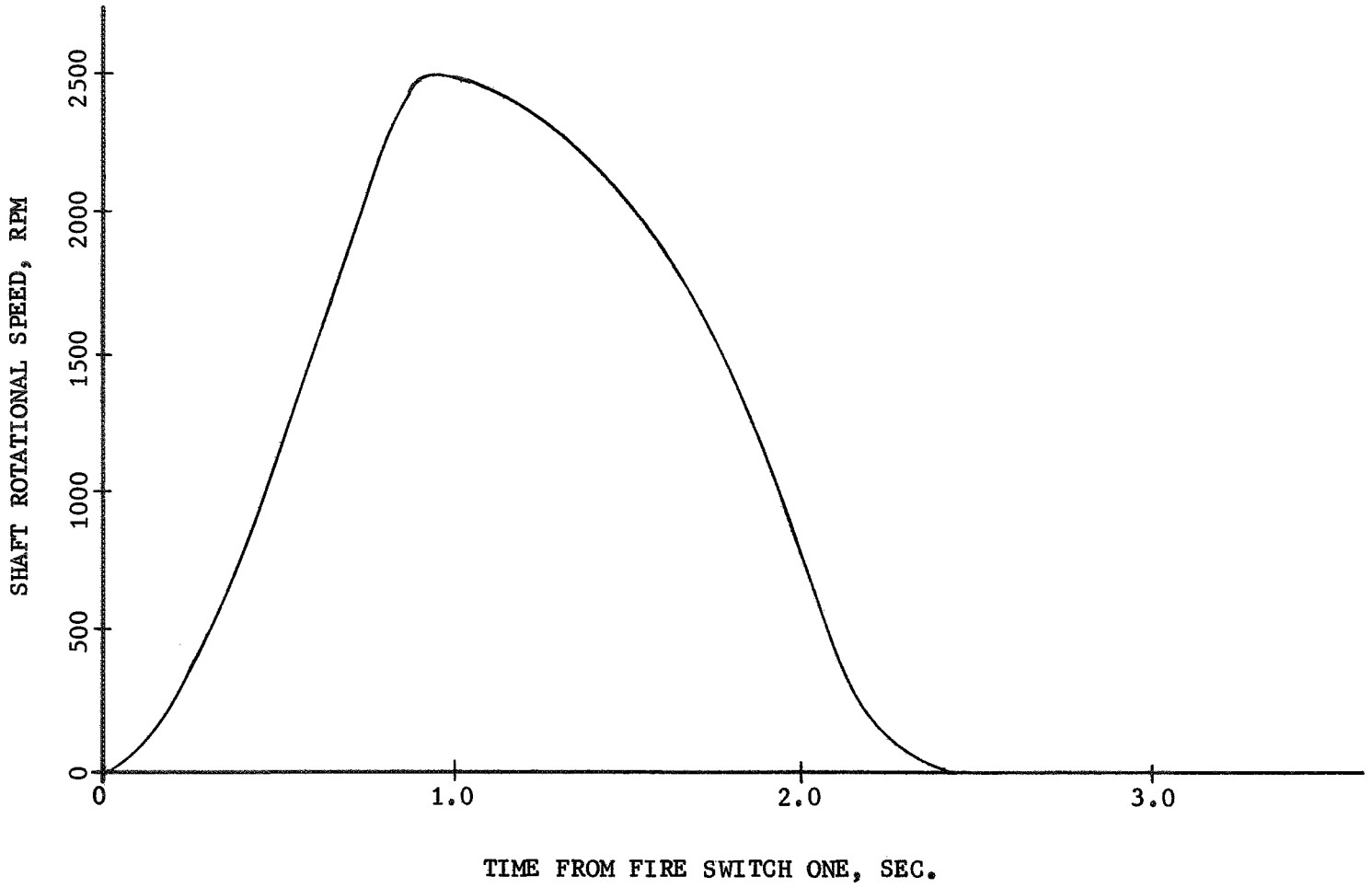

Figure 48. Typical Shaft Speed Transient

second included 119 cycles, and the third had 165 cycles for an accumulative total of 341 equivalent turbopump duty cycles of operation. It was originally intended to conduct a fourth test of 159 additional cycles, but the nosepiece condition after 341 rubbing cycles precluded this possibility.

C. TEST RESULTS

The results of the leakage check conducted before any rubbing action had taken place between the seal and running ring are included as Table VI. These points are plotted on Figure No. 49 and show a fairly closely-defined straight-line relationship between leakages as a function of the pressure drop across the seal face. The data collected after the shaft was manually rotated one-half revolution showed a slight improvement, which could be associated with a "running in" type of action on the surface.

Speeds attained during the first rapid repeat rubbing cycles ranged between a minimum of 2000 rpm to a maximum in excess of 4000 rpm. The speed variations primarily occurred during the first few cycles when adjustments were made in the turbine start valve shut-off timer and the nitrogen supply pressure.

Seal leakage flow rates observed after the first 57 rubbing cycles showed a marked improvement, as indicated on both Table VI and Figure No. 49.

After accumulating 176 equivalent turbopump operating cycles, it can be seen from Figure No. 49 that while the magnitude of leakage was not excessive, the leakage versus pressure drop relationship was markedly different from the earlier data.

The post-test leak test data for the third test (165 rubbing cycles) displayed excessive leakage which indicated that some damage (excessive rubbing wear) had occurred on the interface surfaces.

Based upon the comparatively large magnitude of leakage observed after accumulating 341 rubbing cycles, the unit was partially disassembled to permit inspection of the seal surfaces. Examination of the seal components confirmed that wear had occurred on the sealing nosepiece of the phosphor bronze rotating ring (Figure No. 50). As noted on Figure No. 51, wear had not only occurred on the sealing lip, but on the inner land as well. Despite the wear tracks on the face of the seal, no other damage had occurred. Relapping of the surface would restore the component to serviceable condition.

TABLE VI

LIFT-OFF SEAL STATIC HYDROGEN LEAKAGE TEST RESULTS

Upstream Cavity Pressure, psia	Seal Cavity Pressure, psig	Seal Leakage Flow std cc/sec - H_2
	Pre-Rotational Leak Test	
23.8	0.108	0.959
29.0	0.054	0.875
35.0	0.054	0.821
39.5	0.036	0.561
45.0	0.036	0.647
50.0	0.043	0.701
55.0	0.025	0.534
60.0	0.036	0.564
	Leak Test After 180° Rotation	
40.0	0.029	0.522
50.0	0.036	0.582
60.0	0.025	0.396
	Leak Test After 57 Rubbing Cycles	
40.0	0.018	0.345
45.0	0.018	0.300
50.0	0.018	0.270
60.0	0.014	0.210
	Leak Test After 176 Rubbing Cycles (Accumulative)	
40.0	0.062	0.924
45.0	0.043	0.719
50.0	0.016	0.318
	Leak Test After 341 Rubbing Cycles (Accumulative)	
50.0	15.0	1.98

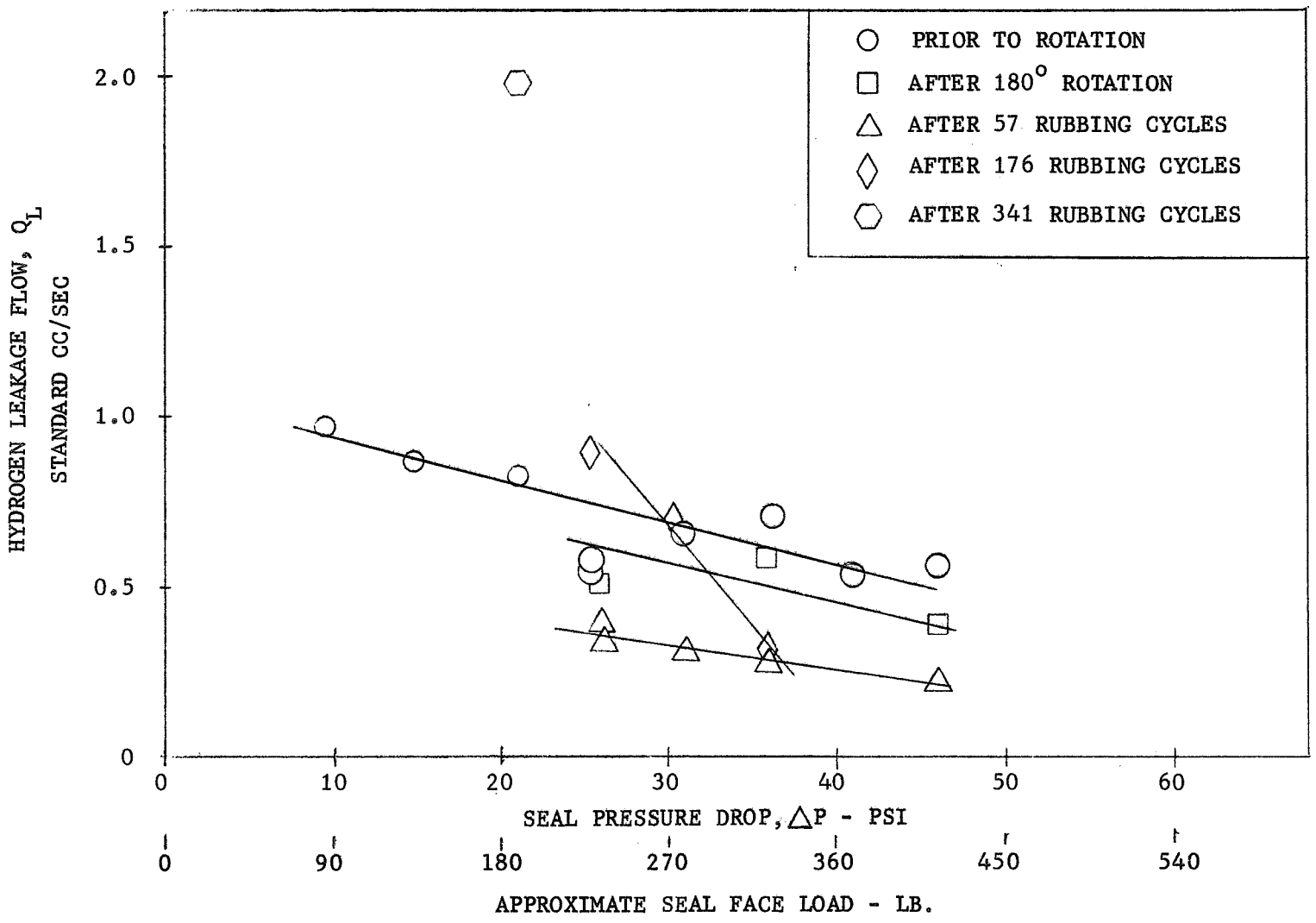

Figure 49. Lift-Off Seal Static Leakage Test Results

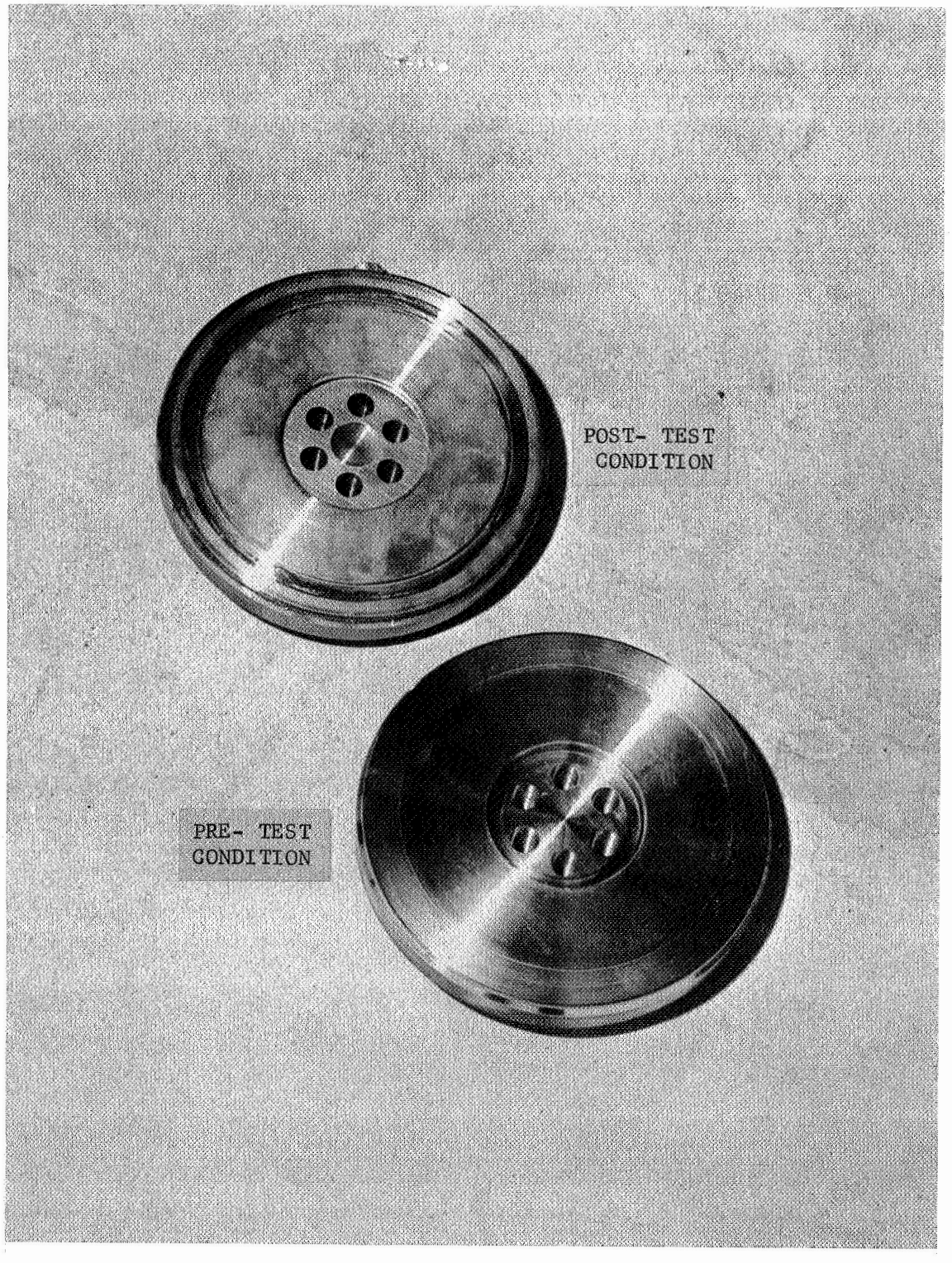

Figure 50. Comparison of Post-Test and Pre-Test Condition of Running-Ring

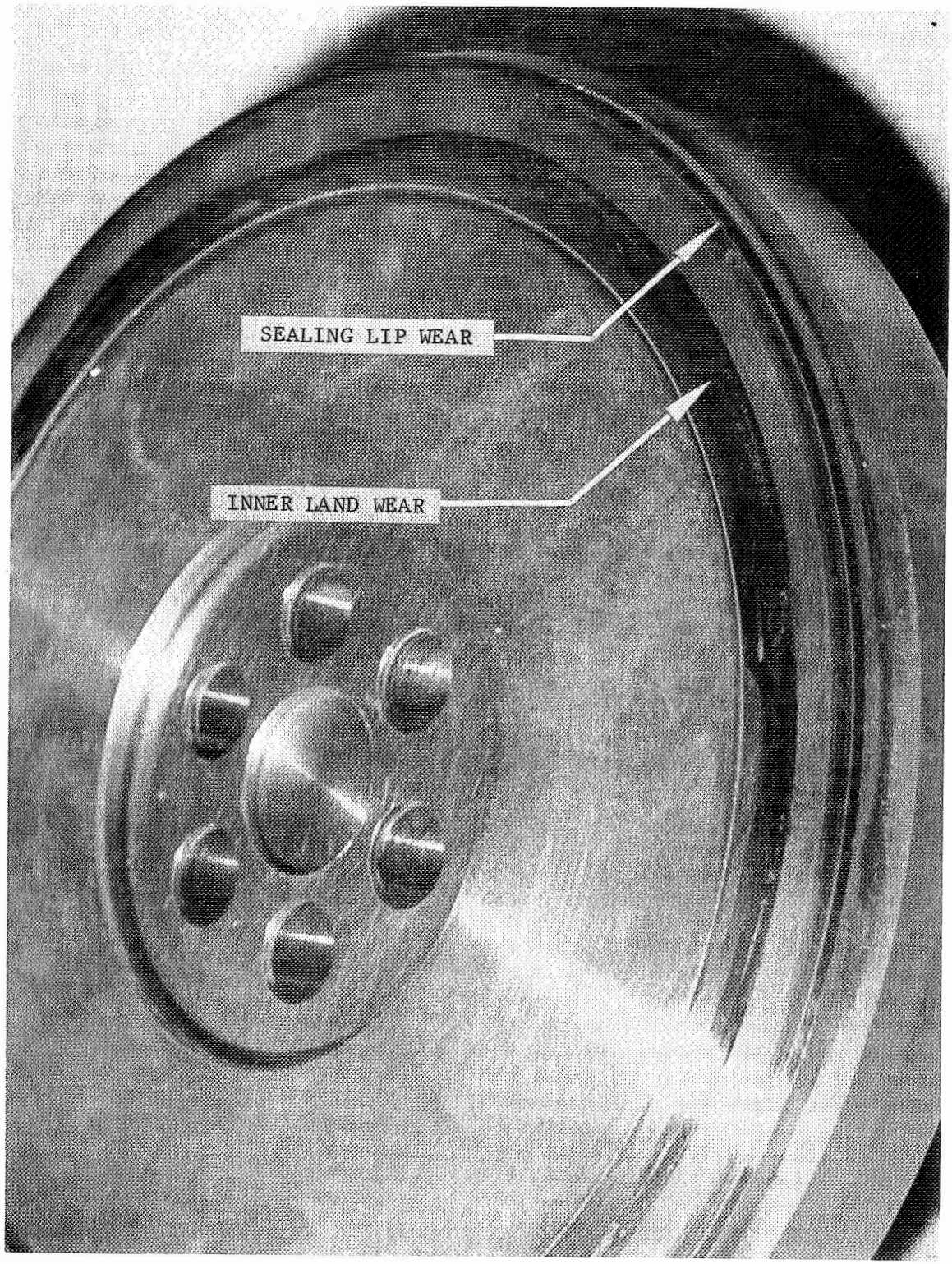

Figure 51. Post-Test Wear Pattern on Rotating Ring

D. CORRELATION OF TEST RESULTS WITH PREDICTIONS

Calculations performed prior to the tests predicted, as indicated earlier in this section, that hydrogen leakage would increase from approximately 0.015 std cc/sec at a pressure drop of 5 psi to 0.045 std cc/sec at a pressure drop of 45 psi. It was not surprising that the magnitude of leakage observed was significantly larger than predicted (approximately two orders of magnitude). The leakage calculations were based upon the flow conductance and modified stress ratio correlations given by Bauer (Reference 2), who pointed out that wide divergence in the correlations occurred in some cases. Specifically, for the seal examined in this program, the actual leakage could vary (plus or minus) by one order of magnitude from the values calculated. Additionally, it is possible that the absence of accurate materials property data at liquid hydrogen temperature contributed to the predicted leakage error. As noted, the predicted trend was for an increase in leakage corresponding with an increase in pressure. It can be observed from Figure 49 that the test data showed a reverse trend. The flow equation of Section V indicated that for a given geometry, the flow basically is a function of the difference of the squares of the two cavity pressures multiplied by the flow conductance parameter (h^3). The flow conductance parameter obtained from Figure No. 25 is a function of the modified stress ratio (R) which is proportional to the applied load. It is found when comparing the predicted leakage at an upstream cavity pressure of 20 psia with that of a 60 psia pressure, there is an increase in pressure effect by a factor of approximately 20 although the flow conductance parameter is reduced by 6. This results in flow increasing by a factor of approximately 3. The reverse trend indicated by the test data is believed to have been caused by changes in seal contact geometry at the progressively higher pressures. The pressure in the upstream cavity (see Figure No. 39) will deflect the rotating ring with subsequent tilting of the nosepiece. This would result in a divergent leak path and a reduction in the seal interface contact width. A change, for example, from a 0.040-in. wide flat surface with 20 psia in the cavity to an effective width of 0.013-in. at the 60 psia cavity pressure would decrease the flow conductance parameter by a factor of 20.

Life calculations, performed prior to testing, predicted that the zero wear life of this configuration should be on the order of 13,000 rubbing cycles while the actual wear life was considerably less. It is clear from the leakage data that the seal operated effectively as a static seal through 57 rubbing cycles. It is possible that the significantly different leakage versus pressure drop relationship after an additional 119 cycles (Figure No. 49) was caused by wear particles accumulating in the pockets of the seal face (Figure No. 52) which would prevent normal contact at the sealing lip interface. At the progressively higher test pressures, the coning of the running ring would reduce the adverse effect of the wear particle entrapment. In terms of leakage magnitude, the seal at this point (176 accumulated rubbing cycles) was operating effectively as a static seal. It was not possible to determine the point at which seal wear completely negated the static sealing function. In any event, the actual life of the seal was approximately two orders of magnitude less

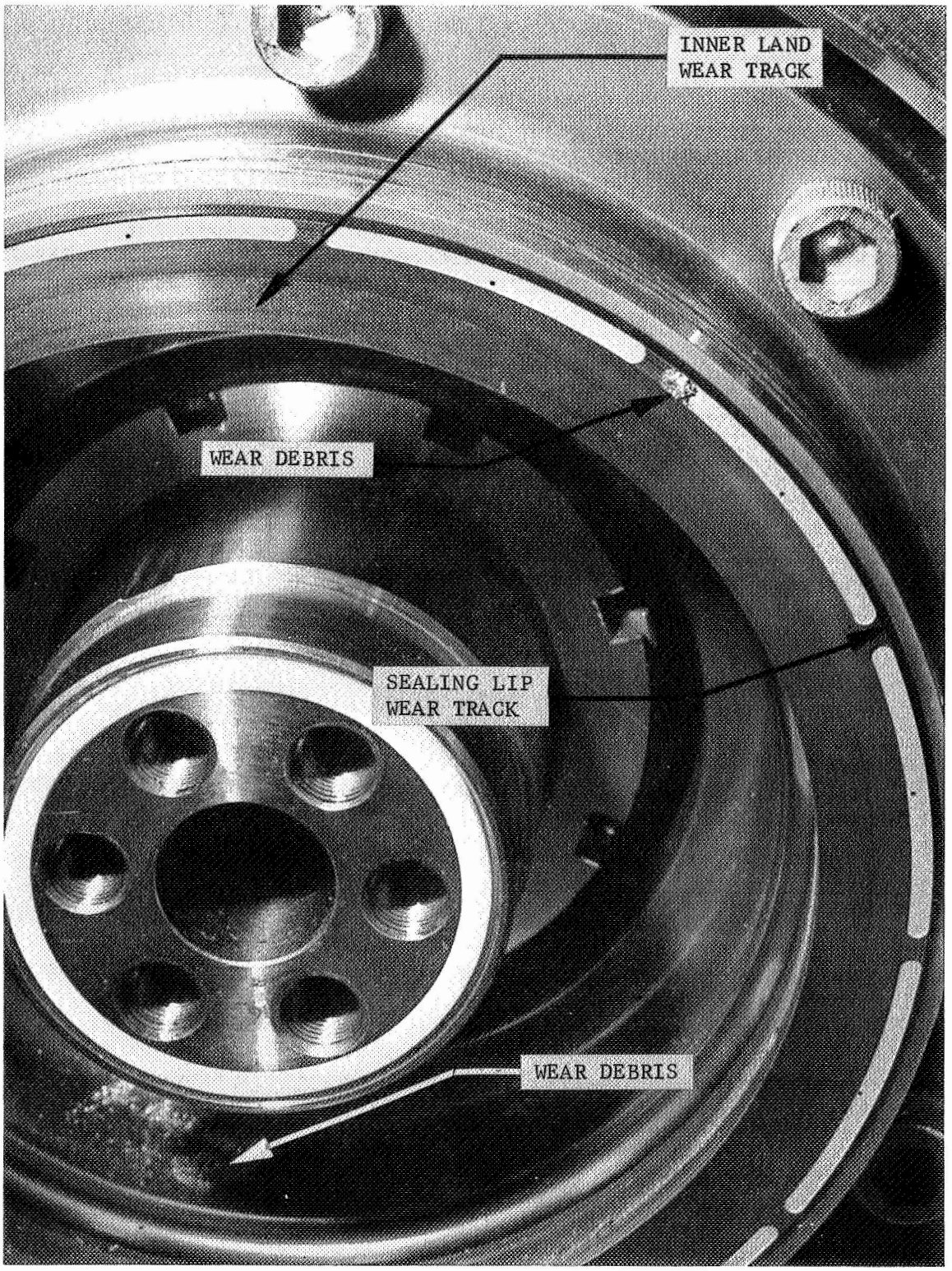

Figure 52. Post-Test Wear Pattern on Lift-Off Seal Face

than the "zero wear" life predictions. As was the case with the leakage predictions, the wear results were not totally unexpected. In utilizing the "zero wear" equations of Section V, it was necessary to assume a magnitude for yield point in shear at liquid hydrogen temperature. Additionally, the relationship between normal stress and shear stress given in Section V includes a stress concentration term and coefficient of friction term, both of which were estimated. The stress concentration term is believed to have the greatest influence because values of from 2 to 1000 can prevail depending upon sharpness of corners (Reference 6). Wear also could be accelerated as a result of heat generated at the sealing interface from the rapid-repeat cycling although no fluid temperature changes were noted during the tests which would confirm this supposition.

VIII. CONCLUSIONS AND RECOMMENDATIONS

The results of liquid hydrogen testing of the lift-off seal investigated during this program effort provide good support for the theoretical leakage, life, and contact load relationships developed. Using 1 std cc/sec as the static hydrogen leakage criteria, useful operating life in excess of 176 cycles was achieved with the seal operating in a rapid-repeat rubbing cyclic test mode. The availability of more accurate materials property data at liquid hydrogen temperature (as discussed in Section VII) would have provided a closer correlation between the predicted and experimental seal performance.

It was not possible to determine the dynamic characteristics of the seal in the lift-off mode because of the hardware discrepancy experienced. However, the design of the hydrostatic face and other elements was accomplished using proven analysis methods and it is reasonable to assume that the hydrostatic performance would have been consistent with predictions.

Based upon the success realized in this program, it is recommended that a detailed pursuit be made to investigate and determine several specific properties of promising materials under cryogenic conditions so as to provide an improved foundation for defining "zero" leakage and "zero" wear. Of particular interest would be the determination of Meyer hardness, Meyer Index, and material transfer factors.

It is further recommended that these specific data be applied to the design, construction, and test evaluation of self-acting hydrostatic lift-off seal of the type described in this report.

REFERENCES

1. Handling Hazardous Materials, NASA SP-5032, National Aeronautics and Space Administration, Washington, D.C., September 1965

2. Bauer, P., Investigation of Leakage and Sealing Parameters, IIT Research Institute Report AFRPL-TR-65-153, August 1965

3. Rabinowicz, E., Friction and Wear of Materials, John Wiley & Sons, New York, 1965

4. Properties of Principal Cryogenics, Aerojet-General Report No. 9050-111-65, November 1965

5. McGregor, C. W., (ed), Handbook of Analytical Design for Wear, Plenum Press, New York, 1964

6. "Designing for Zero-Wear or a Predictable Minimum", Product Engineering, Vol. 37, No. 17, August 15, 1966

7. (U) Advanced Rocket Engine-Storable, Aerojet-General Corporation, Phase I Interim Final Report, Contract AF 04(611)-10830, Report No. AFRPL-TR-67-75, August 1967, (CONF.)

8. Purdy, C. C., Design and Development of Liquid Hydrogen Cooled 120MM Roller, and 110MM Tandem Ball Bearings for M-1 Fuel Turbopump, Contract NAS 3-2555, NASA CR 54826, 24 February 1966

Distribution List for Report No. CR-72796

		Copies
National Aeronautics and Space Administration Lewis Research Center 21000 Brookpark Road Cleveland, Ohio 44135		
Attn:	T. J. Flanagan Mail Stop 500-313	1
	Technical Report Control Office Mail Stop 5-5	1
	Technology Utilization Office Mail Stop 3-16	1
	AFSC Liaison Office Mail Stop 501-3	2
	Library Mail Stop 60-3	1
	M. J. Hartmann Mail Stop 5-9	1
	D. W. Drier Mail Stop 21-4	1
	L. P. Ludwig Mail Stop 23-2	1
	D. D. Scheer Mail Stop 500-204	6
Space Nuclear Propulsion Office-Cleveland National Aeronautics and Space Administration Lewis Research Center 21000 Brookpark Road Cleveland, Ohio 44135		
Attn:	J. C. Montgomery Mail Stop 501-1	1
	R. E. Connelly Mail Stop 501-1	1

	Copies
National Aeronautics and Space Administration Washington, D. C. 20546	
Attn: Code RPX	2
RPL	1
Scientific and Technical Information Facility P. O. Box 33 College Park, Maryland 20740	
Attn: NASA Representative Code CRT	6
National Aeronautics and Space Administration Ames Research Center Moffett Field, California 94035	
Attn: Library	1
National Aeronautics and Space Administration Flight Research Center P. O. Box 273 Edwards, California 93523	
Attn: Library	1
National Aeronautics and Space Administration Goddard Space Flight Center Greenbelt, Maryland 20771	
Attn: Library	1
National Aeronautics and Space Administration John F. Kennedy Space Center Kennedy Space Center, Florida 32899	
Attn: Library	1
National Aeronautics and Space Administration Langley Research Center Langley Station Hampton, Virginia 23365	
Attn: Library	1

	Copies
National Aeronautics and Space Administration Manned Spacecraft Center Houston, Texas 77058	
Attn: Library	1
National Aeronautics and Space Administration George C. Marshall Space Flight Center Marshall Space Flight Center, Alabama 35812	
Attn: Library	1
Keith Chandler	1
Loren Gross	1
Jet Propulsion Laboratory 4800 Oak Grove Drive Pasadena, California 91103	
Attn: Library	1
U. S. Atomic Energy Commission AEC-NASA Space Nuclear Propulsion Office Washington, D. C. 20546	
Attn: F. C. Schwenk	1
Chemical Propulsion Info. Agency Applied Physics Laboratory 8621 Georgia Avenue Silver Spring, Maryland 20910	1
Defense Documentation Center Cameron Station Alexandria, Virginia 22314	1
Office of the Director of Defense Research and Engineering Washington, D. C. 20301	1
Advanced Research Projects Agency Washington, D. C. 20301	
Attn: D. E. Mock	1

	Copies
Research and Technology Division Air Force Systems Command Bolling Air Force Base Washington, D. C. 20332	
Attn: RTD (RTNP)	1
Arnold Engineering Development Center Air Force Systems Command Tullahoma, Tennessee 37389	
Attn: AEOIM	1
Air Force Aero Propulsion Laboratory Research and Technology Division Air Force Systems Command United States Air Force Wright Patterson AFB, Ohio 45433	
Attn: APRP	1
Aeronautical Systems Division Air Force Systems Command Wright Patterson Air Force Base Dayton, Ohio 45433	
Attn: Library	1
Air Force Missile Test Center Patrick Air Force Base, Florida 32925	
Attn: L. J. Ullian	1
Air Force Systems Command Andrews Air Force Base Washington, D. C. 20332	
Attn: SCLT	1
Air Force Rocket Propulsion Laboratory (RPR) Edwards Air Force Base, California 93523	1
Air Force Office of Scientific Research Washington, D. C. 20333	
Attn: SREP, Dr. J. F. Masi	1

	Copies
Office of Research Analyses (OAR) Holloman Air Force Base, New Mexico 88330	
Attn: Library	1
Commanding Officer U. S. Army Research Office (Durham) Box CM, Duke Station Durham, North Carolina 27706	1
U. S. Army Missile Command Redstone Scientific Information Center Redstone Arsenal, Alabama 35808	
Attn: Chief, Document Section	1
Bureau of Naval Weapons Department of the Navy Washington, D. C. 20360	
Attn: J. Kay, Code RTMS-41	1
Commander U.S. Naval Missile Center Point Mugu, California 93041	
Attn: Technical Library	1
Commanding Officer Office of Naval Research 1030 E. Green Street Pasadena, California 91101	1
Director (Code 6180) U.S. Naval Research Laboratory Washington, D. C. 20390	
Attn: H. W. Carhart	1
Picatinny Arsenal Dover, New Jersey 07801	
Attn: Chief, Liquid Propulsion Laboratory	1

	Copies
Aerojet-General Corporation P. O. Box 296 Azusa, California 91703	
Attn: Librarian	1
Aerojet-General Corporation 11711 South Woodruff Avenue Downey, California 90241	
Attn: F. M. West, Chief Librarian	1
Aerojet Liquid Rocket Company P. O. Box 13222 Sacramento, California 95813	
Attn: Tech. Library 9696-2001	1
K. R. Collins	1
R. Jones	1
Aerospace Corporation P. O. Box 95085 Los Angeles, California 90045	
Attn: Library-Documents	1
Allis Chalmers Mfg. Co. Box 512 Milwaukee, Wisconsin 53201	1
Battelle Memorial Institute 505 King Avenue Columbus, Ohio 43201	
Attn: Report Library Room 6A	1
Bell Aerospace Company Box 1 Buffalo, New York 14240	
Attn: Technical Library	1
M. Messina	1

	Copies
The Boeing Company Aerospace Division P. O. Box 3707 Seattle, Washington 98124	
Attn: Ruth E. Peerenboom, Library Processes Sup. (1190)	1
Borg-Warner Mechanical Seals P. O. Box 2017 Terminal Annex Los Angeles, California 90054	1
Brown Engineering Co., Inc. Research Park Huntsville, Alabama 35807	
Attn: Library	1
Chicago Rawhide Mfg., Co. 900 North State Street Elgin, Illinois 60120	
Attn: Robert V. Brink	1
Chrysler Corporation Space Division New Orleans, Louisiana 70150	
Attn: Library	1
Crane Packing Company 6425 Oakton Street Morton Grove, Illinois 60053	
Attn: H. Tankus	1
Curtiss-Wright Corporation Weight Aeronautical Division Woodridge, New Jersey 07075	
Attn: Library	1
Fairchild Stratos Corporation Aircraft Missiles Division Hagerstown, Maryland 20740	
Attn: Library	1

	Copies
The Franklin Institute Research Laboratories Benjamin Franklin Parkway Philadelphia, Pennsylvania 19103	
Attn: Library	1
Garlock, Inc. Palmyra, New York 14522	1
The Garrett Corporation AiResearch Manufacturing Co. 9851 Sepulveda Blvd. Los Angeles, California 90009	
Attn: Library	1
General Dynamics/Astronautics P. O. Box 1128 San Diego, California 92112	
Attn: Library and Information Services (128-00)	1
General Electric Company Advanced Technology Laboratories Schenectady, New York 12301	
Attn: Library	1
General Electric Company Flight Propulsion Laboratory Dept. Cincinnati, Ohio 45215	
Attn: D. Suichu	1
General Motors Corporation Allison Division P. O. Box 24013 Indianapolis, Indiana 46206	
Attn: Library	1
Gits Brothers Mfg. Co. 1846 South Kilbourn Avenue Chicago, Illinois 60623	
Attn: R. H. Jackson	1

	Copies
Grumman Aircraft Bethpage Long Island New York, New York 11714	
Attn: Library	1
IIT Research Institute 10 West 35th Street Technology Center Chicago, Illinois 60616	
Attn: Library	1
Lockheed Missiles and Space Company Propulsion Engineering Division (D. 55-11) Sunnyvale, California 94087	1
Lockheed Propulsion Company P. O. Box 111 Redlands, California 92374	
Attn: Library	1
Marquardt Corporation 16555 Saticoy Street Box 2013 - South Annex Van Nuys, California 91404	
Attn: Library	1
McDonnell Douglas Aircraft Corporation P. O. Box 516 Lambert Field, Missouri 63166	
Attn: Library	1
McDonnell Douglas Astronautics Company Western Division 5301 Bolsa Avenue Huntington Beach, California 92647	
Attn: Library	1
Mechanical Technology Incorporated 968 Albany-Shaker Road Latham, New York 12110	1

	Copies
Metal Bellows Corporation Providence Highway Sharon, Massachusetts 02067	1
Metal Products Division Koppers Co., Inc. 200 Scott Street Baltimore, Missouri 21203	1
Pesco Products Division of Borg-Warner Corp. 24700 N. Miles Road Bedford, Ohio 44146	1
Rocketdyne, A Division of North American Rockwell Corporation 6633 Canoga Avenue Canoga Park, California 91304	
Attn: Library, Dept. 596-306	1
J. Hale	1
K. Rothe	1
R. E. Burcham	1
Rocket Research Corporation 520 South Portland Street Seattle, Washington 98108	1
Sealol, Inc. Warwick Industrial Park Providence, Rhode Island 02905	
Attn: J. B. Stevens	1
Sundstrand Corporation Hydraulics Division Rockford, Illinois 61101	1
Stein Seal Company Twentieth Street and Indiana Avenue Philadelphia, Pennsylvania 19132	1
Sundstrand-Denver Industrial Products Group 2480 W. 70th Street Denver, Colorado 80221	1

	Copies
Systems Development Division IBM Corporation Endicott, New York 13760	1
TRW Systems One Space Park Redondo Beach, California 90278	
Attn: STL Tech. Lib. Doc. Acquisitions	1
United Aircraft Corporation Corporation Library 400 Main Street East Hartford, Connecticut 06118	
Attn: Library	1
United Aircraft Corporation Pratt & Whitney Fla. Res. Development Center P. O. Box 2691 W. Palm Beach, Florida 33402	
Attn: Library J. Hill W. R. Munk	1 1 1
United Aircraft Corporation United Technology Center P. O. Box 358 Sunnyvale, California 94088	
Attn: Library	1
Worthington Corporation Advanced Products Division Harrison & Worthington Avenues Harrison, New Jersey 07029	1